

Masterarbeit

Parton densities from LHC vector boson production at small and large transverse momenta

Einfluss der Partondichten auf die Produktion von
Vektorbosonen am LHC bei kleinen und großen
Transversalimpulsen

Matthias Brandt

Themensteller: Prof. Dr. Michael Klasen
Zweitgutachter: Jun. Prof. Dr. Anna Kulesza

Contents

1. Introduction	1
2. Basics of perturbative QCD	3
2.1. The QCD Lagrangian	3
2.2. The EW Lagrangian	6
2.3. From correlation functions to the scattering matrix - the perturbative approach	11
2.4. Back to QCD - Renormalization and the running coupling	22
2.5. Infrared divergences	31
3. From partons to hadrons - the process of interest	37
3.1. The parton model	37
3.2. Vector boson production in second order QCD	40
3.3. CSS resummation formula	45
4. Parton distribution functions	51
5. Numerical results	57
5.1. Comparison to data	58
5.2. Decomposition of partonic processes	63
5.3. Parton density sensitivity of LHC vector boson production	66
6. Conclusion	71
7. Appendix A	73
A.1. Feynman rules	75
A.2. Useful relations for the calculation of Feynman amplitudes	77
A.3. Calculation of the leading order QCD contributions to weak vector boson production	80
A.4. Quark self energy one loop contribution - example of dimensional regularization	88
A.4.1. Derivative of the self-energy contribution	90
Bibliography	93

Introduction

Due to the Large Hadron Collider (LHC) at CERN particle physicists gained access to higher precision tests of the Standard Model parameters. The Standard Model (SM) of particle physics is the current status of a theory describing the fundamental forces and building blocks of nature.

It is known to be imperfect (in addition to its own problems) and there is hope to find new physics within the energy regime now accessible at the LHC. However, also the search for new physics relies on the precision of the predictions of the SM. An important uncertainty lies in the structure of the initially colliding particles which are protons and lead nuclei.

The protons are believed to be bound states of so-called partons. The part of the SM describing the interactions among these partons is the quantum field theory of strong interactions namely Quantum Chromo-Dynamics (QCD). Unfortunately, this theory does not lead to exactly solvable equations.

A perturbative model of the interactions at high momentum transfers has been developed with great success. But the calculation of bound states of these particles remains inaccessible within perturbation theory. Therefore, this component still has to be determined from experiment. At current status the pool of partons consists of the force mediating gluons and six species of quarks. The substructure of the proton at high momentum transfers is described through so-called Parton Distribution Functions (PDFs).

In former collision experiments like the Deep-inelastic scattering (DIS) of electrons from protons within the HERA physics program at DESY or of neutrinos from nucleons at Fermilab Tevatron in particular the quark distributions have been constrained. The gluon density on the other hand enters only at next-to-leading order in the perturbative predictions for these processes.

The gluon PDF has been constrained mainly based on data from prompt photon production through the so-called QCD Compton process in proton-proton (more generally hadron-hadron) collisions, which is described in perturbation theory by the scattering of a quark from a gluon producing a photon. However, photon isolation and frag-

mentation uncertainties have caused difficulties in the past (although the situation is improving through recent LHC data).

We will consider another important SM process, the production of electroweak vector bosons in proton-proton collisions.

We will investigate the possibility to make improvement on the current uncertainties of PDFs in particular at high partonic momentum fractions (of the parent proton).

At leading order of perturbation theory, the production is described by two subprocesses, namely quark-antiquark and quark-gluon scattering. It will be shown that at high transverse momenta of the created vector boson, the quark-gluon subprocess will become the dominant component, raising the sensitivity of the collision experiment to the gluon distribution.

Furthermore, we will test the reliability of perturbation theory and its resummation (based on non-perturbative fit parameters determined from Tevatron Run 1) while comparing it to LHC data gained from its first run at a center of mass energy of $\sqrt{s} = 7 \text{ TeV}$.

The outline is the following.

Chapter two will deal with the basic features of the quantum field theory of the strong interactions and how to derive predictions for scattering processes starting from the field theoretic Lagrangian. Chapter three will apply the model to the case of weak vector boson production in proton-proton collisions. After a short review of the status of parton densities the numerical results will be presented in chapter five.

Basics of perturbative QCD

The underlying theory of our calculations is the SM of particle physics. It is a dynamical theory of relativistic and quantized fields that describes the electromagnetic, weak and strong interactions between quarks and leptons which are assumed to be the fundamental constituents of matter. The theory can be summarized by its Lagrangian which is invariant under certain local gauge transformations corresponding to the SM gauge group $SU(3)_C \times SU(2)_L \times U(1)_Y$. Our focus lies on the $SU(3)$ component of the SM. However since we are dealing with the production of weak bosons we will have brief look at the electroweak sector too.

We spare a historical review but restrict our attention to the aspects relevant to calculations.

2.1. The QCD Lagrangian

The theory of QCD describes the strong interaction of *color*-charged particles which are quarks and gluons. Mathematically speaking QCD is a non-Abelian gauge theory obeying a local gauge symmetry under transformations of the $SU(3)_C$ (the C holds for the corresponding three colors) group. From experiments one distinguishes in six quark flavors which differ in their masses and electromagnetic charges. Corresponding to their chronological discovery one usually speaks of three generations which come in pairs of so-called up-type and down-type quarks where the former carry a fractional electromagnetic charge of $+2/3e$ and the latter one of $-1/3e$. The first generation consists of light up(u)- and down(d)-quarks, the second of charm(c)- and strange(s)-quarks and the third of heavy bottom(b)- and top(t)-quarks.

However, no isolated quarks could be found yet. So they are assumed to be bound to color-singlet states. Within the model one summarizes these states as so-called hadrons distinguished into baryons and mesons which are characterised by their quantum number giving so-called *valence* quarks. In the case of baryons the latter are three quarks each one of different color and in the case of mesons one has a quark-antiquark pair

with the same type of color (color and anti-color) yielding color neutral states.

The quanta of the gauge group are the so-called gluons mediating the force between quarks while carrying color themselves. The coupling of the gluons to themselves turns out to be an important feature of the theory. As we will discuss later on it will allow to describe interactions of colorless bound states through the interaction of effectively free quarks and gluons.

On the other hand there exist strong arguments how it also can explain the mechanism that hides color to which one refers as color *confinement*. However this can not be described within the approach we are going to follow which is an perturbative treatment of the theory. For further readings on that topic see for example [1].

Our starting point is the classical Lagrangian of QCD given as below

$$\mathcal{L}^d = \sum_q \bar{\psi}_{q,i} (i\gamma^\mu D_{\mu ij} - m_q \delta_{ij}) \psi_{q,j} - \frac{1}{4} G_{\mu\nu}^a G^{a\mu\nu}. \quad (2.1)$$

The quark fields are represented by Dirac spinors coming in three different colors, i.e. by $\psi_{q,j}$ where q denotes the flavor of the quarks with mass m_q and j the color index running from 1 to $N_C = 3$. The γ^μ are labeling the common Dirac matrices and accordingly the adjoint spinor is defined as $\bar{\psi}_{q,i} = \psi_{q,i}^\dagger \gamma^0$.

To ensure the invariance of the Lagrangian under $SU(3)_C$ gauge transformations the derivative $D_{\mu ij}$ is made up in such a way that $D_{\mu ij} \psi_{q,j}$ transforms as $\psi_{q,i}$ under these transformations and it is therefore called covariant derivative. It is defined as

$$D_{\mu ij} = \delta_{ij} \partial_\mu + i g_s t_{ij}^a G_\mu^a. \quad (2.2)$$

The t_{ij}^a are the generators of the $SU(3)$ group in the fundamental representation with a running from 1 to $N_c^2 - 1 = 8$ and they act on the quark fields which are therefore in the fundamental representation, too. To each generator corresponds a gauge field G_μ^a . To get the actual QCD Lagrangian these fields still have to be quantized.

As mentioned above these quanta are the so-called gluons, so we go on referring to the gauge fields as gluon fields. Thus, the second term of the covariant derivative (included in the Lagrangian) represents the interaction of the gluon fields with the quark fields which is just a rotation of the quark colors in $SU(3)$ color space. The strength of the interaction is described universally by the strong coupling constant g_s . The last term of the classical Lagrangian embodies the kinematics of the gluon fields. The gluon field

strength tensor $G_{\mu\nu}^a$ is defined as follows:

$$G_{\mu\nu}^a = \partial_\mu G_\nu^a - \partial_\nu G_\mu^a - g_s f_{abc} G_\mu^b G_\nu^c. \quad (2.3)$$

Here, the f_{abc} are the structure constants of the SU(3) group according to its Lie-algebra $[t^a, t^b] = i f_{abc} t^c$. Expanding the kinematic term yields

$$\begin{aligned} -\frac{1}{4} G_{\mu\nu}^a G^{a\mu\nu} = & -\frac{1}{4} (\partial_\mu G_\nu^a - \partial_\nu G_\mu^a) (\partial^\mu G^{a\nu} - \partial^\nu G^{a\mu}) \\ & + \frac{g_s}{2} f_{abc} (\partial^\mu G^{a\nu} - \partial^\nu G^{a\mu}) G_\mu^b G_\nu^c - \frac{g_s}{4} f_{abc} f_{ade} G_\mu^b G_\nu^c G^{d\mu} G^{e\nu}. \end{aligned} \quad (2.4)$$

The term in the first line represents the free propagation of the gluon fields while the second line shows cubic and quartic self-interaction terms.

Since the gluon fields G_μ^a are Lorentz four-vectors, they exhibit four degrees of freedom but due to gauge invariance and the implied masslessness of the fields (mass term would violate the invariance) only two of them are physical. When it comes to quantize the fields of the classical Lagrangian there arise some technical issues preventing the non-physical degrees of freedom from entering into physical observables while performing the quantization in a consistent manner. For later usage in practical calculations it is best to follow the Faddeev-Popov procedure which leads besides of an gauge-fixing term (applies a covariant gauge) to a term containing additional unphysical fields named ghosts. These ghost fields couple to the gluon fields in such a way that all contributions coming from the unphysical polarization states of the gluon fields cancel. Indicating quantized quantities via the hat symbol, the QCD Lagrangian reads:

$$\begin{aligned} \mathcal{L}_{QCD} = & \sum_q \bar{\psi}_{q,i} \left(i\gamma^\mu \hat{D}_{\mu ij} - m_q \delta_{ij} \right) \psi_{q,j} - \frac{1}{4} \hat{G}_{\mu\nu}^a \hat{G}^{a\mu\nu} \\ & - \frac{1}{2\xi} (\partial^\mu \hat{G}_\mu^a) (\partial^\nu \hat{G}_\nu^a) + \partial_\mu \eta_b^\dagger \hat{D}_{bc}^\mu \eta_c. \end{aligned} \quad (2.5)$$

Here, ξ denotes the gauge parameter. The ghost fields are labeled by η with their color indices b, c running from 1 to 8. They are massless, complex scalar and most remarkably anti-commuting fields. The covariant derivative acting on the ghost fields is very similar to the one acting on the quark fields (still defined as in 2.2 but with quantized fields)

but with its $SU(3)$ group generators being in the adjoint representation:

$$\hat{D}_{\mu bc} = \delta_{bc} \partial_\mu + g_s f_{abc} \hat{G}_\mu^a. \quad (2.6)$$

For further details on the quantization procedure and the explicit form of the quantized fields we refer to [2].

2.2. The EW Lagrangian

The electroweak (EW) part of the SM, known as the *Glashow–Weinberg–Salam* (GWS) model, describes the electromagnetic and weak interactions which take place among all fundamental matter fields, i.e. quarks and leptons, in a single, unified gauge theory with the gauge group $SU(2)_L \times U(1)_Y$. As mentioned in the last section a mass term for gauge bosons violates the local gauge symmetry of the Lagrangian. But indeed, gauge bosons of the EW model will be massive. This is where the so-called Higgs mechanism comes into play. As we will shortly discuss in a moment, the bosons will achieve their masses via the introduction of an additional complex scalar field with a non-vanishing vacuum expectation value which may cause the local gauge symmetry to be spontaneously broken so that only the electromagnetic gauge symmetry $U(1)_{em}$ remains preserved. Out of the four associated gauge bosons one will have three massive bosons which can be identified as the charged vector bosons $W^{+/-}$ and the neutral Z boson and one massless boson that will be identified with the photon γ .

We will consider the classical Lagrangian given below piece by piece.

$$\mathcal{L}_{EW}^{cl} = \mathcal{L}_{EW}^{\text{gauge}} + \mathcal{L}_{EW}^{\text{quarks}} + \mathcal{L}_{EW}^{\text{lepton}} + \mathcal{L}_{EW}^{\text{Higgs}} + \mathcal{L}_{EW}^{\text{Yukawa}}. \quad (2.7)$$

The first piece represents the kinematics of the gauge fields, where the fields corresponding to the $SU(2)$ part are denoted by W_μ^a with $a = 1, 2, 3$ and the one belonging to the $U(1)$ part by B_μ . One has

$$\mathcal{L}_{EW}^{\text{gauge}} = -\frac{1}{4} W_{\mu\nu}^a W^{a\mu\nu} - \frac{1}{4} B_{\mu\nu} B^{\mu\nu}, \quad (2.8)$$

where the field strength tensors are defined by

$$\begin{aligned} B_{\mu\nu} &= \partial_\mu B_\nu - \partial_\nu B_\mu, \\ W_{\mu\nu}^a &= \partial_\mu W_\nu^a - \partial_\nu W_\mu^a - g\epsilon_{abc} W_\mu^b W_\nu^c. \end{aligned} \quad (2.9)$$

The structure constants following from the $SU(2)$ Lie-algebra are given by the total antisymmetric Levi-Civita tensor ϵ_{abc} .

Now the second piece represents the kinematic part of the quark and lepton fields involving the interaction with the gauge fields. The model distinguishes into left- and right-handed fields. The left-handed (L) quarks and leptons transform as doublets under $SU(2)_L$ transformations while the right-handed (R) particles transform as singlets. As quarks, leptons come in three generations, each generation consists of an electron like particle and a corresponding neutrino, namely electron (e), muon (μ) and tauon (τ) and electron-neutrino (ν_e) and so on. We denote the lepton doublets as

$$L_f^L = \begin{pmatrix} \nu_f'^L \\ l_f'^L \end{pmatrix} = \begin{pmatrix} \nu_e'^L \\ e'^L \end{pmatrix}, \begin{pmatrix} \nu_\mu'^L \\ \mu'^L \end{pmatrix}, \begin{pmatrix} \nu_\tau'^L \\ \tau'^L \end{pmatrix}, \quad (f = 1, 2, 3) \quad (2.10)$$

and accordingly the quark doublets as

$$Q_f^L = \begin{pmatrix} u_f'^L \\ d_f'^L \end{pmatrix} = \begin{pmatrix} u'^L \\ d'^L \end{pmatrix}, \begin{pmatrix} c'^L \\ s'^L \end{pmatrix}, \begin{pmatrix} t'^L \\ b'^L \end{pmatrix}, \quad (f = 1, 2, 3).$$

Here the prime symbol serves to distinguish the electroweak quark eigenstates from the physical mass eigenstates. The fields inside the doublets are again described by Dirac spinors. The singlets accordingly are $u_f'^R, d_f'^R$ and $l_f'^R$ where no right-handed neutrinos are included. The electroweak particles carry weak isospin I_3 (third component of the isospin vector, $\begin{pmatrix} +1/2 \\ -1/2 \end{pmatrix}$ for the doublets, 0 for singlets) and hypercharge Y . Both are related to the electric charge Q by $Q = I_3 + Y/2$.

To reduce the number of indices, spinor and matrix multiplication will be understood from now on. Additionally making use of the Dirac slash notation $\gamma_\mu D^\mu = \not{D}$ the fermionic part reads

$$\mathcal{L}_{EW}^{\text{quarks}} + \mathcal{L}_{EW}^{\text{lepton}} = \sum_f \left(\bar{Q}_f^L i \not{D} Q_f^L + \bar{L}_f^L i \not{D} L_f^L + \bar{u}_f'^R i \not{D} u_f'^R + \bar{d}_f'^R i \not{D} d_f'^R + \bar{l}_f'^R i \not{D} l_f'^R \right) \quad (2.11)$$

where the covariant derivative D_μ when acting on doublets is given by

$$D_\mu = \mathbb{1} \partial_\mu + ig \frac{\sigma^a}{2} W_\mu^a + ig' \frac{Y}{2} B_\mu \quad (2.12)$$

and in the case it acts on singlets just by

$$D_\mu = \mathbb{1} \partial_\mu + ig' \frac{Y}{2} B_\mu. \quad (2.13)$$

Here $\sigma^a/2$ are the $SU(2)$ generators represented by the *Pauli*-matrices σ^a .

The crucial ingredient now is a complex scalar field $SU(2)$ doublet with hypercharge $Y = 1$ (\Rightarrow one electrically charged (Φ^+) and one neutral component (Φ^0))

$$\Phi = \begin{pmatrix} \Phi^+ \\ \Phi^0 \end{pmatrix} = \frac{1}{\sqrt{2}} \begin{pmatrix} \Phi_1 + i\Phi_2 \\ \Phi_3 + i\Phi_4 \end{pmatrix} \quad (2.14)$$

which couples to the gauge bosons via the covariant derivative and to itself via the so-called *Higgs*-potential $V(\Phi)$

$$\mathcal{L}_{EW}^{\text{Higgs}} = (D_\mu \Phi)^\dagger (D^\mu \Phi) - V(\Phi) \quad (2.15)$$

where

$$V(\Phi) = -\mu^2(\Phi^\dagger \Phi) + \frac{1}{4}\lambda(\Phi^\dagger \Phi)^2, \quad \lambda, \mu^2 > 0. \quad (2.16)$$

Here μ is a parameter with dimension mass, λ a dimensionless coupling constant.

Now all fields obeying

$$|\Phi|^2 = \frac{v^2}{2}, \quad v = 2\frac{\mu}{\lambda} \quad (2.17)$$

minimize the potential so that the ground state is degenerate with a non-vanishing expectation value of $v/\sqrt{2}$. One may conveniently choose the vacuum state to be

$$\Phi_0 = \frac{1}{\sqrt{2}} \begin{pmatrix} 0 \\ v \end{pmatrix} \quad (2.18)$$

(where we have $\Phi_1 = \Phi_2 = \Phi_3 = 0$). Doing so, the $SU(2)_L \times U(1)_Y$ symmetry will be broken while the state remains invariant under $U(1)_{em}$ transformations since the non-vanishing value affects only the electrically neutral component Φ^0 . Expanding the scalar field doublet around its vacuum expectation value and performing a certain gauge transformation one can write

$$\Phi = \frac{1}{\sqrt{2}} \begin{pmatrix} 0 \\ v + H \end{pmatrix} \quad (2.19)$$

where H remains as the only physical degree of freedom while all other fields can be eliminated by choosing a certain gauge and thus correspond to unphysical degrees of freedom. The corresponding quantum is known as the *Higgs* boson with mass $m_H = \sqrt{2}\mu$.

Expanding the covariant derivative in (2.15) one now finds the following mass terms

$$m_W^2 W_\mu^+ W^{-\mu}, \quad \text{with} \quad W_\mu^\pm = \frac{1}{\sqrt{2}} (W_\mu^1 \mp iW_\mu^2), \quad m_W = \frac{1}{2}gv \quad (2.20)$$

and

$$\frac{1}{2}m_Z^2 Z_\mu Z^\mu, \quad \text{with} \quad Z_\mu = \frac{1}{\sqrt{g^2 + g'^2}} (gW_\mu^3 - g'B_\mu), \quad m_Z = \frac{v}{2}\sqrt{g^2 + g'^2} \quad (2.21)$$

where indeed the fields W_μ^\pm have electrical charge eigenvalues of $Q = \pm 1$ and the field Z_μ of $Q = 0$. The neutral massless field A_μ is given by

$$A_\mu = \frac{1}{\sqrt{g^2 + g'^2}} (g'W_\mu^3 + gB_\mu). \quad (2.22)$$

The physical particles W^\pm , Z^0 and γ are now described by the quanta of these fields. The masses of the W^\pm and Z^0 bosons are quite high (from experiment $m_W \approx 80 \text{ GeV}$, $m_Z \approx 90 \text{ GeV}$) so that the weak interactions are very short ranged.

There is one more term in the Lagrangian which serves to gain masses for the fermions after the symmetry is broken. It describes the interaction of the fermions with the complex scalar fields and reads

$$\mathcal{L}_{EW}^{\text{Yukawa}} = \sum_{f,f'} \left(\bar{Q}_f^L y_{ff'}^u u_{f'}^R \tilde{\Phi} + \bar{Q}_f^L y_{ff'}^d d_{f'}^R \Phi + \bar{L}_f^L y_{ff'}^l l_{f'}^R \Phi + h.c. \right) \quad (2.23)$$

where $\tilde{\Phi} = \begin{pmatrix} \Phi^0 \\ -\Phi^- \end{pmatrix}$ and the respective quark and lepton Yukawa coupling matrices are denoted by $y_{ff'}^u$, $y_{ff'}^d$ and $y_{ff'}^l$.

The massive physical states achieved after the symmetry breaking are related to the electroweak states by

$$u_f^{L(R)} = \sum_i U_{fi}^{u,L(R)} u_i'^{L(R)}, \quad d_f^{L(R)} = \sum_i U_{fi}^{d,L(R)} d_i'^{L(R)}, \quad l_f^{L(R)} = \sum_i U_{fi}^{l,L(R)} l_i'^{L(R)} \quad (2.24)$$

where the matrices $U_{fi}^{u,L}$, $U_{fi}^{u,R}$ and so on are diagonalizing the Yukawa matrices so that the masses after symmetry breaking are given by

$$m_{j,f} = \frac{v}{\sqrt{2}} \sum_{i,k} U_{fi}^{j,L} G_{ik}^j U_{kf}^{j,R\dagger}, \quad j = u, d, l. \quad (2.25)$$

Within the SM the neutrinos are assumed to be massless so that $U_{fi}^{\nu,L}$ can be chosen in such a way that the coupling terms to the physical W^\pm fields read

$$\frac{g}{\sqrt{2}} \sum_{f,f'} \left(\bar{u}_f^L \gamma^\mu W_\mu^+ V_{ff'} d_{f'}^L + \bar{\nu}_f^L \gamma^\mu W_\mu^+ l_{f'}^L + \bar{d}_f^L \gamma^\mu W_\mu^- V_{ff'}^\dagger u_{f'}^L + \bar{l}_f^L \gamma^\mu W_\mu^- \nu_{f'}^L \right) + h.c. . \quad (2.26)$$

Here $V_{ff'} = \sum_i U_{fi}^{u,L\dagger} U_{if}^{d,L}$ denotes the so-called *Cabbibo-Kobayashi-Maskawa* (CKM) quark mixing matrix. The remarkable point here is that the W fields can change the flavor of the matter fields.

On the other hand the couplings to the neutral fields are given by

$$e J_\mu^{em} A^\mu + \frac{g}{\cos \theta_W} (J_\mu^3 - \sin^2(\theta_W) J_\mu^{em}) Z^\mu . \quad (2.27)$$

The above currents are given as

$$J_\mu^3 = \sum_f \left(I_3^u \bar{u}_f^L \gamma_\mu u_f^L + I_3^d \bar{d}_f^L \gamma_\mu d_f^L + I_3^\nu \bar{\nu}_f^L \gamma_\mu \nu_f^L + I_3^l \bar{l}_f^L \gamma_\mu l_f^L \right) \quad (2.28)$$

where I_3^j ($j = u, d, \nu, l$) label the respective third component of the isospin and

$$J_\mu^{em} = \sum_f (e_u \bar{u}_f \gamma_\mu u_f + e_d \bar{d}_f \gamma_\mu d_f + \bar{l}_f \gamma_\mu l_f) \quad (2.29)$$

where e_u and e_d label the electric charge fraction of the up- and down-type quarks. The angle θ_W denotes the so-called *Weinberg* angle given by the relation

$$\cos \theta_W = \frac{m_W}{m_Z} . \quad (2.30)$$

The electromagnetic coupling e is related to the gauge group couplings via

$$e = \frac{gg'}{\sqrt{g^2 + g'^2}} \quad (2.31)$$

All other interaction and self-coupling terms will not be relevant for the calculations. As in the QCD case there will arise problems when quantizing the gauge fields leading to additional gauge-fixing and ghost terms again, but we will not bother them either.

2.3. From correlation functions to the scattering matrix - the perturbative approach ¹

The next step is to derive results from the Lagrangian for physical observables in order to compare them with experimental measurements. Since we deal with particle collisions, the desired quantity is the scattering cross section. The latter is directly related to the scattering matrix S . The matrix elements are defined as transition amplitudes for a set of well-separated particles with definite initial momenta p_1, p_2, \dots which is constructed in the far past evolving in the far future into a desired set of well-separated final particle states with momenta k_1, k_2, \dots . In the Heisenberg picture (states are constant, full time dependence is carried by the operators) it looks like

$$\langle k_1, k_2 \dots | \hat{S} | p_1 p_2 \dots \rangle = \lim_{T \rightarrow \infty} \langle k_1 k_2 \dots | e^{-i\hat{H}(2T)} | p_1 p_2 \dots \rangle. \quad (2.32)$$

Note that although the particles are considered as being well-separated, i.e noninteracting, the given states are eigenstates of the Hamiltonian H corresponding to the **full** Lagrangian and not only to its free fields part. As we will see this is due to the particles self interactions via their self-generated fields. Unfortunately, the QCD Lagrangian - as is the case for all known Lagrangians of field theories in four spacetime dimensions that contain interaction terms - does not lead to analytically exactly solvable equations of motion. To evaluate (2.32) we will follow a perturbative approach. One can extract the exact S -matrix from another rather abstract quantity, the Fourier-transforms of correlation or Green's functions. The correlation functions themselves will be treated perturbatively in terms of fields and the vacuum state corresponding to the free Hamiltonian. To see how this is done, we consider at first the case of a real scalar theory with three different interacting fields for simplicity. The Lagrangian is given by

$$\mathcal{L}_{ABC} = \sum_{i=A,B,C} \frac{1}{2} \left((\partial_\mu \hat{\phi}_i(x)) (\partial^\mu \hat{\phi}_i(x)) - m_i^2 \hat{\phi}_i^2(x) \right) - g \hat{\phi}_A(x) \hat{\phi}_B(x) \hat{\phi}_C(x). \quad (2.33)$$

So in the free field case the fields would just obey the *Klein-Gordon* (KG) equation. In order to use the interaction picture of operators and states we split the corresponding Hamiltonian into the free *Klein-Gordon* part ($\hat{H}_{KG} \equiv \hat{H}_0$) and the interaction part:

$$\hat{H} = \hat{H}_0 + \hat{H}_{\text{int}} = \hat{H}_0 + \int d^3x \hat{\phi}_A \hat{\phi}_B \hat{\phi}_C. \quad (2.34)$$

¹This section roughly follows [3].

In the following we will neglect the subscripts of the fields when there is no need to distinguish between different fields.

Our goal will be to express the n -point correlation function

$$\langle \Omega | T \phi(x_1) \phi(x_2) \dots \phi(x_n) | \Omega \rangle \quad (2.35)$$

in terms of fields and states that are exactly known, i.e. the free ones. To achieve this one turns into the interaction picture (IP). In (2.35) $|\Omega\rangle$ denotes the vacuum state corresponding to the full Hamiltonian. The time-ordering operator T takes care that later terms are placed to the left of earlier ones.

At a certain time t_0 the fields $\hat{\phi}$ can be expanded in terms of creation and annihilation operators as:

$$\hat{\phi}(t_0, \mathbf{x}) = \int \frac{d^3p}{(2\pi)^3} \frac{1}{\sqrt{2E_{\mathbf{p}}}} (a_{\mathbf{p}} e^{i\mathbf{p}\cdot\mathbf{x}} + a_{\mathbf{p}}^\dagger e^{-i\mathbf{p}\cdot\mathbf{x}}). \quad (2.36)$$

In the IP operators now only carry the time dependence of the free Hamiltonian, so that we have for the fields in the interaction picture (denoted by I):

$$\hat{\phi}_I(x) = \hat{\phi}_I(t, \mathbf{x}) = e^{i\hat{H}_0(t-t_0)} \hat{\phi}(t_0, \mathbf{x}) e^{-i\hat{H}_0(t-t_0)}. \quad (2.37)$$

Actually, this IP fields are equal to free fields in the Heisenberg picture.

The states in the IP are related to the constant Heisenberg picture states by

$$|\psi(t)\rangle_I = e^{i\hat{H}_0(t-t_0)} e^{-i\hat{H}(t-t_0)} |\psi_{t_0}\rangle \equiv \hat{U}(t, t_0) |\psi_{t_0}\rangle \quad (2.38)$$

making sure that expectation values are not changed when turning from the Heisenberg picture into the interaction picture. The unitary operator defined in (2.38) also relates the Heisenberg fields to the IP fields:

$$\hat{\phi}(t, \mathbf{x}) = \hat{U}^\dagger(t, t_0) \hat{\phi}_I(t, \mathbf{x}) \hat{U}(t, t_0). \quad (2.39)$$

The unitary operator itself obeys the following equation (easy to check from its definition)

$$i \frac{\partial}{\partial t} \hat{U}(t, t_0) = \hat{H}_{\text{int}}^I \hat{U}(t, t_0), \quad (2.40)$$

where

$$\hat{H}_{\text{int}}^I = e^{i\hat{H}_0(t-t_0)} \hat{H}_{\text{int}} e^{-i\hat{H}_0(t-t_0)} = \int d^3x \hat{\phi}_A^I \hat{\phi}_B^I \hat{\phi}_C^I \quad (2.41)$$

is the interaction Hamiltonian in the interaction picture. Converting (2.40) into an integral equation one can solve it iteratively with the initial condition $\hat{U}(t_0, t_0) = 1$. Using the time-ordering operator one can display the iteration procedure in a very compact form:

$$\hat{U}(t, t_0) = T \exp \left[-i \int_{t_0}^t dt' H_{\text{int}}^I(t') \right]. \quad (2.42)$$

Actually, one can generalize this to arbitrary times (at different initial conditions) and get further useful properties ($t_1 \geq t_2 \geq t_3$):

$$\hat{U}(t_1, t_2) \hat{U}(t_2, t_3) = \hat{U}(t_1, t_3) \quad \text{and} \quad \hat{U}(t_1, t_3) \hat{U}^\dagger(t_2, t_3) = \hat{U}(t_1, t_2). \quad (2.43)$$

Now we concentrate on the vacuum states which are defined by their eigenvalue equations $\hat{H} |\Omega\rangle = E_\Omega |\Omega\rangle$ ($E_\Omega \neq 0$) and $\hat{H}_0 |0\rangle = 0$. One can relate them by acting on $|0\rangle$ with the Heisenberg evolution operator $e^{-i\hat{H}T}$ in the following way. We multiply $e^{-i\hat{H}T}$ by a unity operator in form of a complete set of Heisenberg states and take the limit of very large T in a slightly imaginary direction. Since among all states $|\Omega\rangle$ is the one with the lowest energy we get $e^{-i\hat{H}T} \xrightarrow{T \rightarrow \infty(1-i\epsilon)} e^{-iE_\Omega T} |\Omega\rangle \langle\Omega|$. Acting now in that way on $|0\rangle$ (one has to argue that the both vacuum states have a finite overlap) we can deduce $|\Omega\rangle \xrightarrow{T \rightarrow \infty(1-i\epsilon)} (e^{-iE_\Omega T} \langle\Omega|0\rangle)^{-1} e^{-i\hat{H}T} |0\rangle$. Adding in the limit a small constant and keeping in mind that $\hat{H}_0 |0\rangle = 0$ we arrive at

$$|\Omega\rangle = \lim_{T \rightarrow \infty(1-i\epsilon)} \frac{e^{-iE_\Omega(t_0+T)}}{\langle\Omega|0\rangle} \hat{U}(t_0, -T) |0\rangle, \quad \langle\Omega| = \lim_{T \rightarrow \infty(1-i\epsilon)} \frac{e^{-iE_\Omega(T-t_0)}}{\langle 0|\Omega\rangle} \hat{U}(T, t_0) \langle 0|. \quad (2.44)$$

Now we can put everything together. By imposing the normalization condition $\langle\Omega|\Omega\rangle = 1$ (divide by one in this form) and using (2.44) and (2.42) as well as many times (2.39) and (2.43) one can finally obtain our desired relation for the correlation function in (2.35):

$$\langle\Omega|T\hat{\phi}(x_1)\dots\hat{\phi}(x_n)|\Omega\rangle = \lim_{T \rightarrow \infty(1-i\epsilon)} \frac{\langle 0|T\hat{\phi}_I(x_1)\dots\hat{\phi}_I(x_n)\exp[-i\int_{-T}^T dt H_{\text{int}}^I(t)]|0\rangle}{\langle 0|T\exp[-i\int_{-T}^T dt H_{\text{int}}^I(t)]|0\rangle} \quad (2.45)$$

where the time-ordering operator again allows us to strongly compress the expression (the exponential function has to be written as in infinite series for evaluation of T). Of course, as the equations of motion we cannot solve this relation exactly since it contains an infinite series which cannot be simplified to an analytical expression. But now single terms of the series can be calculated. In other words one hopes that a perturbative

treatment is applicable, i.e. that higher power terms contribute less so that a finite number of terms still gives a meaningful result.

Consider at first the two-point correlation function where we will concentrate on the numerator for now.

The first term of the infinite series then is just the two-point correlation function of the free case (remembering that fields in the IP are just free fields) and actually the Green's function corresponding to the *Klein-Gordon* equation. Let us split the fields in positive (containing all annihilation operators) and negative (containing all creation operators) frequency parts: $\hat{\phi} = \hat{\phi}^+ + \hat{\phi}^-$. Then we have (from now on fields acting on $|0\rangle$ will be in the IP, so we will drop the I label)

$$\langle 0|T\hat{\phi}(x_1)\hat{\phi}(x_2)|0\rangle = \begin{cases} \langle 0|\hat{\phi}^+(x_1)\hat{\phi}^-(x_2)|0\rangle & \text{for } x_1^0 > x_2^0; \\ \langle 0|\hat{\phi}^+(x_2)\hat{\phi}^-(x_1)|0\rangle & \text{for } x_2^0 > x_1^0, \end{cases} \quad (2.46)$$

since $\hat{\phi}^+|0\rangle = 0$ and $\langle 0|\hat{\phi}^- = 0$. So in either case a particle will be created at one spacetime point and destroyed at another and hence one may identify this expression as an amplitude for the propagation of a particle between those points while both directions (which depend on the time order of the events) are included. One can evaluate (2.46) in a way leading to an expression where the time-ordering is incorporated implicitly:

$$\langle 0|T\hat{\phi}(x_1)\hat{\phi}(x_2)|0\rangle = \int \frac{d^4p}{(2\pi)^4} \frac{i}{p^2 - m^2 + i\epsilon} e^{-ip \cdot (x_1 - x_2)} \equiv \Delta_F(x_1 - x_2). \quad (2.47)$$

The symbol Δ_F indicates that this is the so-called *Feynman-propagator* for a KG particle (in coordinate space). The next term in the series is $(\int dt \int d^3x \rightarrow \int d^4y)$

$$\langle 0|(-ig)T\hat{\phi}_A(x_1)\hat{\phi}_A(x_2) \int d^4y \hat{\phi}_A(y)\hat{\phi}_B(y)\hat{\phi}_C(y)|0\rangle = 0 \quad (2.48)$$

where now we have to choose one specific type of fields retroactively. The reason why this yields zero is simple: all operators of different types of fields commute and there is only one of type B and C , respectively.

For the next term we will use Wick's theorem which states that

$$T\hat{\phi}(x_1) \dots \hat{\phi}(x_n) = N \left(\hat{\phi}(x_1) \dots \hat{\phi}(x_n) + \text{all possible combinations of contractions} \right), \quad (2.49)$$

where the term "contraction" is defined between two field operators by

$$\overline{\hat{\phi}(x_1)\hat{\phi}(x_2)} = \begin{cases} [\hat{\phi}^+(x_1), \hat{\phi}^-(x_2)] & \text{for } x_1^0 > x_2^0; \\ [\hat{\phi}^+(x_2), \hat{\phi}^-(x_1)] & \text{for } x_2^0 > x_1^0, \end{cases} \equiv \Delta_F(x_1 - x_2) \quad (2.50)$$

which actually is equal to their *Feynman*-propagator.

Contractions between field operators that are not adjacent still are defined to be *Feynman*-propagators depending on the corresponding spacetime points (definition is included in the proof of the theorem). For example in the case of three field operators one will have

$$\begin{aligned} T\hat{\phi}_1\hat{\phi}_2\hat{\phi}_3 &= N \left(\hat{\phi}_1\hat{\phi}_2\hat{\phi}_3 + \overline{\hat{\phi}_1\hat{\phi}_2}\hat{\phi}_3 + \overline{\hat{\phi}_1\hat{\phi}_3}\hat{\phi}_2 + \overline{\hat{\phi}_2\hat{\phi}_3}\hat{\phi}_1 \right) \\ &= N \left(\hat{\phi}_1\hat{\phi}_2\hat{\phi}_3 + \Delta_F(x_2 - x_3)\hat{\phi}_1 + \Delta_F(x_1 - x_2)\hat{\phi}_3 + \Delta_F(x_1 - x_3)\hat{\phi}_2 \right). \end{aligned}$$

The symbol N labels the normally ordering operator which positions all annihilation to the left of the creation operators. The vacuum expectation value of all normally ordered terms containing uncontracted field operators will therefore yield zero. This theorem holds for different types of particles too, but of course there will be no contractions between them.

By Wick's theorem the term of the next order

$$\langle 0 | \frac{(-ig)^2}{2!} T\hat{\phi}_A(x_1)\hat{\phi}_A(x_2) \int d^4y_1 \hat{\phi}_A(y_1)\hat{\phi}_B(y_1)\hat{\phi}_C(y_1) \int d^4y_2 \hat{\phi}_A(y_2)\hat{\phi}_B(y_2)\hat{\phi}_C(y_2) | 0 \rangle$$

gives

$$\begin{aligned} \frac{(-ig)^2}{2!} \int d^4y_1 \int d^4y_2 & \left(\Delta_F^A(x_1 - x_2)\Delta_F^A(y_1 - y_2) + \Delta_F^A(x_1 - y_1)\Delta_F^A(x_2 - y_2) \right. \\ & \left. + \Delta_F^A(x_1 - y_2)\Delta_F^A(x_2 - y_1) \right) \Delta_F^B(y_1 - y_2)\Delta_F^C(y_1 - y_2). \end{aligned}$$

Thinking of the propagators as lines between two spacetime points one may illustrate these three terms by the diagrams in Fig. 2.1.

Actually, the second and third term will yield the same result after performing integration over y_1 and y_2 . So one may put the second and third diagram together.

Using this rather intuitive way of illustration for the second next (the one in between yields zero again) order term of the series leads to Fig. 2.2.

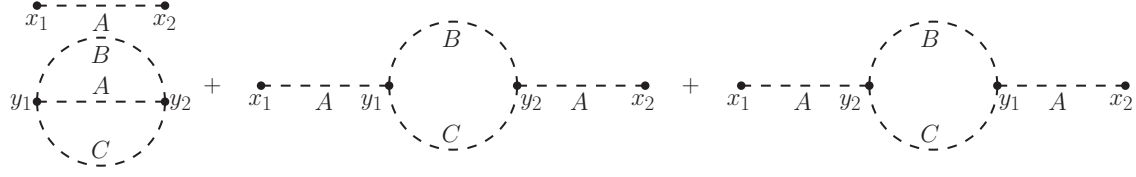


Figure 2.1.: Illustration of the first non-zero correction of a two-point correlation function in a theory of three interacting real scalar fields.

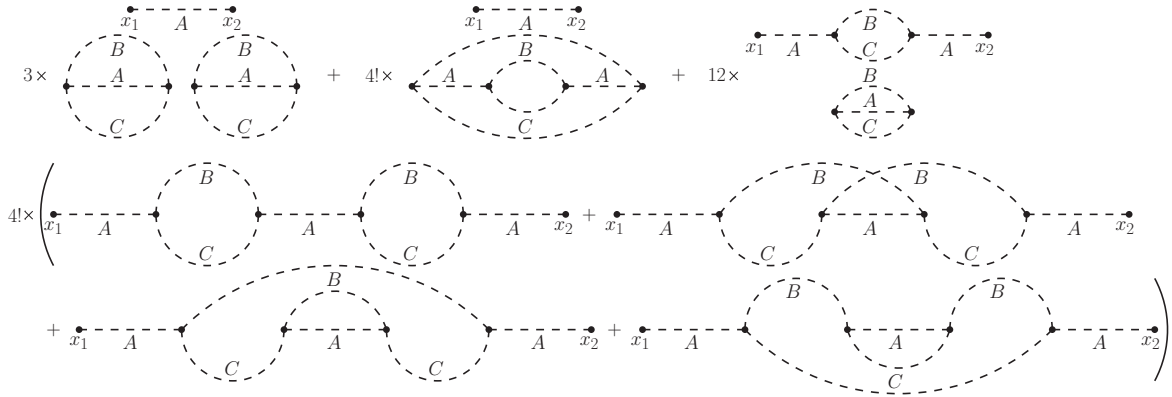


Figure 2.2.: Illustration of the second non-zero correction of a two-point correlation function in a theory of three interacting real scalar fields.

In this case we have factored out all diagrams for which the terms they illustrate give the same result. For each permutation of the integration variables y_i ($i = 1, \dots, 4$) (so we have $4!$ permutations) there is a diagram yielding the same result as one of the diagrams explicitly shown in Fig. 2.2 except for the first and the last diagram in the first line. There are 15 contributing contractions from the A fields and 3 contractions from the B and C fields respectively, so in total a number of 108 diagrams. While all diagrams yield the same result with respect to the contractions of the A fields in each of this cases there is a diagram out of the additional 9 possible B and C contractions with no further diagram yielding the same result. The first and the last diagram of the first line shown in Fig. 2.2 are corresponding this fact.

For the other diagrams the factor of $4!$ cancels exactly the one coming from the series expansion and as one may yet have thought this will be the case in every order.

In both Figures there are diagrams containing pieces which are disconnected from the points x_1 and x_2 . Furthermore the last diagram in the first line of Fig. 2.2 contains a piece disconnected from the other internal points which rather looks like the disconnected piece of the first diagram of Fig. 2.1.

Actually, one can show that all terms represented by these pieces factor out into an exponential function. So using the diagrams the other way around to remember the mathematical expressions the numerator (in the sense of (2.45)) of the two-point correlation function is represented by

$$\exp \left(\text{diagram 1} + \text{diagram 2} + \dots \right) \cdot \left(\text{diagram 3} + \text{diagram 4} + \dots \right)$$

The diagrams are as follows:
 Diagram 1: A dashed circle with a horizontal dashed line through its center. The top arc is labeled 'B', the bottom arc is labeled 'C', and the horizontal line is labeled 'A'.
 Diagram 2: Two dashed circles connected by a horizontal dashed line. The top arcs are labeled 'B', the bottom arcs are labeled 'C', and the horizontal line is labeled 'A'.
 Diagram 3: A horizontal dashed line with two dots at the ends, labeled 'x1' and 'x2', and 'A' in the middle.
 Diagram 4: A horizontal dashed line with two dots at the ends, labeled 'x1' and 'x2', and 'A' in the middle. In the middle of this line is a dashed circle with top arc 'B' and bottom arc 'C'.

But as it turns out the denominator yields exactly this exponential function containing all the disconnected pieces. From (2.44) one can see then that the sum of all terms represented by disconnected pieces is somehow proportional to the vacuum energy E_Ω . Therefore, one often refers to this pieces as vacuum bubbles.

So in the end, one can easily write down the mathematical expression by considering the sum of all possible diagrams where the external points (x_1 and x_2) are connected to all internal points (y_i). For each line one has to write down then a factor of Δ_F corresponding to the type of particle the line represents and the points it connects and a factor of $(-ig)$ and the integral $\int d^4 y_i$ for each internal point.

Let us have a look at the Fourier-transform of the second diagram for instance in Fig. 2.1. Thanks to the considered Fourier-transformation we can simplify the most left propagator to (remember (2.47))

$$\begin{aligned} \int d^4 x_1 e^{ip_1 \cdot x_1} \int \frac{d^4 p}{(2\pi)^4} \frac{i}{p^2 - m_A^2 + i\epsilon} e^{-ip \cdot (x_1 - y_1)} &= \int \frac{d^4 p}{(2\pi)^4} \frac{i(2\pi)^4 \delta^{(4)}(p_1 - p)}{p^2 - m_A^2 + i\epsilon} e^{ip \cdot y_1} \\ &= \frac{i}{p_1^2 - m_A^2 + i\epsilon} e^{ip_1 \cdot y_1}. \end{aligned}$$

Taking into account the integration of the next internal point and the parts of the other associated propagators depending on that point yields

$$\frac{i}{p_1^2 - m_A^2 + i\epsilon} \int d^4 y_1 e^{ip_1 \cdot y_1} e^{-ik_1 \cdot y_1} e^{-ik_2 \cdot y_1} = \frac{i}{p_1^2 - m_A^2 + i\epsilon} (2\pi)^4 \delta^{(4)}(k_1 + k_2 - p_1).$$

So this integration just leads to four-momentum conservation at the internal point. Accordingly the other half of the diagram gives

$$\frac{i}{p_2^2 - m_A^2 + i\epsilon} (2\pi)^4 \delta^{(4)}(k_1 + k_2 - p_2).$$

Keeping this in mind we go back to our original purpose: the derivation of the scattering matrix or more specifically its actual scattering part.

There will always be a probability that particles will pass each other without interfering. Accordingly one can split the \hat{S} -matrix into $S = \mathbb{1} + i\hat{T}$ where \hat{T} is the so-called transition matrix.

Now this transition matrix (cf. (2.32)) can be extracted from the Fourier-transform of the correlation functions in a way given by the Lehmann-Symanzik-Zimmermann (LSZ) reduction formula:

$$\prod_{f=1}^m \int d^4 x_f e^{ik_f \cdot x_f} \prod_{i=1}^n \int d^4 y_i e^{-ip_i \cdot y_i} \langle \Omega | T \hat{\phi}(x_1) \dots \hat{\phi}(x_m) \hat{\phi}(y_1) \dots \hat{\phi}(y_n) | \Omega \rangle$$

$$\xrightarrow[p_i^2 \rightarrow m^2]{k_f^2 \rightarrow m^2} \left(\prod_{f=1}^m \frac{\sqrt{Z}i}{k_f^2 - m^2} \prod_{i=1}^n \frac{\sqrt{Z}i}{p_i^2 - m^2} \right) \langle k_1 \dots k_m | i\hat{T} | p_1 \dots p_n \rangle \quad (2.54)$$

For a better overview the subscripts indicating different types of fields again have been neglected. For different fields one just has to adjust the m 's and Z 's in the formula. So the transition matrix can be won by determining the multiplication factor of the product of several single particle poles of just the form we encountered for the two-point correlation function.

Let us take the example of two to two particle scattering ($AB \rightarrow AB$). The four-point correlation function will be represented by the diagrams in Fig. 2.3.

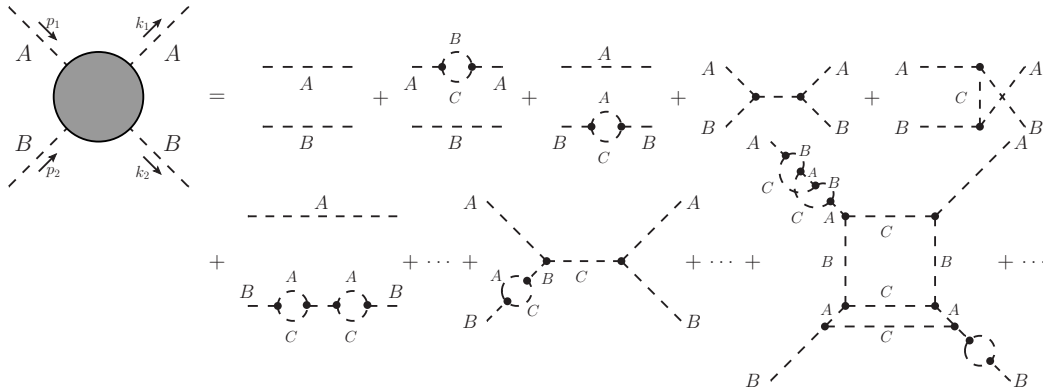


Figure 2.3.: *Feynman*-diagrams for a four-point correlation function in a theory of three interacting real scalar fields. It is shown more specifically the case of $\langle \Omega | \hat{\phi}_A(k_1) \hat{\phi}_B(k_2) \hat{\phi}_A(p_1) \hat{\phi}_B(p_2) | \Omega \rangle$ where the momenta have been omitted in the diagrams for clear vision.

All diagrams where external lines are disconnected from each other will not exhibit a product of four single particle poles and therefore not contribute to the T -matrix

(but actually to the $\mathbb{1}$ in the S -matrix). All other diagrams will contain four external propagator lines somehow connected to each other. Let us move along an external line inwards the diagram to the point where one can split the diagram into the part passed and the rest of the diagram (containing all other external propagators) by cutting a single internal line. All contributions coming from different diagrams moving along the external line up to the respective point will factor out making us able to sum them up just as we did in the case of the two-point function.

The sum will just be a full propagator as determined in (2.51)². Doing so for all external lines we will have

$$\frac{k_f^2 \rightarrow m_f^2}{p_i^2 \rightarrow m_i^2} \frac{Z_A i}{k_1^2 - m_A^2} \frac{Z_B i}{k_2^2 - m_B^2} \frac{Z_A i}{p_1^2 - m_A^2} \frac{Z_B i}{p_2^2 - m_B^2} \cdot \left(\text{sum of all truncated and full connected AB} \rightarrow \text{AB diagrams} \right) \quad (2.55)$$

where truncated here now simply means that the full external propagators have to be removed. This result generalizes to higher correlation functions. Comparing now to the LSZ reduction formula in the end yields

$$\begin{aligned} \langle k_1 \dots k_m | i\hat{T} | p_1 \dots p_n \rangle &= (2\pi)^4 \delta^{(4)} \left(\sum_{i=1}^n p_i - \sum_{f=1}^m k_f \right) \cdot i\mathcal{M} \\ &= (2\pi)^4 \delta^{(4)} \left(\sum_{i=1}^n p_i - \sum_{f=1}^m k_f \right) \cdot (\sqrt{Z})^{m+n} \cdot \left(\text{sum of all truncated and full connected n} \rightarrow \text{m diagrams with external initial momenta } p_i \text{ and final momenta } k_f. \right) \end{aligned} \quad (2.56)$$

where one usually splits the T -matrix defining an invariant matrix element \mathcal{M} up to an overall four-momentum conserving delta function. As we knew already, the latter one also appears within the correlation function (but we have neglected it in (2.55).

²This was the reason deriving the two-point function the way we did i.e. Fourier-transforming only in one variable and setting the other to zero. In a fully connected diagram the second variable of the full propagator will correspond to an internal point leading to Fourier-transforming it and momentum-conservation.

Finally, for an idealized scattering process of two incoming beams the quantity \mathcal{M} is related to the measurable scattering cross section σ in the following way

$$\sigma_{\{2 \rightarrow n\}} = \int d\sigma_{\{2 \rightarrow n\}} = \frac{1}{2E_1 2E_2 |v_1 - v_2|} |\mathcal{M}_{\{2 \rightarrow n\}}|^2 d\text{PS}^{(n)} \quad (2.57)$$

where

$$d\text{PS}^{(n)} \equiv \prod_f^n \int \frac{d^3 k_f}{(2\pi)^3} \frac{1}{2E_{\mathbf{k}_f}} (2\pi)^4 \delta^{(4)} \left(p_1 + p_2 - \sum_f^n k_f \right) \quad (2.58)$$

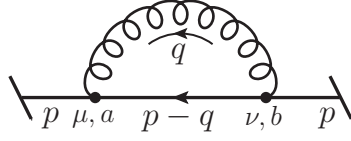
defines the Lorentz invariant phase space of the final state particles. The prefactor in the above equation (2.57) is the incident flux where $|v_1 - v_2|$ is the difference of the two beam velocities in the laboratory frame of the experiment. For a collinear collision $E_1 E_2 |v_1 - v_2|$ can be expressed by $\sqrt{(p_1 \cdot p_2)^2 - m_1^2 m_2^2}$ which is then Lorentz invariant [4]. Additionally, one most often sums(averages) over all internal degrees of freedom of the final (initial) particles which in the case of QCD are the helicities and color charges of the particles, so that one uses $|\overline{\mathcal{M}}|^2 \equiv \sum_{\text{helicity, color}} |\mathcal{M}|^2$ instead in the above expression.

2.4. Back to QCD - Renormalization and the running coupling

Now let us get back to QCD. The *Feynman*-rules for deriving an invariant matrix element will change since we have to deal with particles carrying spin and different forms of interactions. External lines will exhibit spinors or polarization vectors, vertices will involve representations of the gauge group generators. The procedure on deriving the new rules will in principle be the same. In the case of the gauge bosons, however, the quantization problems mentioned in section 2.1 affect the derivation of their *Feynman*-propagator as well so that the canonical approach is not quite the best procedure there. Nevertheless, we are not going to bother with the subtleties on deriving the specific QCD rules but just go ahead using them. The QCD rules are listed in Appendix A.1 as well as the relevant EW rules. At first, we take a look at the full propagator of a quark field. From the Feynman rules and by $i \frac{(\not{p} + m_0)}{p^2 - m_0^2} \rightarrow \frac{i}{\not{p} - m_0}$ it follows by analogy with Eq. (2.51)

$$\text{Diagram: a circle with two external lines labeled } p \text{ and } p \text{ entering from the left and right respectively} = \frac{i}{\not{p} - m_0 - \Sigma^{\bar{q}q}(\not{p}) + i\epsilon} \quad (2.59)$$

where $-i\Sigma^{\bar{q}q}(\not{p})$ here denotes the sum of all 1PI diagrams adapted to the case of quarks (we will not consider different quark masses/flavors in general discussions). One often refers to $-i\Sigma^{\bar{q}q}$ as the quark self-energy. Now take a closer look at the first contribution to it:



$$= \int \frac{d^4 q}{(2\pi)^4} i g_s \gamma^\mu t^a \frac{(-i) g_{\mu\nu} \delta_{ab}}{q^2 + i\epsilon} \frac{i(\not{p} - \not{q} + m_0)}{(p - q)^2 - m_0^2 + i\epsilon} i g_s \gamma^\nu t^b$$

As one can see by comparing powers of q in the numerator and denominator, the integrated function diverges as q goes to infinity. In general this comparison only tells something about the degree of a potential divergence since there may be cancellations between divergences when performing the integration. In our case the integral does diverge. This seems to mess up the perturbative series right at the second term.

But as we know from the last section m_0 is not the physical mass and so an unobservable parameter. Hence it may be an infinite quantity itself representing the shift in the mass when going from free theory to interacting theory.

In the given case the physical mass m is given by

$$[\not{p} - m_0 - \Sigma^{\bar{q}q}(\not{p}, m_0)]|_{\not{p}=m} = 0. \quad (2.60)$$

This equation may serve the other way around to express m_0 in terms of the finite mass m

$$m_0 = m - \Sigma^{\bar{q}q}(\not{p}, m_0)|_{\not{p}=m}$$

what actually has to be solved iteratively. However, to finite order one does:

$$m_0 = m - \left({}^{(1)}\Sigma^{\bar{q}q}(\not{p}, m_0)|_{\not{p}=m, m_0=m} + {}^{(2)}\Sigma^{\bar{q}q}(\not{p}, m_0)|_{\not{p}=m, m_0=m} + \dots \right). \quad (2.61)$$

So no iteration is performed at a given order since it would lead to corrections of higher perturbative order while not taking into account the higher order terms from the perturbative series itself.

Now how to express m_0 in terms of an infinite quantity properly. One will have to make the divergences manifest in some parameter and take the limit of the parameter at the end of the calculations. They are several ways to do that, but nowadays the most commonly used method is *dimensional regularization* first introduced by *Veltman*

and 't Hooft [5]. Its biggest advantage is that it preserves the gauge and Lorentz invariance of the Lagrangian. The concept is easy: one performs the integration in another dimension D where no divergences arise, the divergences will then be manifest in orders of $1/(D-4)$ poles. The execution on the other hand may involve a number of subtleties depending on the respective integral and its parameters.

Applying this method to the first contribution to $-i\Sigma^{\bar{q}q}$ yields (using (A.21),(A.27) and (A.28) to arrive at the first line)

$$\begin{aligned} & -i^{(1)}\Sigma^{\bar{q}q} \xrightarrow{4 \rightarrow D} -\frac{4}{3}g_s^2 \frac{(2\pi\mu)^{4-D}}{(2\pi)^4} \int d^D q \frac{(2-D)(\not{p}-\not{q}) + Dm_0}{(q^2 + i\epsilon)((p-q)^2 - m_0^2 + i\epsilon)} \\ \Rightarrow {}^{(1)}\Sigma^{\bar{q}q} &= -\frac{4}{3} \frac{g_s^2}{(4\pi)^2} \left[\not{p} \left(\Delta - \ln \frac{m_0^2}{\mu} + \frac{m_0^2}{p^2} + \frac{m_0^4 - (p^2)^2}{(p^2)^2} \ln \frac{m_0^2 - p^2 - i\epsilon}{m_0^2} + 1 \right) \right. \\ & \quad \left. - 4m_0 \left(\Delta - \ln \frac{m_0^2}{\mu} + \frac{m_0^2 - p^2}{p^2} \ln \frac{m_0^2 - p^2 - i\epsilon}{m_0^2} + \frac{3}{2} \right) + \mathcal{O}(4-D) \right] \end{aligned} \quad (2.62)$$

where the explicit calculation is shown in Appendix A.4. Here μ denotes an arbitrary parameter of dimension mass to account for the additional powers of mass from the momentum integration in D dimensions. The divergences are contained in the Δ 's defined as $\Delta = 2/(4-D) - \gamma_E + \ln 4\pi$, where γ_E is the *Euler-Mascheroni* constant.

As one can see there is a singular term proportional to \not{p} , so while expressing m_0 in terms of m as described will make the denominator of the propagator finite at $\not{p} = m$ by definition, at arbitrary \not{p} there will remain a divergent term $(\not{p} - m) \cdot \Delta$.

Now again the amplitude for creating a single particle state is given by the residue of the full propagator at the physical mass scale defined by

$$Z^{-1} = 1 - \left. \frac{d}{d\not{p}} \Sigma^{\bar{q}q}(\not{p}) \right|_{\not{p}=m}. \quad (2.63)$$

So at order g_s^2 we have

$$Z \approx 1 + \left. \frac{d}{d\not{p}} {}^{(1)}\Sigma^{\bar{q}q}(\not{p}, m_0) \right|_{\not{p}=m, m_0=m}. \quad (2.64)$$

For now we were dealing with divergences in the limit of high q to which one refers as ultraviolet (UV) divergences. But the derivative of the first contribution will lead to another type of divergence which has its origin in the zero gluon mass and occurs in the limit of low q . To this type of divergence one refers as an infrared (IR) divergence.

Interchanging the order of integration and derivation the part which leads to an IR divergence does not lead to an UV one. So while for UV divergences the integration was performed in the limit $D \rightarrow 4^-$ in the IR case one just does $D \rightarrow 4^+$ instead. The derivative of the first contribution at $\not{p} = m$ then becomes

$$\left. \frac{d}{d\not{p}} {}^{(1)}\Sigma^{\bar{q}q}(\not{p}, m) \right|_{\not{p}=m} = -\frac{4}{3} \frac{g_s^2}{(4\pi)^2} \left(\Delta_{UV} - \ln \frac{m^2}{\mu} - 2 \left(\Delta_{IR} + \ln \frac{m^2}{\mu} - 2 \right) \right) \quad (2.65)$$

where $\Delta_{UV} = \Delta = -\Delta_{IR}$ and the calculation can be found in Appendix (A.4.1). Since Z just reflects the normalization of the quark fields, which is no observable, one may redefine the quark fields in order to normalize Z to unity. Doing so implies that the former remaining divergence $(\not{p} - m) \cdot \Delta$ will be removed, too. We just redefine the fields in the Lagrangian as $\hat{\psi}_q = \sqrt{Z} \hat{\psi}_{q,r}$ where r indicates that the field has been *renormalized*. Then the denominator of the propagator to order g_s^2 becomes (remember m_0 has been expressed as described in (2.61))

$$\begin{aligned} & (\not{p} - m) \left(1 + \left. \frac{d}{d\not{p}} {}^{(1)}\Sigma^{\bar{q}q}(\not{p}, m) \right|_{\not{p}=m} \right) + {}^{(1)}\Sigma^{\bar{q}q}(m, m) - {}^{(1)}\Sigma^{\bar{q}q}(\not{p}, m) \\ &= \not{p} - m + \frac{4}{3} \frac{g_s^2}{(4\pi)^2} \left[\not{p} \left(\frac{m^2}{p^2} + \frac{m^4 - (p^2)^2}{(p^2)^2} \ln \frac{m^2 - p^2 - i\epsilon}{m^2} - 3 \right) \right. \\ & \quad \left. - m \left(4 \frac{m^2 - p^2}{p^2} \ln \frac{m^2 - p^2 - i\epsilon}{m^2} - 2 \right) \right] \end{aligned} \quad (2.66)$$

where we have neglected the infrared part for now, there will be another way to deal with it later on. So in the end, we have an UV finite expression for the quark propagator in terms of the physical mass and a field strength normalized to unity. Furthermore the dependence on the unphysical parameter μ has been removed again.

There will arise other divergences from contributions to the gluon and ghost propagators and the QCD vertices. They can be handled in a similar way after they have been made manifest as before by dimensional regularization. The divergences arising from vertex corrections may just be canceled by an according redefinition of the bare coupling constant while in the case of gluon propagators one may renormalize the gluon fields as we did for the quark fields. Following our previous conditions, one would renormalize the gluon fields then by the value of the residue at $p^2 = 0$ and redefine the coupling constant for example at zero momentum transfer. Doing it in this way is the so-called on-shell renormalization.

But as long as this might be great to do in quantum electrodynamics, in QCD one

cannot properly determine the quark masses since they are not found as isolated particles. As we will discuss the coupling grows so strong at low momentum scales that an perturbative approach becomes invalid.

So one might consider to impose other conditions at other momentum scales where experiments have access to the parameters of the theory leading to perturbative reasonable results. The new redefined quantities will be somehow related to the on-shell quantities by a finite shift. To perform the so-called renormalization procedure in a consistent manner in practice one most often does the following.

At first one rewrites the bare parameters and fields in terms of the renormalized ones while the rescaling coefficients are initially arbitrary. So we have

$$\hat{\psi}_q = \sqrt{Z_q} \hat{\psi}_{q,r}, \quad \hat{G}_\mu^a = \sqrt{Z_G} \hat{G}_{r,\mu}^a, \quad \eta^a = \sqrt{Z_\eta} \eta_r^a \quad (2.67)$$

and

$$m_{q,0} = Z_m m_{q,r}, \quad g_s = Z_g g_{s,r}, \quad \xi = Z_\xi \xi_r. \quad (2.68)$$

Then one splits the Lagrangian into a part equal to the original Lagrangian just with the bare characters replaced by the renormalized ones and a part containing the so-called counter-terms. Accordingly the first part will lead to the same expressions and divergences again just with the rescaled quantities instead of the bare ones. The other part will lead to "new" *Feynman*-rules and -diagrams which have to be included in calculations. The counter-terms will then be adjusted to fulfill whatever renormalization condition is imposed. Note again: the rescaling factors of the fields now have not to be the residues of the physical particle mass poles.

The counter-term Lagrangian \mathcal{L}_{ct} is given by (to reduce the number of indices spinor and matrix multiplication is understood, cf. 2.5)

$$\begin{aligned} \mathcal{L}_{ct} = & \sum_q \bar{\psi}_{q,r} (i(Z_q - 1)\gamma^\mu \partial_\mu - (Z_q Z_m - 1)m_{q,r}) \hat{\psi}_{q,r} \\ & + (Z_g Z_q \sqrt{Z_G} - 1) i g_{s,r} \sum_q \bar{\psi}_{q,r} t^a \hat{G}_{r,\mu}^a \hat{\psi}_{q,r} \\ & - (Z_G - 1) \frac{1}{4} (\partial_\mu \hat{G}_{r,\nu}^a - \partial_\nu \hat{G}_{r,\mu}^a) (\partial^\mu \hat{G}_r^{a\nu} - \partial^\nu \hat{G}_r^{a\mu}) \\ & + \left(Z_g \sqrt{Z_G^3} \right) \frac{g_{s,r}}{2} f_{abc} \left(\partial^\mu \hat{G}_r^{a\nu} - \partial^\nu \hat{G}_r^{a\mu} \right) \hat{G}_{r,\mu}^b \hat{G}_{r,\nu}^c \\ & - (Z_g^2 Z_G^2) \frac{g_{s,r}^2}{4} f_{abc} f_{ade} \hat{G}_{r,\mu}^b \hat{G}_{r,\nu}^c \hat{G}_r^{d\mu} \hat{G}_r^{e\nu} \\ & + (Z_\eta - 1) (\partial_\mu \eta_r^{\dagger a}) (\partial^\mu \eta_r^a) - (Z_g Z_\eta \sqrt{Z_G} - 1) g_{s,r} f_{abc} (\partial_\mu \eta_r^{\dagger a}) \hat{G}_r^{b\mu} \eta_r^c. \end{aligned} \quad (2.69)$$

As indicated yet since only one rescaling factor for the coupling was defined one can proof that the universality of the coupling constant due to gauge invariance carries over to the renormalized coupling. So the different constants coming from the interaction counter terms are all related to each other and one may derive Z_g in four possible ways according to the four counter-terms involving it. This has been proven up to all orders of perturbation theory by *Slavnov* and *Taylor* generalizing a former proof of 't Hooft on the renormalizability of massless *Yang-Mills* fields [6],[7]. So, as it was not mentioned yet, it has been shown that arising divergences up to all orders indeed can be subtracted by the finite number of constants, introduced in (2.67),(2.68), order by order in perturbation theory.

Let us get back once more to the example of the quark propagator. To determine the self-energy one now has to include the counter-term diagrams. The order $g_{s,r}^2$ contribution to it then is

$$= -i {}^{(1)}\Sigma^{\bar{q}q}(\not{p}, m_r, g_{s,r}) - i ((Z_q - 1)\not{p} - (Z_q Z_m - 1)m_r) ,$$

where we have kept ${}^{(1)}\Sigma^{\bar{q}q}(\not{p}, m_r, g_{s,r})$ to be the self-energy contribution coming from the non-counter-term part of the Lagrangian which we already know.

For the sake of getting rid of divergences one may just choose the counter-terms to cancel only the poles itself which is done in the so-called minimal subtraction (MS) scheme. In the modified MS ($\overline{\text{MS}}$) scheme one additionally cancels the typical $\gamma_E - \ln 4\pi$ constant i.e. one cancels Δ as a whole. So from (2.62) we deduce

$$\begin{aligned} & -\frac{4}{3} \frac{g_{s,r}^2}{(4\pi)^2} \Delta \cdot (\not{p} - 4m_r) + (Z_q - 1)\not{p} - (Z_q Z_m - 1)m_r + \text{finite terms} \stackrel{!}{=} \text{finite} \\ \Rightarrow Z_q^{\overline{\text{MS}}} &= 1 + \frac{4}{3} \frac{g_{s,r}^2}{(4\pi)^2} \Delta + \mathcal{O}(g_{s,r}^4) \quad \text{and} \quad Z_m^{\overline{\text{MS}}} = 1 + 4 \cdot \frac{4}{3} \frac{g_{s,r}^2}{(4\pi)^2} \Delta + \mathcal{O}(g_{s,r}^4) \end{aligned} \quad (2.70)$$

while one often defines then $Z_q \equiv 1 + \delta Z_q$ and $Z_m \equiv 1 + \delta Z_m$. Both factors depend on the gauge where we used the *Feynman*-gauge yet in the definition of the *Feynman*-rules in the Appendix. Depending on the gauge there even might disappear some divergences but the general problem of UV singularities cannot be solved by choosing the right gauge.

Contrary to the on-shell scheme, the final result for the propagator in the $\overline{\text{MS}}$ scheme now will depend on μ . Accordingly, the renormalized mass m_r has to depend on μ too and must be determined from experiment once a specific value of μ has been chosen. The same thing holds for the coupling constant. But except for the on-shell scheme the renormalized mass and coupling constant will depend on a mass scale in other schemes too. But while in other schemes one imposes conditions on how to subtract the divergences at a certain momentum scale in the $\overline{\text{MS}}$ scheme the μ coming from the regularization procedure somehow plays the role of the renormalization scale.

Now for example for the vertex corrections one encounters terms $\sim \ln(p^2/\mu^2)$ where p^2 here actually is an aggregate of momenta and masses. So if the deviation of p^2 from μ^2 grows, the logarithm might become large enough to spoil the perturbative approach. It may become necessary to renormalize the theory at another scale μ to reestablish the validity of the perturbative series. Not to lose predictive power we need to get some knowledge about the dependence of the parameters on μ . We defined the renormalized theory to be numerically the same as the bare one (cf. (2.67),(2.68)) which should be independent of any renormalization scale. However, at finite order the dependence of a observable on μ cannot completely get canceled (except for special cases) [8], but atleast we can get information about it in this way. We will restrict our attention to the implications for the strong coupling constant.

To compare between renormalized and bare theory, we regularize both theories in the dimensional regularization scheme with mass parameter μ_0 at first. We introduced the parameter to account for the extra dimensions when performing the momentum integrations but where does it actually enter into the theory? In D dimensions the QCD Lagrangian should have dimension $[\mathcal{L}] = \text{mass}^D$; so looking at the several terms in the Lagrangian one encounters $[\hat{G}_\mu] = \text{mass}^{(D-2)/2}$ and $[\hat{\psi}_q] = \text{mass}^{(D-1)/2}$ so that the interaction terms have a missing mass dimension of $(4-D)/2$, so one assigns the additional mass parameter to the coupling constant, redefining

$$g_s = g_s^0 \mu_0^\epsilon, \quad \epsilon = (4-D)/2, \quad (2.71)$$

where g_s^0 is kept dimensionless.

In a general subtraction scheme defined at a certain momentum scale μ_r , while regularizing in the same manner as before, the renormalization prescription $g_s = Z_g g_{s,r}$ yields

$$g_s = Z_g \left(g_{s,r}^R(\mu_r) \mu_0^\epsilon, \mu_r, m_r(\mu_r), \xi_r(\mu_r) \right) g_{s,r}^R(\mu_r) \mu_0^\epsilon \quad (2.72)$$

where the R indicates the "running" of the coupling, i.e. its dependence on the scale μ_r , while $g_{s,r}^R$ is dimensionless and $g_{s,r} = g_{s,r}^R \mu_0^\epsilon$. Actually the μ_0 dependence in the end will cancel out.

In the $\overline{\text{MS}}$ scheme, now the mass parameter from the regularization becomes the renormalization scale and might be varied to an arbitrary μ_r . Furthermore contrary to other schemes in the $\overline{\text{MS}}$ scheme the scaling factor of the coupling constant Z_g depends neither on the renormalized mass nor on the gauge nor explicit on the scale simplifying things a lot. So here we have

$$g_s = Z_g(g_{s,r}^R(\mu_r)) g_{s,r}^R(\mu_r) \mu_r^\epsilon \quad (2.73)$$

To the first order of non-zero correction one determines the scaling factor to be [9]

$$Z_g^{\overline{\text{MS}}} = 1 - \frac{(g_{s,r}^R)^2}{(4\pi)^2} \cdot \Delta \left(\frac{11}{2} - \frac{1}{3} n_f \right) + \mathcal{O}((g_{s,r}^R)^4). \quad (2.74)$$

where n_f is the number of quark flavors. Now it follows using $\frac{d}{d\mu_r} g_s = 0$

$$\begin{aligned} \mu_r \frac{d}{d\mu_r} g_{s,r}^R(\mu_r) &= \mu_r \frac{d}{d\mu_r} \frac{g_s \mu_r^{-\epsilon}}{Z_g} = -\epsilon \frac{g_s \mu_r^{-\epsilon}}{Z_g} - \mu_r \frac{g_s \mu_r^{-\epsilon}}{Z_g} \frac{d}{d\mu_r} Z_g \\ &= -\epsilon g_{s,r}^R(\mu_r) - \mu_r g_{s,r}^R(\mu_r) \frac{\partial Z_g}{\partial g_{s,r}^R} \frac{d}{d\mu_r} g_{s,r}^R(\mu_r) \\ &= -\epsilon g_{s,r}^R(\mu_r) + \frac{(g_{s,r}^R(\mu_r))^2}{(4\pi)^2} \Delta \left(11 - \frac{2}{3} n_f \right) \mu_r \frac{d}{d\mu_r} g_{s,r}^R(\mu_r) \\ \Rightarrow \mu_r \frac{d}{d\mu_r} g_{s,r}^R(\mu_r) &= -\frac{(g_{s,r}^R(\mu_r))^3}{(4\pi)^2} \left(11 - \frac{2}{3} n_f \right) + \mathcal{O}((g_{s,r}^R)^5, \epsilon). \end{aligned} \quad (2.75)$$

In a higher context, one refers to this equation as the *renormalization group equation* (RGE) of the strong coupling at leading order.

One may integrate this equation yielding

$$\alpha_s^R(\mu_r) = \frac{\alpha(\mu_{r,0})}{1 + \alpha(\mu_{r,0}) \frac{\beta_0}{2\pi} \ln \left(\frac{\mu_r}{\mu_{r,0}} \right)} \quad (2.76)$$

where we have defined $\alpha_s^R = (g_{s,r}^R)^2/(4\pi)$ and $\beta_0 = 11 - 2/3 \cdot n_f$ to achieve the more commonly used expression for the so-called *running* coupling constant. The denotation of the constant as β_0 occurs since one often refers to the left hand side of Eq. (2.75) as the *beta-function* of the strong coupling. Once the initial value of the coupling constant $\alpha_s(\mu_{r,0})$ has been determined by experiments one may choose yet another

scale μ_r at which to evaluate theoretical calculations. To ensure the validity of the perturbative approach and to reduce the effects of the scale parameter one will have to choose a proper value for the scale parameter when it comes to theoretical predictions for certain processes due to the involved $\ln(p^2/\mu_r^2)$ terms. In this way, the running coupling gains dependence on the physical scale of the process and becomes a sort of an effective coupling. The simplest method is to take a typical value of the momentum invariants of the considered process, for example a momentum transfer Q , assigning it to all orders of α_s^R involved in the calculation. To estimate the renormalization scale uncertainty, one varies the scale by multiplying/dividing by a factor of two. We will use this method throughout this work (for further reading on more sophisticated methods see for example [8]).

Now let us get to the properties of the running coupling itself.

Since at first sight Eq. (2.76) looks like the strong coupling may depend on two initial constants one often comes across another notation of the equation

$$\alpha_s^R(\mu_r) = \frac{2\pi}{\beta_0 \ln(\frac{\mu_r}{\Lambda_{QCD}})}, \quad \Lambda_{QCD} = \mu_{r,0} \exp\left(-\frac{2\pi}{\alpha_s(\mu_{r,0})\beta_0}\right) \quad (2.77)$$

defining the so-called *QCD scale parameter* Λ_{QCD} . As long as there are less than 16 quark flavors β_0 will be positive. So as the scale decreases Λ_{QCD} describes the value at which the running coupling becomes strong. Of course the given formula cannot describe the true behavior at low scales since the *beta*-function approximation will become invalid as the coupling grows large. Higher order corrections might reveal another zero of the derivative of the coupling constant (in addition to $g_s^R, r = 0$). Instead of blowing to infinity the strong coupling might evolve to a finite fixed point. Nevertheless the growing of the running coupling at low momentum scales or accordingly large distances constitutes the fact that no isolated quarks or gluons have been observed so far. Experiments typically estimate the value of Λ_{QCD} at a few 100 MeV.

On the opposite site now the running coupling decreases as the scale is growing ultimately tending to zero $\alpha_s^R(\mu_r) \xrightarrow{\mu_r \rightarrow \infty} 0$. This is the so-called *asymptotic freedom* property of QCD (or non-abelian gauge theories in general). So in the end this allows to describe strong interaction processes in the limit of high energy scales by a perturbative series in α_s^R . The property of asymptotic freedom has been confirmed up to an order of four loop corrections [10], where from now on we will use the term *loop* corrections to refer to Feynman diagrams with closed circles of internal lines.

The introduced perturbation theory has been found to become valid at about $\mu_r \approx 1 - 3 \text{ GeV}$ [11]. Besides Λ_{QCD} one commonly uses the value of $\alpha_s(\mu_{r,0})$ defined at a

reference scale which is chosen to be the mass of the weak Z -boson $\mu_{r,0} = M_Z$. Including higher corrections to the *beta*-function it has been determined by experiments to $\alpha_s(M_Z) \approx 0.1183$ (world average [12]).

Actually in our calculations we will include the next-to-leading order term in the expansion of the *beta*-function and thus for the running coupling the solution to

$$\mu \frac{d}{d\mu_r} \alpha_s^R(\mu_r) = -\frac{\beta_0}{4\pi} (\alpha_s^R)^2(\mu_r) - \frac{\beta_1}{16\pi^2} (\alpha_s^R)^3(\mu_r) \quad (2.78)$$

where now the second contribution has been found to be $\beta_1 = 102 - (38/3)n_f$.

One should mention that besides the μ_r dependence the predictions in general underlie another uncertainty. Although the leading and next-to-leading order of the *beta*-function turns out to be scheme independent this is not the case anymore in subsequent orders making the running coupling even renormalization scheme dependent.

Apart from all that it is worth mentioning that the running mass vanishes sufficiently fast in the limit of high scales so that it can be safely neglected as will be done in our calculations [9].

2.5. Infrared divergences

Until now, we skipped over the infrared divergence arising in the quark propagator self-energy which will contribute to a scattering cross section via the normalization factors \sqrt{Z} in the LSZ formula (Z being the residue of an external quark propagator). Furthermore, there will be a variety of infrared divergences from other diagrams, too. At first, we take a look at one of the simplest scattering processes involving strong interacting particles, the electron-positron annihilation into a quark anti-quark pair via a virtual photon (or neutral electroweak boson). We actually did not use the term *virtual* before which in Feynman diagram language refers to a particle propagating on internal lines so that its four-momentum squared is not bounded to the corresponding physical mass of that type of particle, one says it is off mass-shell.

Only considering QCD corrections at one loop order, the invariant matrix element squared will be represented by the following diagrams (note that the external propagators have been removed according to the LSZ formula but replaced by external lines

representing their spinor properties as defined in the Appendix A.1).

$$\begin{aligned}
 |\mathcal{M}|^2 = & \left(\begin{array}{c} e^- \\ \swarrow \\ \gamma, Z \\ \nwarrow \\ e^+ \end{array} \begin{array}{c} \nearrow \\ q \\ \nwarrow \\ \bar{q} \end{array} \right)^2 + \left(\begin{array}{c} e^- \\ \swarrow \\ \gamma, Z \\ \nwarrow \\ e^+ \end{array} \begin{array}{c} \nearrow \\ q \\ \nwarrow \\ \bar{q} \end{array} \right)^* \left(\begin{array}{c} e^- \\ \swarrow \\ \gamma, Z \\ \nwarrow \\ e^+ \end{array} \begin{array}{c} \nearrow \\ q \\ \nwarrow \\ \bar{q} \end{array} \begin{array}{c} \nearrow \\ g_s \\ \nwarrow \\ g_s \end{array} \right) \\
 & + \left(\begin{array}{c} e^- \\ \swarrow \\ \gamma, Z \\ \nwarrow \\ e^+ \end{array} \begin{array}{c} \nearrow \\ q \\ \nwarrow \\ \bar{q} \end{array} \right) \left(\begin{array}{c} e^- \\ \swarrow \\ \gamma, Z \\ \nwarrow \\ e^+ \end{array} \begin{array}{c} \nearrow \\ q \\ \nwarrow \\ \bar{q} \end{array} \begin{array}{c} \nearrow \\ g_s \\ \nwarrow \\ g_s \end{array} \right)^* + 2\alpha_s z_1 \left(\begin{array}{c} e^- \\ \swarrow \\ \gamma, Z \\ \nwarrow \\ e^+ \end{array} \begin{array}{c} \nearrow \\ q \\ \nwarrow \\ \bar{q} \end{array} \right)^2
 \end{aligned}$$

where the leading order diagrams have to be interfered with the loop corrected ones to obtain a result at fixed order ($\alpha^2\alpha_s$). Here \sqrt{Z} (corresponding to the quarks) has been expanded as $\sqrt{Z} \approx 1 + \alpha_s z_1 + \dots$.

Now due to the incorporated infrared singularities from the one loop corrections this quantity will diverge (although there are some cancellations between them).

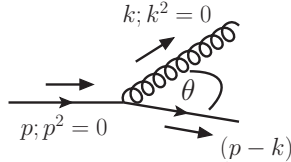
But one can argue that this process will be indistinguishable from a process where a quark in the final state emits a gluon in the limit of vanishing (or below some experimental cut) gluon-energy. The corresponding diagrammatic contributions

$$\begin{aligned}
 & \left(\begin{array}{c} e^- \\ \swarrow \\ \gamma, Z \\ \nwarrow \\ e^+ \end{array} \begin{array}{c} \nearrow \\ q \\ \nwarrow \\ \bar{q} \end{array} \begin{array}{c} \nearrow \\ g_s \\ \nwarrow \\ g_s \end{array} \right)^2 + \left(\begin{array}{c} e^- \\ \swarrow \\ \gamma, Z \\ \nwarrow \\ e^+ \end{array} \begin{array}{c} \nearrow \\ q \\ \nwarrow \\ \bar{q} \end{array} \begin{array}{c} \nearrow \\ g_s \\ \nwarrow \\ g_s \end{array} \right)^* \left(\begin{array}{c} e^- \\ \swarrow \\ \gamma, Z \\ \nwarrow \\ e^+ \end{array} \begin{array}{c} \nearrow \\ q \\ \nwarrow \\ \bar{q} \end{array} \begin{array}{c} \nearrow \\ g_s \\ \nwarrow \\ g_s \end{array} \right) \\
 & + \left(\begin{array}{c} e^- \\ \swarrow \\ \gamma, Z \\ \nwarrow \\ e^+ \end{array} \begin{array}{c} \nearrow \\ q \\ \nwarrow \\ \bar{q} \end{array} \begin{array}{c} \nearrow \\ g_s \\ \nwarrow \\ g_s \end{array} \right) \left(\begin{array}{c} e^- \\ \swarrow \\ \gamma, Z \\ \nwarrow \\ e^+ \end{array} \begin{array}{c} \nearrow \\ q \\ \nwarrow \\ \bar{q} \end{array} \begin{array}{c} \nearrow \\ g_s \\ \nwarrow \\ g_s \end{array} \right)^* + \left(\begin{array}{c} e^- \\ \swarrow \\ \gamma, Z \\ \nwarrow \\ e^+ \end{array} \begin{array}{c} \nearrow \\ q \\ \nwarrow \\ \bar{q} \end{array} \begin{array}{c} \nearrow \\ g_s \\ \nwarrow \\ g_s \end{array} \right)^2
 \end{aligned}$$

are indeed of the same order as the virtual loop correction diagrams.

The phase space integral of the emitted gluon will yet lead to another divergence in the limit of vanishing energy of the gluon. As it turns out the arising singularities cancel exactly against the residual divergences of the virtual corrections so that the scattering cross section becomes finite if one incorporates this phase space contribution and sums over all left indistinguishable final states (color and polarization of the emitted gluon). To one loop order this follows from the *Bloch-Nordsieck* [13] theorem known from Quantum Electro-Dynamics (QED). In QED, this statement holds in every order of perturbation theory. In a physical scenario (for now ignoring confinement), the cross section will then depend on the energy cut-off value as long as no full inclusive cross section (i.e $e^-e^+ \rightarrow q\bar{q}X$) where the full (only constrained by the momentum conserving delta function) gluon phase space is taken into account then is considered. However, in QCD the situation might change in higher orders due to the gluon self-couplings and

a new type of divergence. The same type of divergence arises in the limit of massless quarks, what we are going to consider in our calculations. Picture the emission of a gluon from an external massless quark :



Expanding the denominator of the propagator yields ($p^2 = 0, k^2 = 0$)

$$(p - k)^2 = -2p \cdot k = -2p^0 k^0 + 2|\mathbf{p}||\mathbf{k}| \cos(\theta) = -2p^0 k^0 (1 - \cos(\theta)). \quad (2.79)$$

where θ denotes the angle between the (three-)momenta of the emitted particle and the emitting particle. This expression vanishes if the four-momentum of the emitted gluon becomes zero ($k \rightarrow 0$) giving rise to a so-called *soft* singularity (after the phase space integration is performed in the corresponding region) which also appears in QED when a photon becomes soft. As its name implies, the new type of divergence, the so-called *collinear divergence*, shows up when the (three-)momentum of the emitted gluon becomes parallel to the momentum of the emitting quark ($\theta \rightarrow 0$). Since this divergence is avoided by a non-zero mass one also refers to it as a *mass singularity*. Both singularities are logarithmic. Furthermore there will be an overlap of both types eventually giving rise to a double logarithmic divergence. If instead a gluon splits into an quark anti-quark pair the soft divergence gets canceled.

Now generally it depends on the gauge in which diagram singularities arise. We will deal with the situation of Feynman gauge. Note that there appears in general no divergence when an external particle is attached to two internal lines since in general the virtual particles have non-zero invariant mass. Now regularizing potential divergences via dimensional regularization Fig. 2.4 summarizes the arising divergences from real emissions and virtual corrections in next-to-leading-order QCD.

Following the *Bloch-Nordsieck* approach one will now have to take into account the collinear emissions of gluons from quarks yet at one loop order (being not able to resolve collinear final state particles). As can be shown from another theorem, the *Kinoshita-Poggio-Quinn* theorem, the total (summing/averaging over all final/initial color and helicity states and carrying out the final state momentum phase space) inclusive electron-positron annihilation cross section remains finite up to all orders even

Real corrections	Virtual corrections	Singularity
		$1/\epsilon, 1/\epsilon^2$
		$1/\epsilon$
		$1/\epsilon, 1/\epsilon^2$
		$1/\epsilon$
		$1/\epsilon, 1/\epsilon^2$
		$1/\epsilon, 1/\epsilon^2$
		$1/\epsilon$

Figure 2.4.: Real emission and virtual correction contributions within NLO QCD giving rise to singularities (in Feynman gauge). One may identify the grey blob with a leading order process. It is distinguished into initial state (top) and final state situations (bottom). The self energy corrections again enter via the LSZ formula. This figure/table has been taken from (slightly modified) [14].

in QCD.

Considering the process in reverse, i.e $q\bar{q} \rightarrow e^-e^+$ the world looks different.

Taking into account all indistinguishable final states will not yield a finite result. For

example, we now have to distinguish between collinear divergences that are soft and those which are semi-hard. This is because the gluon is now emitted from an initial state quark, so that in the case of a non-soft but collinear gluon, the process will be distinguishable from the two-to-two particle process. Making the different types of divergences explicit, for example through an momentum and angular cutoff, it turns out that all soft (including overlapping divergences) still cancel out at one loop order in the total cross section so that only purely collinear terms survive.

Actually, this has been shown to become untrue at two-loop level (see [15]).

Furthermore, it is important to note that also when carrying out the full phase space integration the result still suffers collinear divergences. In order to get a finite result one has to take into account contributions from soft and collinear initial states.

This is the statement of the so-called *Kinoshita-Lee-Nauenberg* theorem [16]. It states that the power series expansion of a transition probability is infrared (soft and collinear) finite if one sums over all degenerate (same energy eigenvalues) initial and final states. Unfortunately, there may arise the necessity of the inclusion of disconnected diagrams which then leads to an infinite series of diagrams at every order of perturbation theory. However, when it comes to an application of these elementary particle scatterings within the framework of hadron collisions one deals with these problems in another way, one subtracts the remaining divergences into a quantity from a non-perturbative region as we will see in the next chapter.

From partons to hadrons - the process of interest

3.1. The parton model

Quarks and gluons are not observed as isolated particles, once a quark anti-quark pair may be created both particles will end up on a timescale roughly about $\sim 1/\Lambda_{QCD} \approx \mathcal{O}(1 \cdot 10^{-24})$ s within color singlet bound states i.e. hadrons. Our perturbative treatment is restricted to interactions among free quarks and gluons in the limit of high momentum transfers/short distances.

Consider the parton model suggested by Feynman.

The parton model states that a proton consists of the three quantum number giving valence quarks uud and an unknown bunch of quark anti-quark pairs and gluons. As mentioned earlier one refers to all constituents collectively as partons.

Picture a proton-proton collision in the center-of-mass frame in the limit of high center-of-mass energy: Both protons see each other relativistically contracted to flat discs. Furthermore the lifetime of the partonic virtual state of the protons in their rest frames becomes large in the center-of-mass frame. Thus, the interaction takes place on a timescale where the partons are approximately "frozen" in a specific configuration. There will be a specific probability for each parton to carry a certain momentum fraction of the whole proton. Interchanging a high momentum the virtual particle carrying it can only cover a short distance. If the partons are randomly spread over the protons sphere and their density is not too high we then may describe the interaction between the two protons perturbatively as a hard scattering between effectively free partons one from each proton, respectively. The subsequent interactions of eventual strong final state particles of the hard parton scattering and the proton remnants will also be considered to take place on a longer time scale.

Let us move on to our concrete process of interest: the inclusive single weak vector boson production in proton-proton collisions $p + p \rightarrow V + X$ where X may be any

hadronic final state and V can be either a Z or a W boson. The scattering process is schematically illustrated in Fig. 3.1.

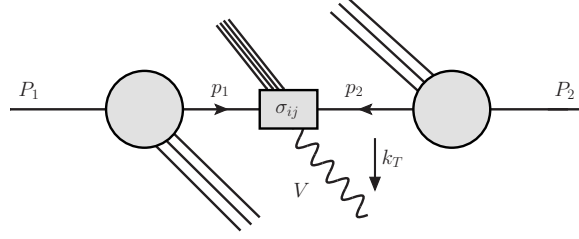


Figure 3.1.: Schematic illustration of a proton-proton collision resulting in the production of a weak boson V .

We will consider the cross section differential in the transverse momentum (with respect to the collision axis) of the weak boson denoted by k_T .

According to the above described parton model, the inclusive differential cross section at leading order in QCD ($\alpha_s \alpha_w$) factorizes into (up to higher inverse powers of the hard scattering momentum transfer)

$$\frac{d\sigma_{pp \rightarrow V X}}{dk_T^2 dy}(P_1, P_2, \mu_r) = \sum_{i,j} \int dx_1 \int dx_2 f_{i/A}(x_1) \frac{sd\sigma_{ij}^{(1)}}{dt du}(p_1, p_2, \mu_r) f_{j/B}(x_2) \quad (3.1)$$

where $f_{i/A}(x_1)$ and $f_{j/B}(x_2)$ are the so-called *parton-distribution-functions* (PDFs) giving the probability of finding a parton of type i, j inside the respective proton A, B carrying a longitudinal momentum fraction $x_1, x_2 \in [0, 1]$ of the parent proton.

Representing the nature of the hadronic proton state these are non-perturbative functions which should be process independent and have to be determined from experiments. We will go into some more detail in section 4. The other piece in Eq. (3.1), $sd\sigma_{ij}^{(1)}/dt/du$, is the perturbative calculable partonic differential cross section for each contributing configuration of initial partons i, j which we sum over incoherently (the (1) indicates the order in α_s).

We neglect all contributions from top quark channels and assume all quarks of the left five flavors to be massless, even more we treat the whole proton state as massless in the high energy limit.

In the above formula P_1 and P_2 are the momenta of the incoming protons and $p_1 = x_1 P_1$ and $p_2 = x_2 P_2$ the ones of the partons entering the hard (high momentum transfer) partonic scattering process. Furthermore, we defined the so-called Mandelstam variables

as

$$s = (p_1 + p_2)^2, \quad t = (p_1 - k_1)^2, \quad u = (p_2 - k_1)^2 \quad (3.2)$$

where k_1 is the momentum of the outgoing weak vector boson with mass $k_1^2 = m_V^2$. Furthermore we have $\sqrt{\mathbf{k}_{1T}^2} \equiv k_T = ut/s$.

The rapidity y of the weak boson in the center of mass frame of the colliding protons is given by

$$y = \frac{1}{2} \ln \frac{E_V + k_L}{E_V - k_L} \quad (3.3)$$

where $E_V = k^0$ is the energy of the weak vector boson and k_L its longitudinal momentum along the collision axis in that frame.

At leading order, only two typological different partonic subprocesses, quark anti-quark $q\bar{q}(\bar{q}') \rightarrow Z(W)g$ and quark gluon scattering $qg \rightarrow Z(W)q(q')$, contribute. One has to distinguish between the case of the neutral Z boson and the flavor changing charged $W^{+/-}$ bosons. In the latter case, the participating quarks have to be of different flavor in accord with the weak isospin doublets as described in section 2.2. In the case of W bosons, we sum over W^+ and W^- contributions. Each subprocess is represented by two Feynman diagrams, illustrated in Fig. 3.2. With respect to the subsequent orders

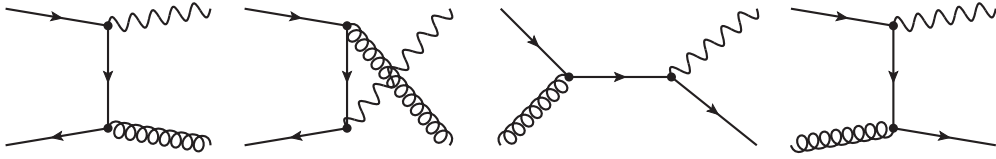


Figure 3.2.: *Feynman*-diagrams for the leading order QCD subprocesses of weak vector boson production, i.e. $q\bar{q}(\bar{q}') \rightarrow Z(W)g$ and $qg \rightarrow Z(W)q(q')$.

one has to compute the first order result in $d = 4 - 2\epsilon$ yet although it is finite in the limit of vanishing ϵ . We actually will deal with the production of real or more precisely stable weak bosons and avoid the subtleties arising in calculations due to their finite width.

For the interested reader who has not yet derived transition probabilities via the Feynman rules by himself the calculation of the leading order contributions to the partonic cross sections is shown in Appendix A.3 (for the case of a W boson).

Note that already the leading order cross section obeys a divergence in the limit $k_T \rightarrow 0$. As long as perturbation theory comes on its own we do not consider low values of k_T but are interested in the k_T dependence where perturbation theory becomes valid. The contributions from the zeroth order ($q\bar{q}(\bar{q}') \rightarrow Z(W)$) which arise approximately only at $s = m_V^2$ and $k_T = 0$ have therefore been neglected. In the case we are interested in

the low k_T regime we will use a resummation technique which will be treated in section 3.3.

3.2. Vector boson production in second order QCD

At next-to-leading order in QCD (we do not consider any corrections from weak or electromagnetic interactions) new production channels become possible and one has to consider a variety of diagrams. The new subprocesses are $q\bar{q}'(\bar{q}) \rightarrow Z(W)q\bar{q}'(\bar{q})$, $qq(q') \rightarrow Z(W)qq(q')$, $q\bar{q}' \rightarrow Zq\bar{q}'$, $gg \rightarrow Z(W)q\bar{q}(\bar{q}')$, the leading order channels will be extended by a final state gluon. The diagrams for virtual corrections are depicted in Fig. 3.3 and have to be interfered with the leading order diagrams as described in section 2.5. As can be seen from the LSZ formula (Eq. (2.54)) since it only distinguishes final and initial states by the sign of the Fourier-transform momentum the matrix element with a particle of (three-)momentum \mathbf{p} in the initial state can be gained from the one with an anti-particle with momentum $-\mathbf{p}$ in the final state by analytical continuation. One refers to this relation as crossing symmetry.

All possible quark gluon scattering diagrams are simply related by crossing to the ones for quark anti-quark scattering, so we only present the latter case. For all contribu-

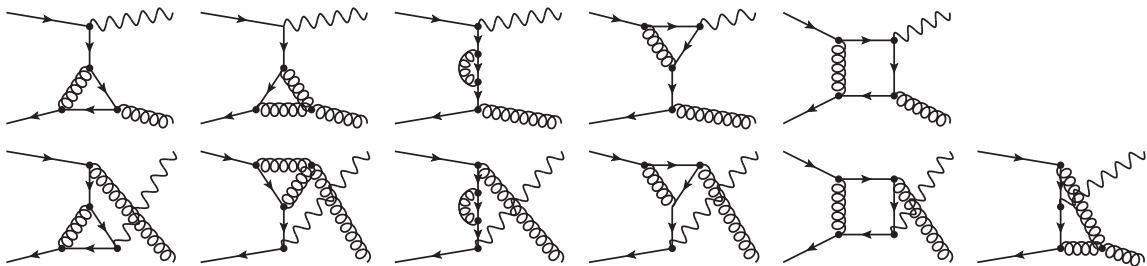


Figure 3.3.: *Feynman*-diagrams for the virtual corrections in second order QCD to the subprocess $q\bar{q}(\bar{q}') \rightarrow Z(W)g$.

tions from squared and interfered diagrams involving gluon loops one has to subtract the contributions from the corresponding diagrams with all possible ghost loops (not shown).

For the real emission correction diagrams we only show a certain set at this point as will be discussed in a moment. To carry out the calculation of the second order contributions here is beyond the scope of this thesis. Furthermore it has been performed a long time ago and the full results can be found in [17],[18]. Nowadays there are several software packages allowing to reproduce the analytical results quite fast (for example FeynArts [19] + FormCalc [20] + FeynCalc [21] + LoopTools [22]). However no very

illuminating insight is gained by presenting lengthy analytic expressions here. As indicated, in section 2.5 the soft divergences (including overlaps) cancel out completely between virtual corrections and real emissions but some of the purely collinear divergences survive. As it turns out, one can attribute the latter ones to initial state singularities. The uncanceled collinear divergences arising from initial state emissions show up in diagrams illustrated in Fig. 3.4.

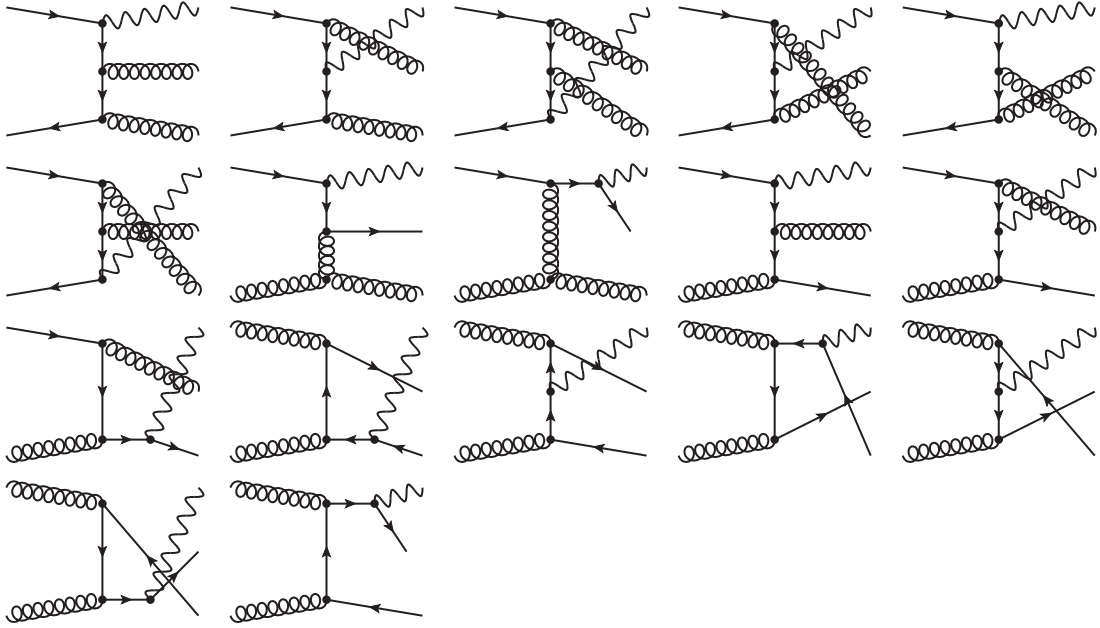


Figure 3.4.: *Feynman*-diagrams for the second order QCD subprocesses of weak vector boson production giving rise to uncanceled collinear divergences from initial state emissions.

We take a closer look at an example shown in Fig. 3.5. One may argue that in the

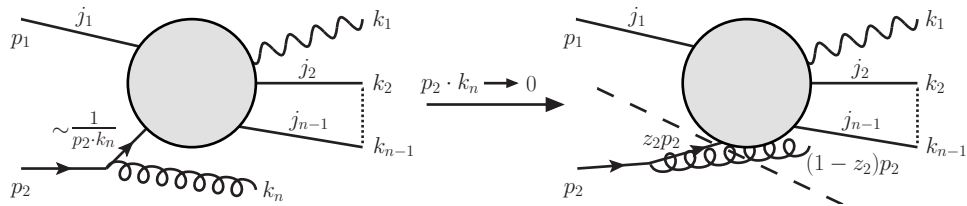


Figure 3.5.: Illustration of an hard scattering process with initial state emission in the collinear limit. The straight lines represent any valid configuration of partons j_1, \dots, j_n . In the considered limit the quasi-real quark entering the hard scattering process carries the longitudinal momentum fraction z_2 of its parent quark. The dashed line indicates the splitting of the corresponding squared matrix element.

limit where the mass of the intermediate propagator vanishes ($p_2 \cdot k_n \rightarrow 0$ in Fig. 3.5) and the virtual particle becomes quasi-real the propagation time of that particle becomes that large that in some sense the splitting into two particles decouples from the hard scattering process and has to be assigned to the long-distance part, i.e. the proton structure.

Indeed, it can be shown that independent of the subsequent hard scattering process in Fig. 3.5 it is possible to factorize the matrix element in the collinear limit, so that one schematically has

$$|\mathcal{M}|_{j_1 q \rightarrow W/Z j_2 \dots j_n g}^2(p_1, p_2) \xrightarrow{p_2 \cdot k_n \rightarrow 0} g_{q \rightarrow qg}(p_2, k_n, z_2) |\mathcal{M}|_{j_1 q \rightarrow W/Z j_2 \dots j_n}^2(p_1, z_2 p_2) \quad (3.4)$$

where z_2 is the longitudinal fraction of the momentum p_2 .

Consider for example the averaged/summed matrix element squared of the first two diagrams (top row left) of Fig. 3.4 which we denote with C_1 and C_2 , so we consider $|\overline{C_1 + C_2}|^2$. Considering the region of the three particle phase space (defined in Eq. 2.58) where $p_2 \cdot k_3$ (denotation according to Fig. 3.5) vanishes in the collinear limit, performing the integration via dimensional regularization one can deduce

$$d\sigma_{C_1+C_2}^{p_2 \cdot k_3 \rightarrow 0}(p_1, p_2) \rightarrow \int_0^1 dz_2 \frac{\alpha_s}{2\pi} P_{\bar{q} \leftarrow \bar{q}}(z_2) \left(\Delta_{IR} - \ln \frac{\mu_r^2}{m_V^2} + \text{finite terms} \right) d\sigma_{q\bar{q}}^{(1)}(p_1, z_2 p_2) \quad (3.5)$$

where the coefficient of the collinear singularity

$$P_{\bar{q} \leftarrow \bar{q}}(z) = P_{q \leftarrow q}(z) = \frac{4}{3} \left(\frac{1+z^2}{(1-z)_+} + \frac{3}{2} \delta(1-z) \right) \quad (3.6)$$

is known as one of the *Altarelli-Parisi splitting functions* at leading order [23]. Actually, the expression here has yet been adjusted to take care of the overlapping region with the soft divergence, since this part will cancel against virtual corrections. Therefore, one defines a so-called plus-distribution by

$$\int_0^1 \frac{f(z)}{(1-z)_+} = \int_0^1 \frac{f(z) - f(1)}{(1-z)} \quad (3.7)$$

where $f(z)$ is any smooth function with regular boundaries.

One can find similar expressions for all the possible splittings shown in the left column of the table in Fig. 2.4. The corresponding coefficients of the divergences are given by

the other lowest order *Altarelli-Parisi splitting functions*:

$$P_{q \leftarrow g}(z) = \frac{1}{2} (z^2 + (1-z)^2) \quad (3.8)$$

$$P_{g \leftarrow q}(z) = \frac{4}{3} \left(\frac{1 + (1-z)^2}{z} \right) \quad (3.9)$$

$$P_{g \leftarrow g}(z) = 6 \left(\frac{1-z}{z} + \frac{z}{(1-z)_+} + z(1-z) \right) + \left(\frac{11}{2} - \frac{n_f}{3} \right) \delta(1-z). \quad (3.10)$$

Remember in our case we have $n_f=5$. One may interpret the functions as the probability for finding a certain parton with longitudinal momentum fraction z inside another parton.

Now as it turns out, it is possible to factor out all residual collinear singularities (there are also some from the propagator corrections of the initial states) from the partonic cross section allowing to do the following. One introduces a factorization scale parameter μ_f to separate the perturbative from the non-perturbative regime and subtracts the divergences into the PDFs defining in a similar fashion to the UV renormalized quantities an observable parton-distribution-function $\tilde{f}_{i/A}(x, \mu_f)$ in terms of the bare PDFs [18]

$$\tilde{f}_{i/A}(x, \mu_f) = \sum_j \int_x^1 \frac{dz}{z} \left(\delta_{ij} \delta(1-z) + \frac{\alpha_s}{2\pi} R_{i \leftarrow j}(z, \mu_f^2) \right) f_{i/A}\left(\frac{x}{z}\right) \quad (3.11)$$

where we have defined

$$R_{i \leftarrow j}(z, \mu_f^2) = P_{i \leftarrow j}(z) \left(\Delta_{IR} - \ln \frac{\mu_r^2}{\mu_f^2} \right) + C_{i \leftarrow j}^{f.s.}(z). \quad (3.12)$$

At lowest order, both PDFs agree since there is no splitting of partons into partons. The additional term $C_{i \leftarrow j}^{f.s.}(z)$ denotes the finite part which one likes to remove in addition dependent on the chosen factorization scheme, we will apply the $\overline{\text{MS}}$ factorization with $C_{i \leftarrow j}^{\overline{\text{MS}}}(z) \equiv 0$.

Accordingly, one now has a renormalized partonic cross section

$$\begin{aligned} \frac{sd\tilde{\sigma}_{ij}}{dtdu}(p_1, p_2, \mu_r) &= \frac{sd\sigma_{ij}^{(1)}}{dtdu}(p_1, p_2, \mu_r) + \frac{sd\sigma_{ij}^{(2)}}{dtdu}(p_1, p_2, \mu_r) \\ &\quad - \frac{\alpha_s}{2\pi} \sum_k \int_0^1 dz_1 R_{k \leftarrow i}(z_1, \mu_f^2) \frac{sd\sigma_{kj}^{(1)}}{dtdu}(z_1 p_1, p_2, \mu_r) \\ &\quad - \frac{\alpha_s}{2\pi} \sum_k \int_0^1 dz_2 R_{k \leftarrow j}(z_2, \mu_f^2) \frac{sd\sigma_{ik}^{(1)}}{dtdu}(p_1, z_2 p_2, \mu_r). \end{aligned} \quad (3.13)$$

Here $\frac{sd\sigma_{ij}^{(2)}}{dtdu}$ incorporates all second order QCD contributions from virtual corrections and real emissions. This expression will now yield a finite result.

The factorization of the residual singularities has been shown for a series of other processes such as DIS, so that the definition of the observable PDFs applies to all of them allowing to compare between theory and experiment in order to use the PDFs to predict results for future experiments.

For further details on factorization of short and long distance parts in general see for example [24].

As one can see the cross section will besides the renormalization scale now additionally depend on the factorization scale. As most often done, we will set $\mu_r = \mu_f$ in our calculations. Although the PDFs themselves are not calculable within perturbative QCD their evolution to higher scales is. Similar to the case of the running coupling one can derive evolution equations for the observable PDFs by imposing the independence of the scattering cross section on the factorization scale, the so-called Dokshitzer-Gribov-Lipatov-Altarelli-Parisi (DGLAP) [23] equations. At leading order this set of coupled evolution equations reads

$$\begin{aligned} \mu \frac{d}{d\mu} \tilde{f}_{g/H}(x, \mu) &= \frac{\alpha_s(\mu)}{2\pi} \int_x^1 \frac{dz}{z} \left(P_{g \leftarrow q}(z) \sum_f \left(\tilde{f}_{q_f/H} \left(\frac{x}{z}, \mu \right) + \tilde{f}_{\bar{q}_f/H} \left(\frac{x}{z}, \mu \right) \right) \right. \\ &\quad \left. + P_{g \leftarrow g}(z) \tilde{f}_{g/H} \left(\frac{x}{z}, \mu \right) \right), \end{aligned} \quad (3.14)$$

$$\mu \frac{d}{d\mu} \tilde{f}_{q_f/H}(x, \mu) = \frac{\alpha_s(\mu)}{2\pi} \int_x^1 \frac{dz}{z} \left(P_{q \leftarrow q}(z) \tilde{f}_{q_f/H} \left(\frac{x}{z}, \mu \right) + P_{q \leftarrow g}(z) \tilde{f}_{g/H} \left(\frac{x}{z}, \mu \right) \right), \quad (3.15)$$

$$\mu \frac{d}{d\mu} \tilde{f}_{\bar{q}_f/H}(x, \mu) = \frac{\alpha_s(\mu)}{2\pi} \int_x^1 \frac{dz}{z} \left(P_{q \leftarrow q}(z) \tilde{f}_{\bar{q}_f/H} \left(\frac{x}{z}, \mu \right) + P_{q \leftarrow g}(z) \tilde{f}_{g/H} \left(\frac{x}{z}, \mu \right) \right) \quad (3.16)$$

where H denotes the type of hadron and f the quark flavor. In higher orders also a splitting of quarks into antiquarks or quarks of different flavor will become possible through subsequent gluon splittings. Then the splitting functions will also gain a μ dependence through $\alpha_s(\mu)$ when expanded to higher orders.

A somewhat more physical approach to derive these equations leads to the interpretation of a growing resolution of more and more partons inside the proton at higher momentum scales.

After all other singularities have been made manifest and canceled one can perform the phase space integration and the convolution of the finite partonic cross section with the PDFs determined from experiments numerically and hence derive the results for the hadronic scattering process which are shown in chapter 5. One should note that there are several subtleties to cancel the singularities properly so that the phase space can be integrated numerically, see [18] for further details.

3.3. CSS resummation formula ¹

While the transverse momentum k_T is of the order of its invariant mass, the calculations of the last section are reliable. But although all infrared poles got canceled the finite remains of the soft and collinear, real and virtual corrections lead to large logarithmic contributions which spoil the perturbative approach. The perturbative series in the region $k_T^2 \ll M_V^2$ is dominated by the following contributions

$$\frac{d\sigma_{pp \rightarrow VX}}{dk_T^2 dy} \sim \frac{\alpha_w \alpha_s}{k_T^2} \ln \left(\frac{M_V^2}{k_T^2} \right) \left(c_1 + c_2 \alpha_s \ln^2 \left(\frac{M_V^2}{k_T^2} \right) + c_3 \alpha_s^2 \ln^4 \left(\frac{M_V^2}{k_T^2} \right) + \dots \right) \quad (3.17)$$

This series is the so-called leading-logarithm approximation. Now at sufficiently low k_T the perturbative series will be effectively an expansion in $\alpha_s \ln^2(M_V^2/k_T^2)$ rather than simply in α_s . The double logarithms correspond to virtual or real corrections from the overlapping region where they are both, soft and collinear.

The overall factor of $1/k_T^2$ comes from the first order contribution which yet diverges in the limit $k_T^2 \rightarrow 0$ as stated in section 3.1. The divergence can be canceled by including the virtual corrections to the zeroth order or formally introducing a negative delta function singularity at the origin.

Fortunately the coefficients c_i of the above series are not independent but can be expressed in terms of c_1 such that it is possible to sum the series exactly yielding an

¹This section closely follows [25] and section 3.2 of [26].

exponential factor.

Technically it is even possible to resum all terms that are at least singular as $1/k_T^2$ as $k_T \rightarrow 0$ which are

$$\frac{d\sigma_{pp \rightarrow VX}}{dk_T^2 dy} \sim \frac{\alpha_w}{k_T^2} \sum_{n=1}^{\infty} \sum_{m=0}^{2n-1} n c_m \alpha_s^n \ln^m \left(\frac{M_V^2}{k_T^2} \right). \quad (3.18)$$

Now to achieve a resummation of all these terms one follows the ideas of renormalization theory. Consider a general quantity $R(M^2, m^2)$ obeying an infrared sensitivity where the scale m^2 measures the distance from the critical region and M^2 represents a hard scale. Then the idea is to show that R can be factorized in the limit $m^2 \ll M^2$ into

$$R(M^2, m^2) = H \left(\frac{M^2}{\mu^2} \right) S \left(\frac{m^2}{\mu^2} \right) \quad (3.19)$$

involving a factorization scale μ . In general it is not quite easy to find such a factorization and it might even be necessary to switch from the original momentum space to a conjugate space (in our case this would be from transverse momentum to transverse position space, i.e. impact parameter space) to perform the factorization.

Although introducing new potentially large ratios, these can be handled using the independence of R on μ . Acting with $\mu d/d\mu$ on R one obtains

$$\frac{d \ln H}{d \ln \mu^2} = \gamma_S(\mu^2) = - \frac{d \ln S}{d \ln \mu^2}. \quad (3.20)$$

With reference to renormalization group theory the gained coefficient function $\gamma_S(\mu^2)$ is called anomalous dimension.

Solving the evolution equations for S , and H yields

$$H \left(\frac{M^2}{\mu^2} \right) = H(1) \exp \left[- \int_{\mu^2}^{M^2} \frac{d\lambda^2}{\lambda^2} \gamma_S(\lambda^2) \right] \quad (3.21)$$

and

$$S \left(\frac{m^2}{\mu^2} \right) = S(1) \exp \left[- \int_{m^2}^{\mu^2} \frac{d\lambda^2}{\lambda^2} \gamma_S(\lambda^2) \right]. \quad (3.22)$$

Inserting both results in equation 3.19 we obtain

$$R(M^2, m^2) = H(1) S(1) \exp \left[- \int_{m^2}^{M^2} \frac{d\lambda^2}{\lambda^2} \gamma_S(\lambda^2) \right]. \quad (3.23)$$

As one can see H and S do not depend on any large ratios any more but all scale dependence on M^2 and m^2 has been moved into the exponential function to which one often refers as the Sudakov form factor. So both functions can be determined by perturbation theory and large logarithms are resummed into the exponential factor. Also the anomalous dimension can be calculated as a series in α_s .

Now Collins, Soper and Sterman (CSS) found a similar (re-)factorized (to distinguish in this case from the former achieved factorization) expression obeying evolution equations for the differential cross section in back-to-back hadron jet production in electron-positron annihilation [27]. Short after it they applied their procedure to the case of Drell-Yan pair- (virtual photon-) ($pp \rightarrow \gamma^* X \rightarrow l^+ l^- X$) and W/Z-production [28]. The actual derivation is quite expensive so just the result will be presented. The resummed expression (only terms at least singular as $1/k_T^2$ as $k_T \rightarrow 0$ have been included) reads

$$\begin{aligned} \frac{d\sigma_{pp \rightarrow VX}}{dk_T^2 dy}(\text{resum}) &= \frac{4\pi^3 \alpha_w}{3S} \int \frac{d^2 b}{(2\pi)^2} e^{i\mathbf{b} \cdot \mathbf{k}_T} \sum_{k,l} e_{kl}^2 W_{kl}(b, M_V, x_1, x_2), \\ W_{kl}(b, M_V, x_1, x_2) &= \exp \left[- \int_{C_1^2/b^2}^{C_2^2 M_V^2} \frac{d\lambda^2}{\lambda^2} \left(\ln \left(\frac{C_2^2 M_V^2}{\lambda^2} \right) A(\alpha_s(\lambda^2)) + B(\alpha_s(\lambda^2)) \right) \right] \\ &\quad \times \sum_i \int_{x_1}^1 \frac{dz_1}{z_1} C_{k \leftarrow i} \left(\frac{x_1}{z_1}, \alpha_s(C_3/b) \right) f_{i/A}(x_1, \alpha_s(C_3/b)) \\ &\quad \times \sum_j \int_{x_1}^1 \frac{dz_2}{z_2} C_{l \leftarrow j} \left(\frac{x_2}{z_2}, \alpha_s(C_3/b) \right) f_{j/B}(x_2, \alpha_s(C_3/b)) . \quad (3.24) \end{aligned}$$

The indices i and j are the initial parton flavors and k, l the once entering the Z/W vertex, so that e_{kl} adjusts the coupling respectively. The values at which the PDFs are evaluated are the dominant values at low k_T given by $x_1 = e^{+y} M_V / \sqrt{S}$ and $x_2 = e^{-y} M_V / \sqrt{S}$ where \sqrt{S} is the center of mass energy of the colliding protons.

Furthermore, b is the conjugate to k_T and thus the transverse position or the impact parameter. The parameters C_1 , C_2 and C_3 are arbitrary and unphysical and will be chosen to $C_1 = C_3 = 2e^{-\gamma_E} \equiv b_0$ and $C_2 = 1$. The functions $A(\alpha_s)$, $B(\alpha_s)$ and $C(x, \alpha_s)$

have perturbative expansions in α_s :

$$A(\alpha_s) = \sum_{n=1}^{\infty} A^{(n)} \left(\frac{\alpha_s}{2\pi} \right)^n, \quad B(\alpha_s) = \sum_{n=1}^{\infty} B^{(n)} \left(\frac{\alpha_s}{2\pi} \right)^n$$

and

$$C(x, \alpha_s) = \delta(1-x) \sum_{n=1}^{\infty} C^{(n)}(x) \left(\frac{\alpha_s}{2\pi} \right)^n \quad (3.25)$$

where the coefficients of the series depend implicitly on the parameters C_i .

Now truncating the series at $A^{(n)}$, $B^{(n)}$ and $C^{(n-1)}$ corresponds to the following expansion (suppressing the coefficients of the logarithms)

$$\frac{d\sigma_{pp \rightarrow VX}}{dk_T^2 dy} \sim \frac{\alpha_w}{k_T^2} (\alpha_s Z_1 + \alpha_s^2 Z_2 + \dots + \alpha_s^n Z_n + h.c.) \quad (3.26)$$

where

$$\begin{aligned} \alpha_s Z_1 &\sim \alpha_s (L+1) + \alpha_s^2 (L^3 + L^2) + \alpha_s^3 (L^5 + L^4) + \dots \\ \alpha_s^2 Z_2 &\sim \alpha_s^2 (L+1) + \alpha_s^3 (L^3 + L^2) + \dots \\ \alpha_s^n Z_n &\sim \alpha_s^n (L+1) + \dots \end{aligned} \quad (3.27)$$

with $L = \ln(M_V^2/k_T^2)$. Each term of the series expansion now is smaller by α_s rather than $\alpha_s L^2$ so that one effectively has reorganized the former expansion (3.18) into a perturbation series in α_s again. The coefficients $A^{(n)}$, $B^{(n)}$ and $C^{(n-1)}$ may be determined by comparison with the original fixed-order perturbation result. We will truncate the series at $n = 2$ which corresponds to the next-to-leading order term in (3.26). One refers to it as the next-to-leading logarithmic (NLL) accuracy.

The relevant coefficients can be found in [25].

When the impact parameter becomes of the order $b \gtrsim 1/\Lambda_{QCD}$ the resummed expression itself becomes unreliable (or even ill-defined since the running coupling in NLO obeys a pole at $\mu = \Lambda_{QCD}$) and non-perturbative effects have to be taken into account. CSS suggested the introduction of an non-perturbative (np) function so that

$$W_{kl}(b) = W_{kl}^{per}(b_*) W_{kl}^{np}(b) \quad (3.28)$$

where

$$b_* = \frac{b}{\sqrt{1 + (b/b_{max})^2}}. \quad (3.29)$$

In this way $W_{kl}^{per}(b_*)$ can be safely evaluated for all values of b since b_* never goes beyond b_{max} . CSS deduced via a renormalization group analysis that $W_{kl}^{np}(b)$ has the following functional form to all orders of perturbation theory (we now write Q^2 instead of M_V^2 since the formula also applies to other Drell-Yan like processes)

$$W_{kl}^{np}(b, Q, x_1, x_2) = \exp \left[-h_1(b) \ln \left(\frac{Q^2}{Q_0^2} \right) - h_{k/A}(x_1, b) - h_{l/B}(x_2, b) \right] \quad (3.30)$$

where the three functions which in general depend on the specific initial parton flavor have to be determined by experiments constrained through $W_{kl}^{np}(b=0) = 1$. However in practice one actually uses simple parametrizations as [29] the Davies-Webber-Stirling (DWS) form

$$\exp \left[\left(-g_1 - g_2 \ln \left(\frac{Q}{2Q_0} \right) \right) b^2 \right], \quad (3.31)$$

the Ladinsky-Yuan (LY) form with three parameters and a logarithmic x -dependence linear in b

$$\exp \left[\left(-g_1 - g_2 \ln \left(\frac{Q}{2Q_0} \right) \right) b^2 - (g_1 g_3 \ln(100x_1 x_2)) b \right] \quad (3.32)$$

or the Brock-Landry-Nadolsky-Yuan (BLNY) form which is just a pure Gaussian version of the former one

$$\exp \left[\left(-g_1 - g_2 \ln \left(\frac{Q}{2Q_0} \right) - g_1 g_3 \ln(100x_1 x_2) \right) b^2 \right]. \quad (3.33)$$

In [29] all three parametrizations were compared to several sets of data coming from Drell-Yan pair and vector boson production in a global fit. The data stemmed from the experiments R209, E605, E288, and Tevatron Run 1 Z. Based on a statement "It is evident that the Gaussian BLNY parametrization fits the whole data sample noticeably better than the other two parametrizations. . ." in [29], we have applied the BLNY form with the respective values for the parameters determined in [29], which are:

$$g_1 = 0.21, \quad g_2 = 0.68, \quad \text{and} \quad g_3 = -0.60 \quad (3.34)$$

where the starting scale has been chosen to be $Q_0 = 1.6 \text{ GeV}$ and the maximum value of the impact parameter to be $b_{max} = 0.5 \text{ GeV}^{-1}$.

Since the resummed expression contains only the most singular part of the former fixed-order result one does the following. One expands the resummed expression to

second order in α_s again and extracts the $1/k_T^2$ terms, while the running coupling and the PDFs are now evaluated at the renormalization/factorization scale of the conventionally determined second order perturbation result. The result, by Arnold and Kauffman called the "asymptotic" (asym) result, is then subtracted from the latter one, i.e the second order perturbative (pert) result. So one has

$$\frac{d\sigma_{pp \rightarrow VX}}{dk_T^2 dy}(\text{total}) = \frac{d\sigma_{pp \rightarrow VX}}{dk_T^2 dy}(\text{resum}) + \frac{d\sigma_{pp \rightarrow VX}}{dk_T^2 dy}(\text{pert}) - \frac{d\sigma_{pp \rightarrow VX}}{dk_T^2 dy}(\text{asym}). \quad (3.35)$$

However, since the PDFs of the resummed and asymptotic result are determined at fixed values of x_1, x_2 , both results continue to fall as $1/k_T^2$ at growing k_T in opposite to the corresponding perturbative result which falls faster (the PDFs also fall with increasing k_T). Since the asymptotic term incorporates only pieces up to second order in α_s there will remain terms uncanceled from the resummed result, so that the total falling will not be that fast as its supposed to be. Furthermore at high k_T the resummed result even passes zero so that the uncanceled terms lead to a negative total result. Thus one has to switch back to the pure perturbative result at some point.

Parton distribution functions

As treated in the last chapter the structure of the proton or generally any hadron can not be described perturbatively and is hence subject to experiments. It is described by the parton distribution functions also referred to as parton density functions which give the probability of finding a certain parton i at a momentum scale $\mu_f = Q$ inside a certain hadron H carrying a longitudinal momentum fraction x . However, we will only deal with proton PDFs. Due to the proton quantum numbers they have to obey certain sum rules besides the completeness relation

$$\sum_i \int_0^1 dx x f_{i/P}(x, Q) = 1. \quad (4.1)$$

The proton is assumed to be a bound state of the three quantum number giving valence quarks, which are two up-quarks and one down-quark, and an unknown admixture of quark-antiquark pairs to which one often refers as sea-quarks. Thus there should be an excess of two u and one d quark over the according antiquarks, which implies the following rules

$$\int_0^1 dx (f_{u/P}(x, Q) - f_{\bar{u}/P}(x, Q)) = 2, \quad \text{and} \quad \int_0^1 dx (f_{d/P}(x, Q) - f_{\bar{d}/P}(x, Q)) = 1. \quad (4.2)$$

For all other flavors there should be the same amount of quarks and antiquarks.

Once the PDFs have been gained from experiment at a certain scale their evolution to higher scales is governed by the DGLAP equations as stated in the last chapter. Now there are several methods to parametrize the x dependence at the starting scale Q_0 in order to fit the data, leading to different sets of PDFs. Usually the parameterizations are of the form (suppressing specific parton indices) [30]

$$f(x, Q_0) = a_0 x^{a_1} (1 - x)^{a_2} P(x) \quad (4.3)$$

The x_1^a term reflects a Regge like behavior in the small x limit, while the term $(1 - x)^{a_2}$ describes the physics in the limit $x \rightarrow 1$ and is mostly affected by the valence quark

sum rules. On the other hand $P(x)$ is a phenomenological smooth function with a few more parameters to achieve more flexibility. The ansatz for this function varies among experimental physics groups.

For the valence (v) quarks for example the CTEQ (The Coordinated Theoretical-Experimental Project on QCD) uses [31]

$$P_v(x, Q_0 = 1.3 \text{ GeV}) = \exp(a_3 x + a_4 x^2 + a_5 \sqrt{x}) \quad (4.4)$$

while the MSTW (Martin-Stirling-Thorne-Watt) collaboration uses [32]

$$P_v(x, Q_0 = 1 \text{ GeV}) = 1 + a_3 \sqrt{x} + a_4 x. \quad (4.5)$$

These collaborations provide PDF sets won by global analyses of experimental data. The next-to-leading order best CT10 global fit [31] will be used for our numerical calculations as a baseline together with its provided uncertainty band. The difficulties of error estimation and propagation in global fit analysis are a whole subject of their own and will not be treated here. We will only have a brief look at the so-called *Hessian method*. The CT10 PDF parametrizations include in total 26 free parameters. At first the whole data sample is fitted using the 26 parameters. Then the best set of fit parameters (we will from now refer to the corresponding fit f_0 as the central value/central fit) is obtained by minimizing the χ^2 of the global fit. The assumption then is that one can approximate χ^2 near the global minimum by a quadratic expansion in the fit parameters a_i ($i = 1, \dots, 26$). One obtains the Hessian error matrix

$$\Delta\chi^2 = \frac{1}{2} \sum_{i,j}^{26} H_{ij} (a_i - a_i^0) (a_j - a_j^0) \quad (4.6)$$

where a_i^0 corresponds to the respective value of the parameter in the central fit. Diagonalizing the matrix yields a basis of 26 orthonormal eigenvectors each one probing a direction in the PDF parameter space. The largest (smallest) eigenvalues corresponding to the eigenvectors represent the best (worst) determined directions. Varying in each eigenvector direction up(+) and down(-) up to a given tolerance one gains a set of 52 PDF fits corresponding to the respective parameter values. Although the plus and minus variations are symmetric in parameter space they will not always cause symmetric variations of an observable depending on the corresponding fit values. To estimate the error of an observable caused by the PDF uncertainties based on the given set of 52 PDFs there exist different methods. However, we will use the one recommended by

CT10. One computes the result for a physical observable $R(f)$ for each of the provided PDFs f_i ($i = 1, \dots, 52$), then the positive and negative error estimates for $R(f)$ are given by

$$\Delta R^+(f) = \sqrt{\sum_{i=1}^{26} \left(\max(R(f_i^+) - R(f_0), R(f_i^-) - R(f_0), 0) \right)^2} \quad (4.7)$$

$$\Delta R^-(f) = \sqrt{\sum_{i=1}^{26} \left(\max(R(f_0) - R(f_i^+), R(f_0) - R(f_i^-), 0) \right)^2} \quad (4.8)$$

where $\max()$ determines the respective maximum value.

For now we will deal with the PDFs themselves (so $R(f) = f$). The 52 f_i^\pm PDFs are provided by CT10 at a confidence level of 90%. In order to estimate the bias coming from the different parametrizations of the x dependence (and other sources of error), also the best NLO fits of the global analyses MSTW08 [32] and NNPDF2.1 (Neural Network Parton Distribution Functions) [33] are presented. All PDF sets have been taken from the LHAPDF (Les Houches Accord PDF) library [34].

In Fig. 4.1 the gluon PDF (reduced by a factor of 20) and the up-quark and strange-quark PDFs are shown at the factorization scale $Q = M_Z$ (top), adequate for electroweak boson production at low transverse momenta, and at the higher scale of $Q = 1 \text{ TeV}$ (bottom), relevant at high transverse momenta of the vector bosons.

Since the PDFs are highly peaked one usually plots $xf_i(x, Q)$ rather than $f(x, Q)$.

As one can see, the densities of gluons and sea quarks at small x increase from low (top) to high (bottom) scales, at the same time PDFs at large x are reduced (mostly valence quarks, here up quarks). According to the DGLAP equations partons at high x tend to split decreasing their momentum to lower x . In addition the splitting produces new partons with low x . Thus the PDFs decrease at large x and increase more rapidly at small x with growing Q^2 . One says, the proton is resolved on finer and finer distance scales. In this region the sea-quark contributions dominate, so that the up-(incorporating valence and sea quarks) and strange-quark PDFs largely overlap, so only the PDF uncertainties are shown in Fig. 4.1 for the latter while the central values are omitted for better visibility.

The PDF uncertainty highly increases below values of $x = 10^{-3}$ where little information is available from pre-LHC experiments. Since the Q^2 dependence can be calculated perturbatively using the DGLAP equations, the PDFs at high Q become less dependent on the non-perturbative input at the starting scale Q_0 , so that their uncertainty

due to the fit of the unknown x dependence at Q_0 to experimental data is reduced.

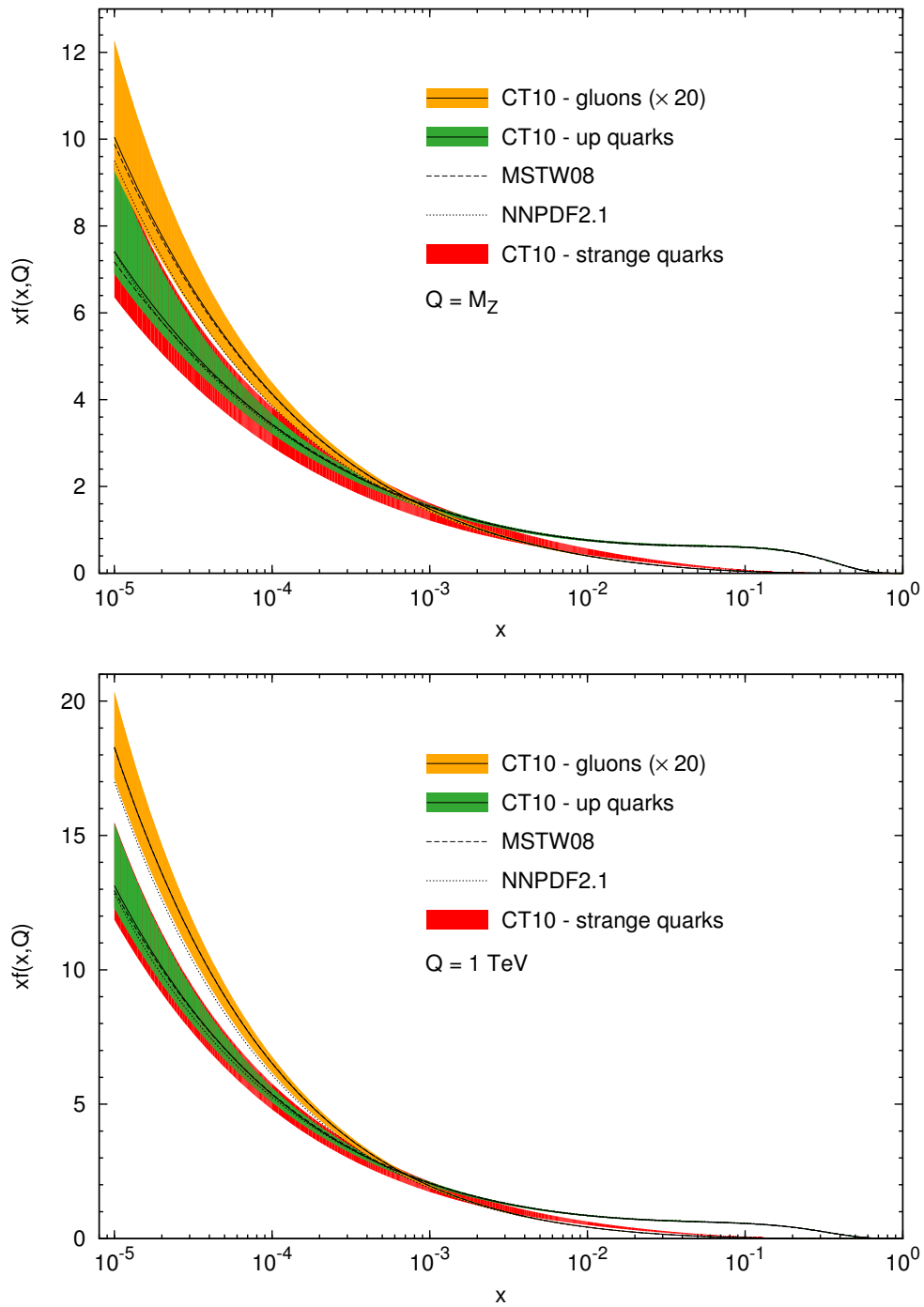


Figure 4.1.: Parton distribution functions (PDFs) on a logarithmic x scale, emphasizing the low x region, at the factorization scale $Q = M_Z$ (top) and 1 TeV (bottom) from different collaborations. PDF uncertainties are only shown for the CT10 group. PDFs are printed for gluons, up quarks and strange quarks.

The shift of the PDFs (in particular for up-quarks) from larger to smaller x values with the evolution from $Q = M_Z$ to $Q = 1$ TeV can actually better be seen when plotting on a linear x axis, which is shown in Fig. 4.2. Emphasizing the high x -region in this way, the up- and strange-quark PDFs are well separated due to the contributions of valence quarks to the up quark PDF, so that also the central values for the strange quark distributions are shown in this case.

Furthermore, one can see that the CT10 uncertainty, induced by experimental data, does not cover in all regions the central values of MSTW08 and NNPDF2.1, demonstrating the important influence of the theoretical bias on the x parametrization at initial scale Q_0 .

Focusing now on the gluon PDF at large x , one can see that it is much less constrained than the up-quark PDF, which in opposite to the former one got directly probed in DIS experiments (the gluon PDF enters only at next-to-leading order QCD).

At the lower scale $Q = M_Z$, the gluon uncertainty parametrized by CT10 at $x = 0.3$ and $x = 0.4$ exhibits considerably large values which amount to $\approx +21\% / -18\%$ and $\approx +40\% / -30\%$, respectively. The evolution to $Q = 1$ TeV does not change this uncertainty significantly, which there amounts to $\approx +22\% / -17\%$ and $\approx +43\% / -28\%$, respectively. Contrary to the strange-quark PDFs, the central MSTW08 and NNPDF2.1 gluon PDF fits are covered by the CT10 uncertainty bands.

In the three global analyses considered here, LHC data have not yet been included.

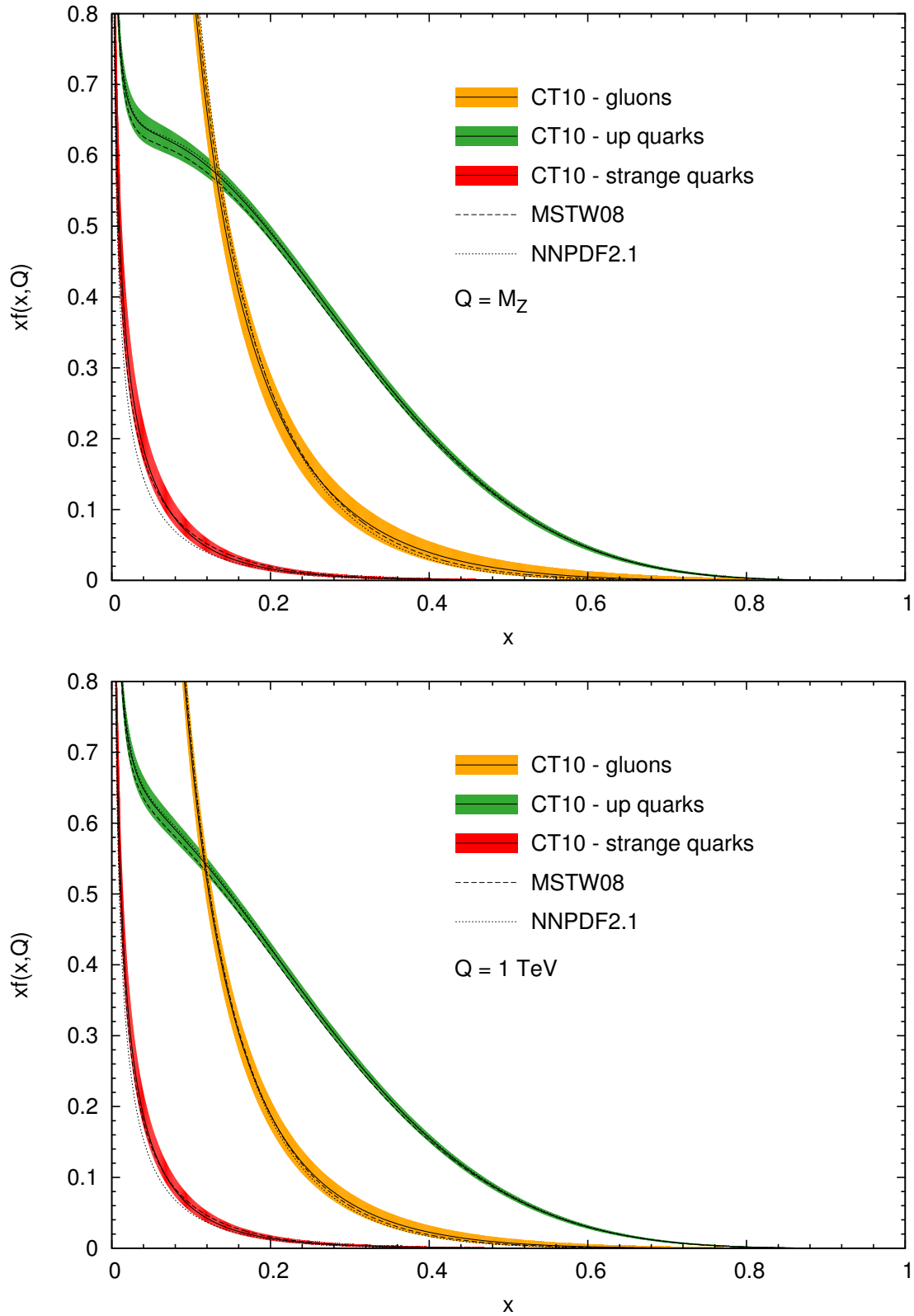


Figure 4.2.: Same as in Fig. 4.1, but on a linear x -scale, emphasizing the high- x region.

Numerical results ¹

The calculations are based on a Fortran program code developed by P.B. Arnold, M. H. Reno and R. P. Kauffman in [18],[25].

All PDF sets (CT10 [31], MSTW08 [32] and NNPDF2.1 [33]) have been included in the calculations via the LHAPDF interface [34]. Some packages of the CERNLIB 2006 library [36] have been used.

As stated in section 3.3 for the non-perturbative function W_{kl}^{np} entering in the CSS resummation formula a pure Gaussian parametrization has been used

$$W_{kl}^{np}(b, Q, Q_0, x_1, x_2) = \exp \left[\left(-g_1 - g_2 \ln \left(\frac{Q}{2Q_0} \right) - g_1 g_3 \ln(100x_1 x_2) \right) b^2 \right] \quad (5.1)$$

with the parameters as determined in [29]

$$g_1 = 0.21, \quad g_2 = 0.68, \quad \text{and} \quad g_3 = -0.60 \quad (5.2)$$

and the starting scale chosen to be $Q_0 = 1.6 \text{ GeV}$ and the maximum value of the impact parameter chosen to be $b_{max} = 0.5 \text{ GeV}^{-1}$.

For the electroweak bosons the following mass values have been used [37]

$$M_W = 80.385 \quad \text{and} \quad M_Z = 91.1876. \quad (5.3)$$

The electroweak bosons are treated as stable. Contributions of top quarks, and the mixing of the bottom quarks to lighter quarks have been neglected. The results for W^+ and W^- production have been summed.

With respect to standard practice from now on the transverse momentum of the respective vector boson will be denoted by p_T . Furthermore, results are presented for the cross section differential in p_T rather than p_T^2 . The center of mass energy in the center of mass frame of the colliding protons will be denoted by \sqrt{s} rather than \sqrt{S} .

¹The results of this thesis and so basically this chapter have been published yet before submitting the thesis in [35].

The factorization and renormalization scales have been equally set to $\mu_f = \mu_r = \mu = \sqrt{M_V^2 + p_T^2}$ with respect to the relevant momentum scales of the process.

At first the theoretical predictions will be compared to LHC data.

5.1. Comparison to data

In the upper part of Fig. 5.1 the theoretical predictions for Z -boson production at a center of mass energy of $\sqrt{s} = 7$ TeV are compared to CMS data. In experiments the Z bosons are detected via their decay products, i.e lepton-antilepton pairs (electrons and muons). Since the subsequent decay of the Z boson has not been included in our theoretical calculations, we are considering the differential cross section normalized to the total cross section. The CMS data were presented in [38] by the CMS collaboration normalized to the total cross section and with combined statistical and systematic uncertainties, individually for decay electrons and muons with pseudorapidity (rest masses neglected) $|\eta| < 2.1$ and as a combination. However, only the combined error is presented. The data extend to values of 600 GeV for the p_T of the Z boson.

The theoretical differential cross section has been computed with the central value of CT10 and integrated over the rapidity range of the Z boson of $|y| < 2.1$ according to the experimental constrain on the pseudorapidity of the leptons which directly translates into the same (despite of the neglected lepton masses) constrain on the Z boson rapidity.

As can be observed, the region where resummation is needed to describe the data extends to values of $p_T \simeq 75$ GeV. Below this point, the perturbative calculation (dotted) diverges logarithmically due to multiple-soft-gluon radiation and needs to be resummed (dashed), while above this point the regular, non-logarithmic terms due to hard, non-collinear radiation can no longer be neglected as is done in the pure resummation result. The transition region can be described as stated in section 3.3 by the subtraction of the asymptotic term.

As can be seen the theoretical predictions for Z boson production can describe the experimental data within the given uncertainties over the full region in p_T .

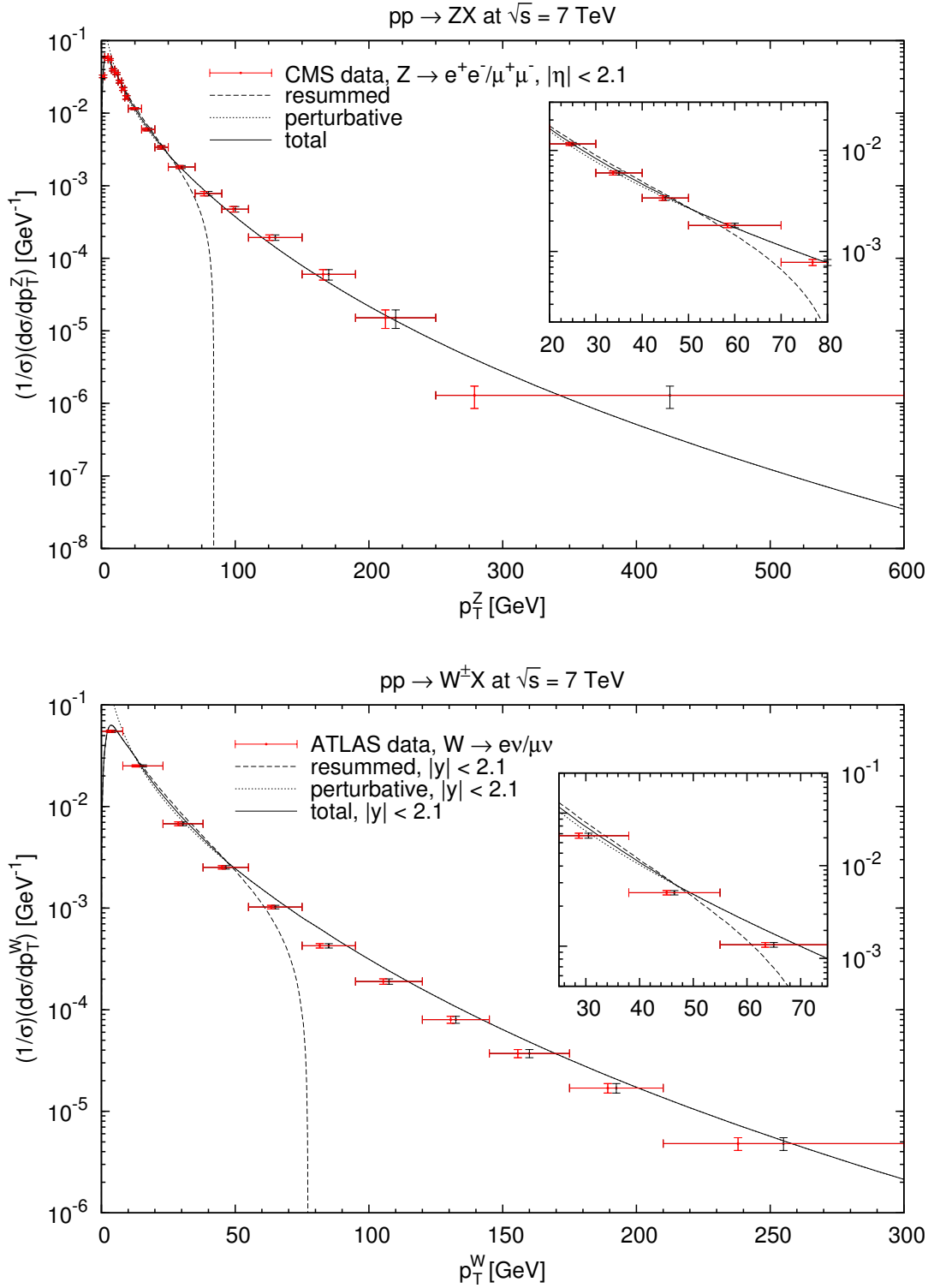


Figure 5.1.: Transverse-momentum spectra of Z (top) and W (bottom) bosons at the LHC with $\sqrt{s} = 7$ TeV, normalized to the total cross section. CMS (top) and ATLAS (bottom) data are compared with theoretical predictions at NLL+NLO in the rapidity range $|y| < 2.1$ using CT10 PDFs. The data points are positioned at the theoretical centers of gravity of the bins (red) and at the centers of the bins (black).

In the lower part of Fig. 5.1 the theoretical predictions for W boson production, as well as at $\sqrt{s} = 7$ TeV, together with ATLAS data [39]. Similarly to CMS, the ATLAS collaboration present their results normalized to the total cross section providing a combined uncertainty estimate for W boson decays into electrons and muons. The W boson decays into an electron (muon) and an electron-antineutrino (muon-antineutrino). The experimental rapidity cut for the electron and muons is given by $\eta < 2.4$. The neutrinos escape detection and enter only through missing energy. The experimental p_T spectrum for the W boson is obtained through a two-step unfolding procedure up to values of 300 GeV. On the other hand we can not determine a rapidity constrain on the W boson in this case, so the presented theoretical predictions calculated in the rapidity range of $|y| < 2.1$ only give a rough estimate in this case.

The theoretical behavior is very similar to the one for Z boson production except that the transition from the region dominated by large logarithms to the perturbative regime occurs at slightly smaller values of $p_T \simeq 65$ GeV, which can be attributed to the other hard scale of the process, i.e. the W boson mass which is with 80.385 GeV somewhat smaller than the Z boson mass of 91.1876 GeV.

The same results are plotted in Fig. 5.2 using a logarithmic x axis to show more clearly the agreement of theoretical predictions and experimental data in the low p_T -regime. In addition the central values for MSTW08 and NNPDF2.1 are presented.

One may ask how the resummation and perturbative regions change when moving from current LHC experiments with $\sqrt{s} = 7(8)$ TeV to those in future, which will be conducted with collision energies up to 14 TeV. The results of a calculation at $\sqrt{s} = 14$ TeV are shown in Fig. 5.3.

The value where the pure resummation result starts to deviate strongly from the total result is given roughly by $p_T \simeq 90$ GeV for Z bosons and by $p_T \simeq 80$ GeV for W bosons. On the other hand, the calculations indicate the reach in p_T , formerly 600(300) for $Z(W)$ bosons produced at $\sqrt{s} = 7$ TeV with an integrated luminosity of 35.9 (31) pb^{-1} , should increase to the multi-TeV range, i.e at least 2 TeV, at $\sqrt{s} = 14$ TeV and an assumed integrated luminosity of 100 fb^{-1} .

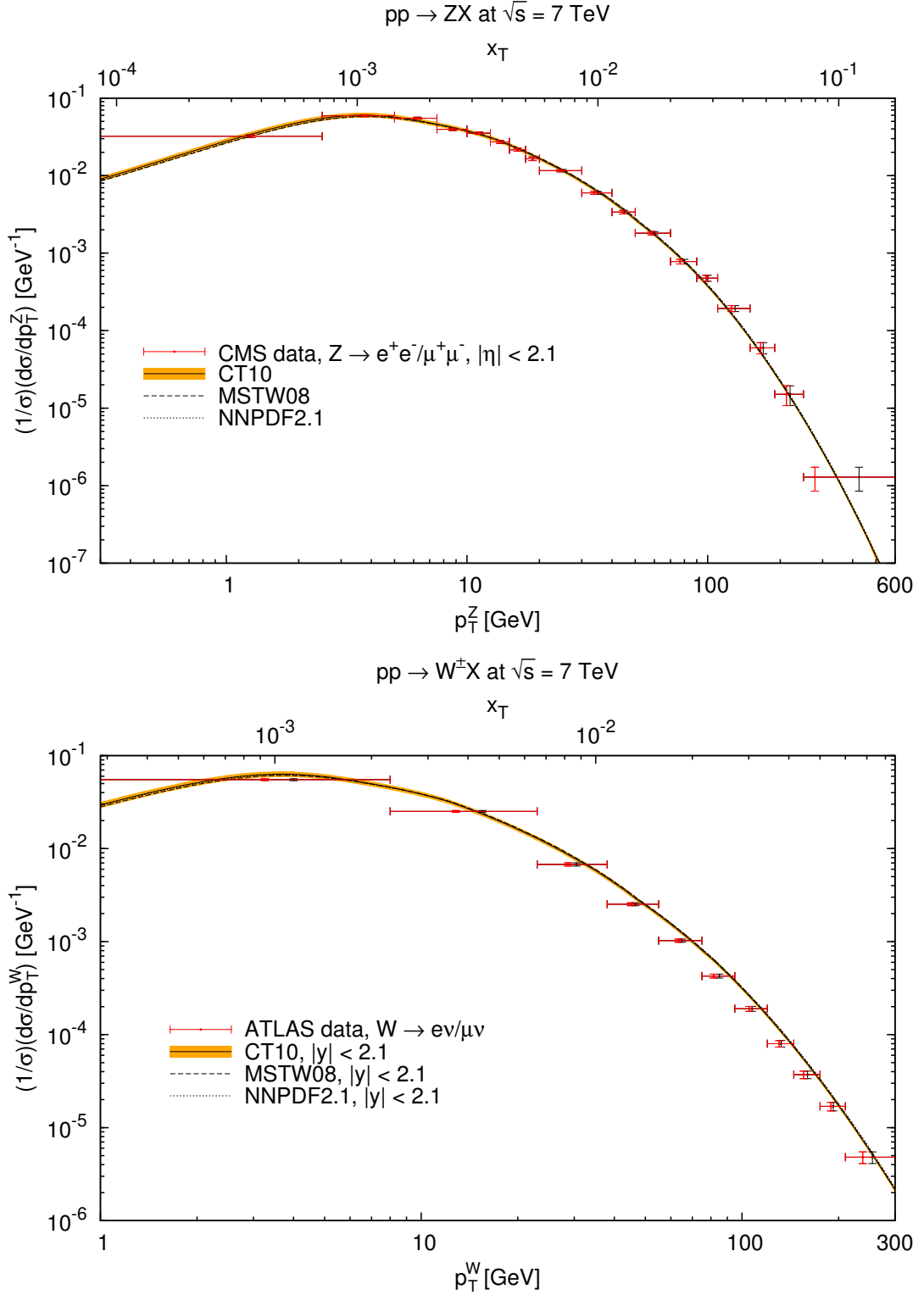


Figure 5.2.: Normalized transverse momentum spectra for Z (top) and W (bottom) bosons. The theoretical calculations at NLO combined with resummation for the rapidity range $|y| < 2.1$ and using various PDFs are shown in comparison with CMS and ATLAS data on a logarithmic x axis. The data points are positioned at the theoretical center of gravity of the bins (red) and at the center of the bins (black). The orange band represents the CT10 PDF uncertainty.

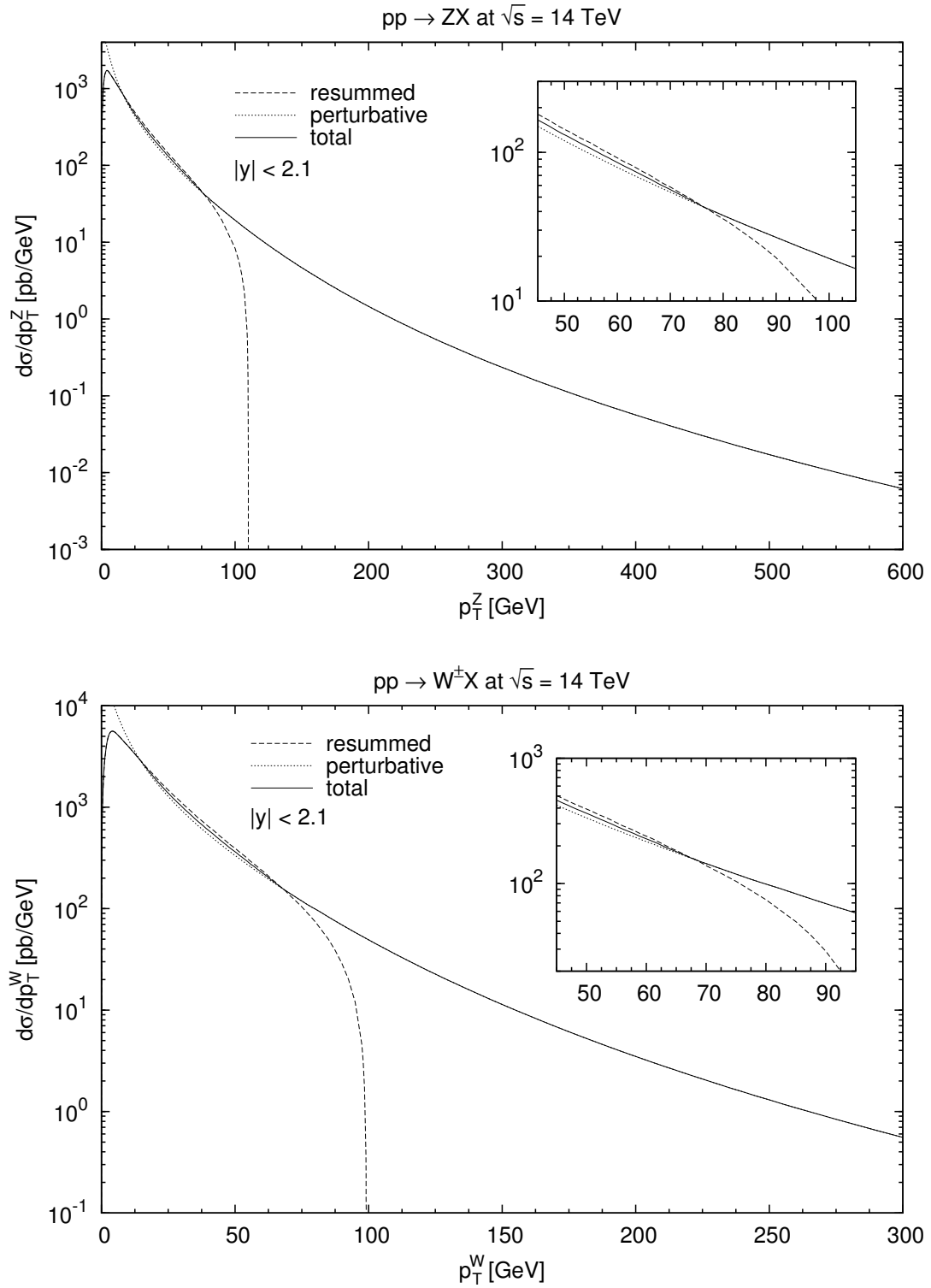


Figure 5.3.: Transverse-momentum spectra of Z (top) and W (bottom) bosons at $\sqrt{s} = 14$ TeV derived in NLL+NLO accuracy in the rapidity range $|y| < 2.1$ using CT10 PDFs.

5.2. Decomposition of partonic processes

The next question under consideration is at which values of p_T electroweak boson production starts to be dominated by the QCD "Compton" process $qg \rightarrow Z(W)q(q')$. The importance of the quark-gluon scattering subprocess can be seen in Fig. 5.4. At a collision energy of $\sqrt{s} = 7$ TeV it is sufficient for the transverse momentum of the produced Z (top) or W (bottom) boson to exceed 20 or 15 GeV. The contribution of the quark-gluon subprocess then remains at a level of 75%–80%, almost up to the kinematic limit, more precisely, up to 3 TeV before quark-antiquark fusion takes over again (not shown here). We show only the results for the leading order subprocesses, the contributions from the subprocesses $q\bar{q}'(\bar{q}) \rightarrow Z(W)q\bar{q}'(\bar{q})$, $qq(q') \rightarrow Z(W)qq(q')$, $q\bar{q}' \rightarrow Zq\bar{q}'$ and $gq \rightarrow Z(W)q\bar{q}'(\bar{q})$ arising at NLO as mentioned in section 3.2 remain at the level of a few percent. This statement actually depends on the factorization scheme and scale, in our case the $\overline{\text{MS}}$ scheme and $\mu_f = \sqrt{M_V^2 + p_T^2} = \mu_r$ as stated above. In principle this choice should provide a reasonable stability of the perturbative calculations in the low- and high- p_T regions.

The dominance of the qg subprocess persists at higher collision energies of $\sqrt{s} = 14$ TeV, as can be observed in Fig. 5.5. The peak contribution is even a bit larger and reaches more than 85% at $p_T \simeq 100$ GeV. A local minimum of about 70% exists at intermediate values of $p_T \simeq 1.5$ TeV. In Fig 5.4 and 5.5 a second, upper x axis has been introduced. It shows an estimator for the values of x at which the parton distributions in the colliding protons are probed given by $x_T = 2p_T/\sqrt{s}$. At the very large values of p_T accessible with the high LHC luminosities and energies, it should be possible to probe and constrain the gluon density where it is not well known.

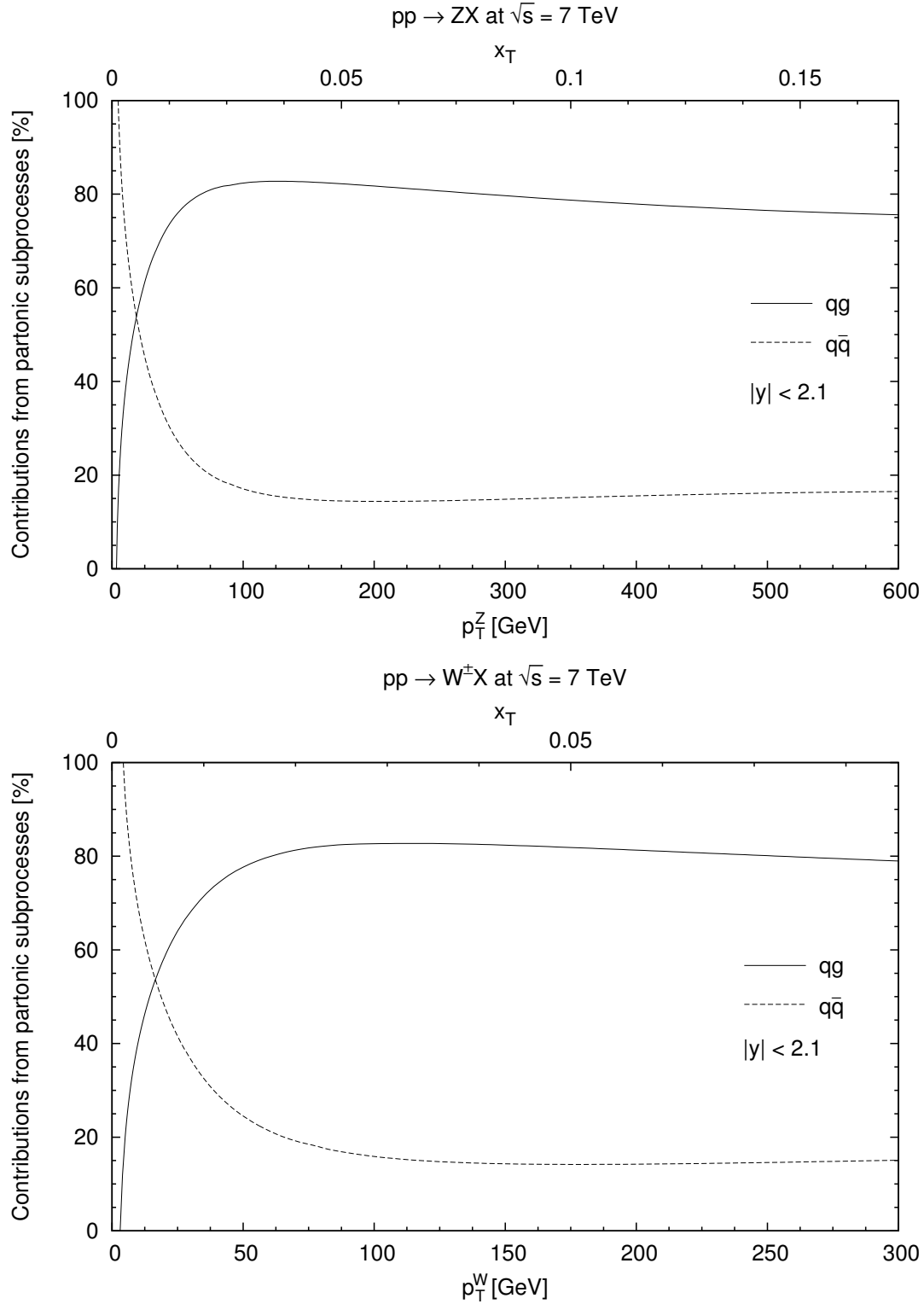


Figure 5.4.: Relative contributions at NLO of the quark-antiquark (dashed lines) and QCD "Compton" (solid lines) subprocesses to the production of Z (top) and W bosons (bottom) at the LHC with $\sqrt{s} = 7$ TeV. Subdominant partonic subprocesses which enter only at NLO or higher orders are not shown.

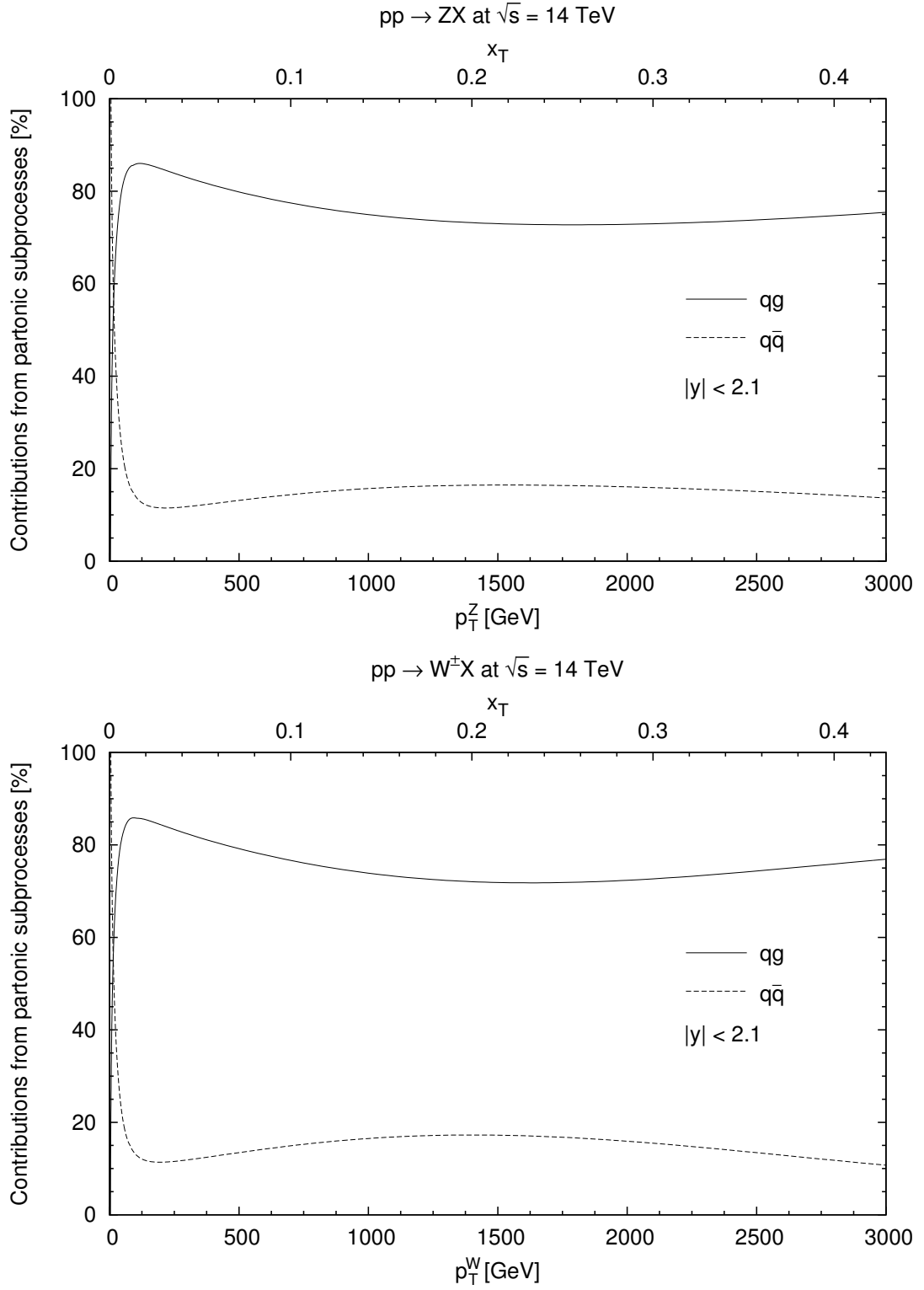


Figure 5.5.: Same as Fig. 5.4 for $\sqrt{s} = 14$ TeV here.

5.3. Parton density sensitivity of LHC vector boson production

Having established the reliability of the theoretical calculations in the resummation and perturbative regimes, as well as the dominance of the quark-antiquark and quark-gluon subprocesses at small and intermediate to large transverse momenta, we can now confront the current status of uncertainties on the quark and gluon PDFs in the proton with the prospects for improving on their determination with electroweak boson production at the LHC.

In Fig. 5.6 ratios of transverse-momentum spectra are shown for Z (top) and W (bottom) bosons using various PDFs to our baseline prediction with CT10 PDFs. While this figure shows results for the LHC with $\sqrt{s} = 7$ TeV, Fig. 5.7 shows these ratios for Z boson production at $\sqrt{s} = 14$ TeV.

If one accounts for a rescaling of transverse momenta by a factor of 2, these figures are very similar. With a total luminosity of more than 23 pb^{-1} collected by ATLAS and CMS at the end of 2012 each at $\sqrt{s} = 8$ TeV, a range in p_T up to 1 TeV or eventually even more can be expected. This corresponds to values of x_T of about 0.3 or more.

In Chapter 4 we observed that the gluon uncertainty at $x = 0.3$ and $x = 0.4$ parametrized by CT10 is quite large and reaches at the scale $Q = 1$ TeV values of $+22\%/-17\%$ and $+43\%/-28\%$, respectively. Since the QCD "Compton" process contributes here more than 75% to the total cross section, this uncertainty is directly reflected in Figs. 5.6 and 5.7 through the orange CT10 uncertainty bands.

The quark PDFs are dominated in this region by the valence contribution and add only a little to the total uncertainty. The alternative PDF determinations by MSTW08 (dashed) and NNPDF2.1 (dotted) follow in this region the lower boundary of the CT10 uncertainty band, based on the Hessian treatment of the experimental statistical error with fixed tolerance ($\Delta\chi^2 = 100$). The MSTW08 and NNPDF2.1 uncertainty bands are smaller than the one from the CT10, in particular due to a dynamic and smaller tolerance ($\Delta\chi^2 \sim 25$) and a different (Monte Carlo) sampling of the statistical error and cross-section validation, respectively, but also due to different input data, values of α_s , treatments of heavy quarks and experimental systematic errors etc.

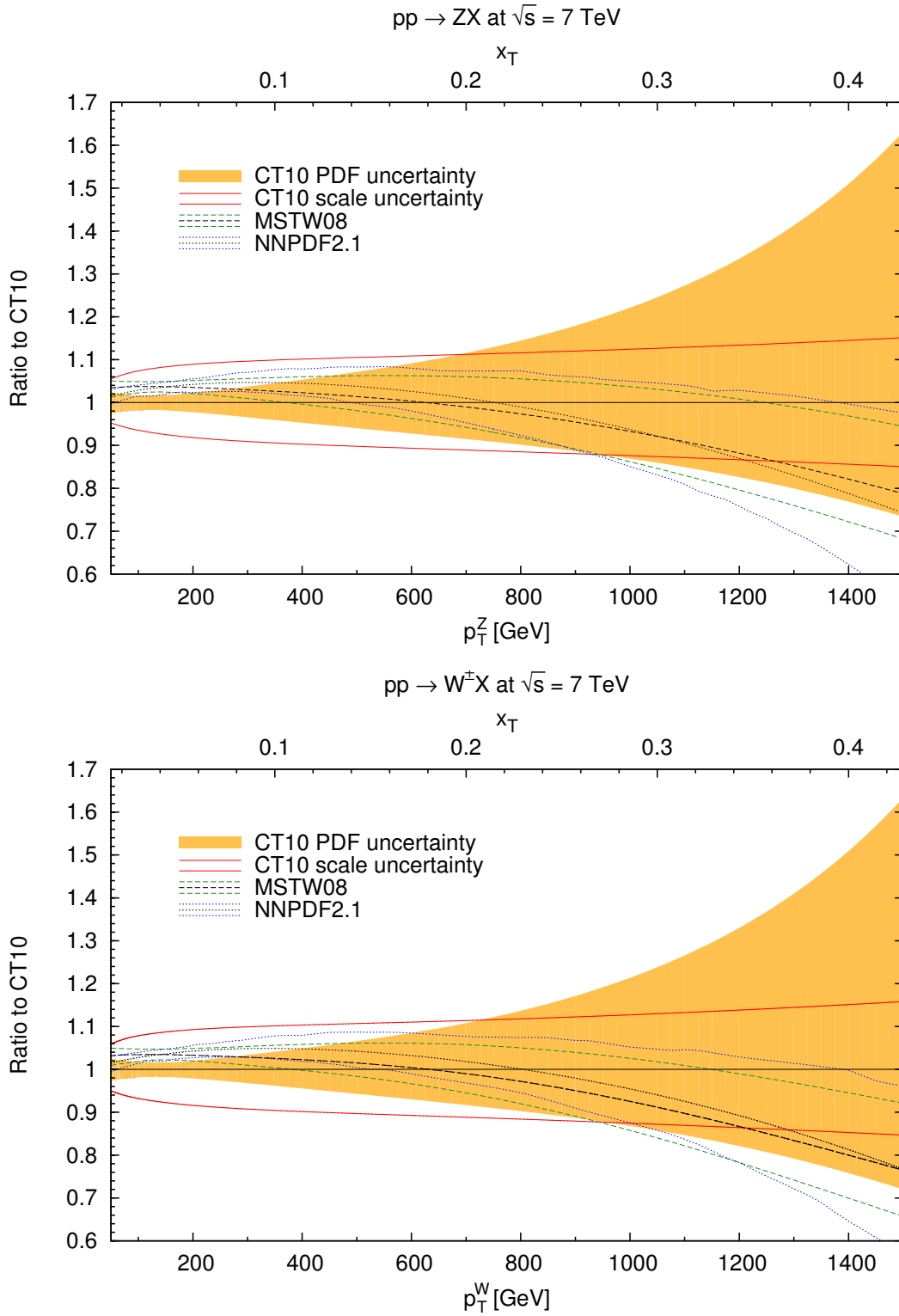


Figure 5.6.: Ratios of Z - (top) and W -boson (bottom) p_T distributions at $\sqrt{s} = 7$ TeV computed with different scales and PDFs to the baseline predictions with CT10 and central scale.

The scale uncertainty (red lines), estimated in the conventional way by varying the factorization and renormalization scales simultaneously by a factor of 2 up and down about the central scale, stays, with $\pm 10\%$ to $\pm 15\%$, considerably smaller than the CT10 PDF uncertainty alone, and of course also the envelope of all three PDF uncertainties. Measurements of electroweak boson production with transverse momenta of 1 TeV or beyond at $\sqrt{s} = 7, 8$ or 14 TeV at the LHC will thus help to improve on the determination of the gluon PDF in the large- x regime.

At low p_T , corresponding to x values of 0.01 to 0.1, the situation is quite different. The quark-gluon process still dominates, but the gluon PDF is quite well determined here through the evolution with errors below 10% at the scale $Q = M_Z$ (see Chapter 4). At the same time, the up- and down-quark PDFs are still strongly influenced by the well-constrained valence contribution.

In contrast, the uncertainty induced by the unphysical scales persists at the level of 10% and thus represents the dominant source of theoretical uncertainty. Taken together, these observations leave little room for improvement of the gluon PDF through electroweak boson production at small transverse momenta.

Since the rapidity of the produced vector boson enters exponentially in the expressions for the partonic momentum fractions ($x_{1,2} = e^{\pm y} M_V / \sqrt{s}$), it is clear that moving away from central to forward rapidity creates a more asymmetric situation, where the partons of one incoming proton are probed at much larger values, and those of the other proton at much smaller values of x . This is reflected in Fig. 5.8, where the cross-section ratios obtained with different PDFs from those obtained with CT10 for the production of electroweak bosons with rapidities of $|y| \in [2; 3]$ are shown.

These rapidities are still covered by the CMS and ATLAS electromagnetic endcap calorimeters, while muons are only detected up to $|\eta| < 2.4$ and 2.5, respectively. As expected, the PDF uncertainties in the forward region are much larger and reach easily a factor of 2. For the reasons mentioned above, the MSTW08 uncertainty band is much smaller than the CT10 band, but it has a very different shape, while the NNPDF2.1 band widens at the same p_T values as the CT10 band, but can even lead to negative cross sections. The envelope of all error bands is thus even larger than the error band of CT10 alone. This demonstrates the potential of corresponding measurements to pin down the gluon PDFs, depending on the transverse momenta that can be reached there.

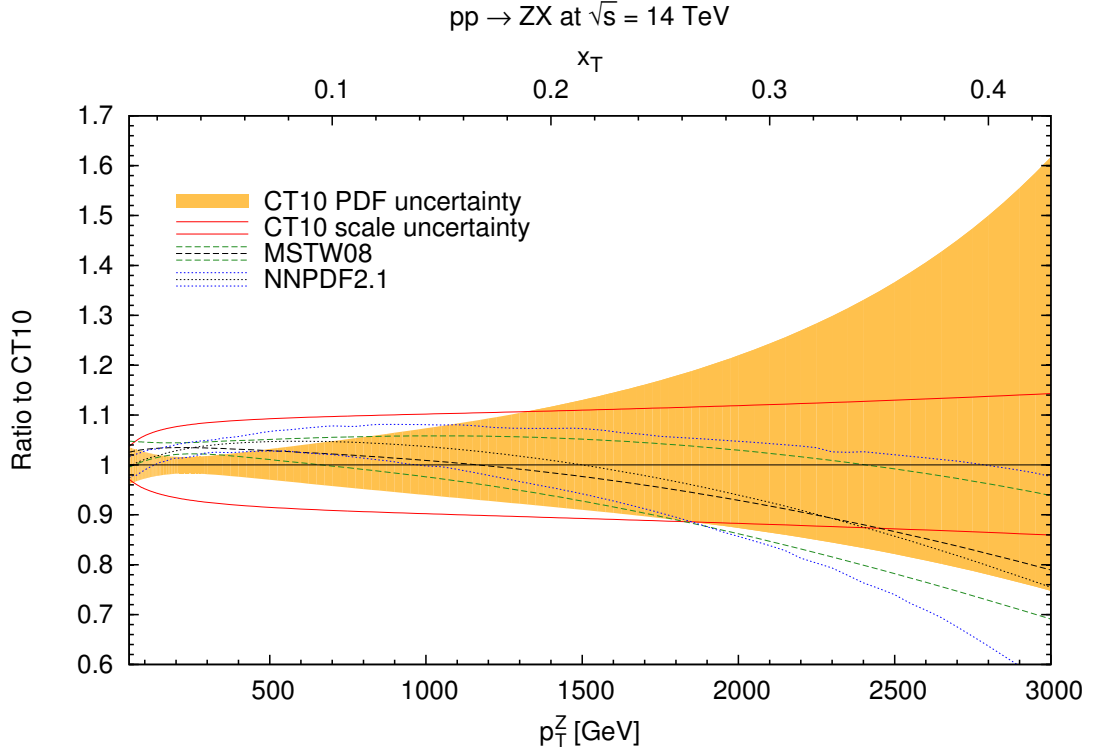


Figure 5.7.: Same as Fig. 5.6 for Z bosons at $\sqrt{s} = 14$ TeV.

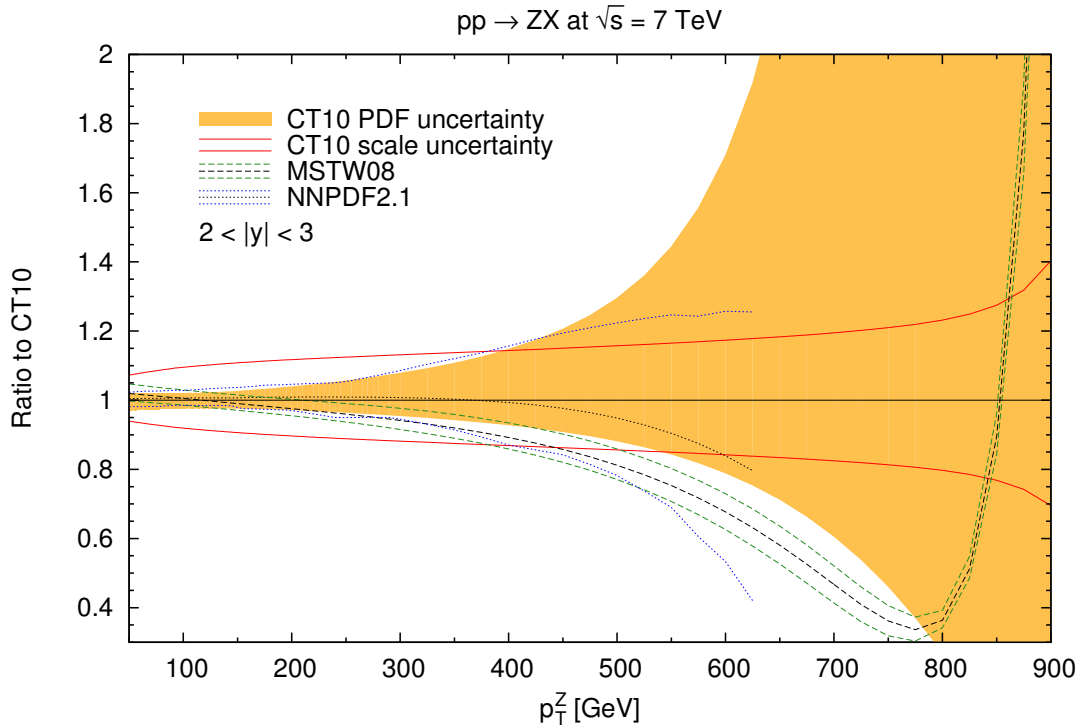


Figure 5.8.: Same as Fig. 5.6 for Z bosons at forward rapidity $|y| \in [2; 3]$.

Conclusion

In conclusion, the possibility to better constrain the parton densities in the proton at large momentum fractions has been investigated. These parton densities are of fundamental importance not only for our description of hadronic and nuclear structure, but also for reliable predictions for new heavy-particle searches at colliders.

The theoretical background has been described in Chapters 2 and 3. The basic concepts of a perturbative treatment of quantum field theories (in particular QCD) have been explained and applied to the case of weak vector boson production in proton-proton collisions. A few insights have been given to the wide topic of arising problems when dealing with long-distance QCD effects.

After a short review of the current status of CT10, MSTW08 and NNPDF2.1 parton distribution functions, the perturbative and resummed cross sections for electroweak vector boson production at the LHC, computed in NLO QCD matched to NLL resummation, have been found to be in good agreement with published CMS and ATLAS data for Z and W bosons at $\sqrt{s} = 7$ TeV up to p_T values of 600 and 300 GeV, respectively. The differential cross section for W and Z production has been found to be dominated by the "Compton" subprocess at transverse momenta beyond about 20 GeV, inducing a large sensitivity of the cross sections on the gluon PDFs. It has been shown that with the luminosities reached in future 14 TeV runs, transverse momenta in the TeV range should be measurable, thus providing access to the gluon PDF at large values of x , where it is currently badly constrained. The theoretical scale uncertainty has been shown to stay sufficiently small there, so that a measurement of electroweak boson production can help to improve on the determination of the gluon PDF in the large- x regime. At smaller transverse momenta, little improvement can be made on the determination of gluon and quark PDFs through the proposed process.

It is to be hoped that the ATLAS and CMS collaborations will soon make available analyses of electroweak boson production at large transverse momenta, so that they can be used in future global analyses of the parton distribution functions in the proton.

Appendix A

A.1. Feynman rules

In QCD and EW theory we deal with particles having spin. So external lines of Feynman diagrams receive Dirac spinors or polarization vectors. For EW theory only the relevant rules will be shown.

One has the following rules for external lines of quarks corresponding to the free particle solutions of the Dirac equations (s denotes the spin, p the momentum of the particle) and their color:

quarks:

$$\longrightarrow \bullet = u(p, s)c \quad (\text{initial}), \quad \bullet \longrightarrow = \bar{u}(p, s)c^\dagger \quad (\text{final}), \quad (\text{A.1})$$

antiquarks:

$$\longleftarrow \bullet = \bar{v}(p, s) \quad (\text{initial}), \quad \bullet \longleftarrow = v(p, s) \quad (\text{final}). \quad (\text{A.2})$$

Here the arrow indicates the particle number flow, not a momentum direction.

For bosons one has polarization vectors (the polarization is denoted by λ):

electroweak bosons:

$$\sim \bullet = \epsilon(p, \lambda) \quad (\text{initial}), \quad \bullet \sim = \epsilon^*(p, \lambda) \quad (\text{final}). \quad (\text{A.3})$$

gluons:

$$\text{~~~~~} \bullet = \epsilon(p, \lambda) \quad (\text{initial}), \quad \bullet \text{~~~~~} = \epsilon^*(p, \lambda) \quad (\text{final}). \quad (\text{A.4})$$

Now for the relevant propagators we have

$$\text{quark propagator} = \bullet \longrightarrow \bullet = i \frac{\not{p} + m}{p^2 - m^2 + i\epsilon}. \quad (\text{A.5})$$

$$\text{gluon propagator} = \bullet \text{---} \text{---} \text{---} \bullet = -i \frac{g_{\mu\nu}}{p^2 + i\epsilon} \delta_{ab}. \quad (\text{A.6})$$

where a, b run over the eight gluon colors. The propagator is given in Feynman gauge. We have to take into account contributions from ghosts:

$$\text{ghost propagator} = \bullet \cdots \cdots \bullet = -i \frac{\delta_{ab}}{p^2 + i\epsilon}. \quad (\text{A.7})$$

The QCD vertices are given by

$$\begin{array}{c} \text{---} \text{---} \text{---} \\ | \\ \bullet \\ / \quad \backslash \\ \text{---} \quad \text{---} \end{array}^{a, \mu} = -ig_s t^a \gamma^\mu, \quad (\text{A.8})$$

$$\begin{array}{c} p_2, \nu, b \\ | \\ \text{---} \text{---} \text{---} \\ / \quad \backslash \\ p_1, \mu, a \quad p_3, \lambda, c \end{array} = -g_s f_{abc} (g_{\mu\nu} (p_1 - p_2)_\lambda + g_{\nu\lambda} (p_2 - p_3)_\mu + g_{\lambda\mu} (p_3 - p_1)_\nu), \quad (\text{A.9})$$

$$\begin{array}{c} p_2, \nu, b \quad p_3, \lambda, c \\ \diagup \quad \diagdown \\ \text{---} \text{---} \text{---} \\ \diagdown \quad \diagup \\ p_1, \mu, a \quad p_4, \rho, d \end{array} = -ig_s (f_{abe} f_{cde} (g_{\mu\lambda} g_{\nu\rho} - g_{\mu\rho} g_{\nu\lambda}) + f_{ade} f_{bce} (g_{\mu\nu} g_{\lambda\rho} - g_{\mu\lambda} g_{\nu\rho}) + f_{ace} f_{dbe} (g_{\mu\rho} g_{\nu\lambda} - g_{\mu\nu} g_{\lambda\rho})),$$

$$\begin{array}{c} \text{---} \text{---} \text{---}^{\mu, b} \\ | \\ \bullet \\ / \quad \backslash \\ \text{---} \quad \text{---} \\ a \quad c \\ \backslash \quad / \\ p \end{array} = -g_s f_{abc} p^\mu \quad (\text{A.10})$$

Due to the anti-commutation property of fermions, one has to take into account an additional minus sign in every closed fermion loop, ghosts also obey anti-commutation.

The relevant EW vertices are given as below.

for W bosons to quarks

$$\begin{array}{c} \text{Wavy line } W, \mu \\ \uparrow \\ \text{Vertex} \\ \swarrow \text{f}' \quad \searrow \text{f} \end{array} = -i \frac{g}{\sqrt{2} \gamma^\mu} \frac{1 - \gamma^5}{2} V_{ff'}, \quad (\text{A.11})$$

for W bosons to leptons

$$\begin{array}{c} \text{Wavy line } W, \mu \\ \uparrow \\ \text{Vertex} \\ \swarrow l \quad \searrow \nu \end{array} = -i \frac{g}{\sqrt{2} \gamma^\mu} \frac{1 - \gamma^5}{2}, \quad (\text{A.12})$$

and for Z bosons to any fermion

$$\begin{array}{c} \text{Wavy line } Z, \mu \\ \uparrow \\ \text{Vertex} \\ \swarrow f \quad \searrow f \end{array} = \frac{-ig}{\cos(\theta_W)} \gamma^\mu \left(\left(I_3^f - \sin^2(\theta_w) e_f \right) \frac{1 - \gamma^5}{2} - \sin^2(\theta_w) e_f \frac{1 + \gamma^5}{2} \right). \quad (\text{A.13})$$

A.2. Useful relations for the calculation of Feynman amplitudes

This appendix shows a list of relations which are useful for simplification of terms arising during the calculation of Feynman amplitudes.

Be v a column vector and A, B matrices ($T \hat{=}$ transposed) then one has

$$(AB)^T = B^T A^T \quad (\text{A.14})$$

and

$$v^T A v = \text{Trace}[A v v^T]. \quad (\text{A.15})$$

The adjoint spinor reads as

$$\bar{u}(p, s) = u^\dagger(p, s) \gamma^0 \quad (\text{same for } v). \quad (\text{A.16})$$

Furthermore, there are the following helicity completeness relations:

For quarks the sum over all spin states is given by

$$\sum_{\text{spins } s} u(p, s) \bar{u}(p, s) = \not{p} + m \mathbb{1}, \quad \sum_{\text{spins } s} v(p, s) \bar{v}(p, s) = \not{p} - m \mathbb{1}. \quad (\text{A.17})$$

for external massless bosons in **non**-physical gauge one has

$$\sum_{\text{polarizations } \lambda} \epsilon_{\mu}^*(p, \lambda) \epsilon_{\mu'}(p, \lambda) = -g_{\mu\mu'} \quad (\text{A.18})$$

and for external massive gauge bosons in physical-gauge ($p^2 = m^2$) the relation reads

$$\sum_{\text{polarizations } \lambda} \epsilon_{\mu}^*(p, \lambda) \epsilon_{\mu'}(p, \lambda) = -g_{\mu\mu'} + \frac{p_{\mu} p_{\mu'}}{m^2}. \quad (\text{A.19})$$

From the $SU(3)_C$ group one has the following color rules

$$\sum_{\text{colors}} c c^{\dagger} = \mathbb{1}_{3 \times 3}. \quad (\text{A.20})$$

$$\text{Tr}[t^a t^b] = \frac{1}{2} \delta^{ab}, \quad \sum_a t^a t^a = C_f \cdot \mathbb{1}_{3 \times 3}, \quad C_f = \frac{N^2 - 1}{2N} \stackrel{SU(3)}{=} \frac{4}{3}. \quad (\text{A.21})$$

$$\begin{aligned} t^a t^b t^a &= \left(C_f - \frac{1}{2} N_C \right) t^b, \quad N_C = 3 \\ f^{abc} t^b t^c &= \frac{1}{2} i C_f t^a \\ f^{acd} f^{bcd} &= C_f \delta^{ab}. \end{aligned} \quad (\text{A.22})$$

The Dirac matrices γ are 4×4 matrices obeying a Clifford algebra defined by

$$\{\gamma^{\mu}, \gamma^{\nu}\} = \gamma^{\mu} \gamma^{\nu} + \gamma^{\nu} \gamma^{\mu} = 2g^{\mu\nu} \mathbb{1}, \quad (\text{A.23})$$

where in D dimensions the Lorentz indices are running from 0 to $D - 1$ and $\mathbb{1}$ denotes the 4×4 unity matrix. From this equation we get the properties

$$(\gamma^0)^2 = \mathbb{1} \quad \text{and} \quad (\gamma^i)^2 = -\mathbb{1} \quad \text{with} \quad i = 1, 2, \dots, D - 1, \quad (\text{A.24})$$

$$(\gamma^\mu)^\dagger = \gamma^0 \gamma^\mu \gamma^0, \quad (\text{A.25})$$

of the Dirac matrices and taking into account the slash notation/relation

$$\not{p} = \gamma^\mu p_\mu, \quad \not{p}\not{q} = 2(p \cdot q)\mathbb{1} - \not{q}\not{p} \quad \rightarrow \quad \not{p}\not{p} = p^2\mathbb{1} \quad (\text{A.26})$$

we also have the following list of contraction relations in D dimensions:

$$\gamma^\mu \gamma_\mu = g_\mu^\mu = D, \quad (\text{A.27})$$

$$\gamma^\mu \not{p} \gamma_\mu = (2 - D)\not{p}, \quad (\text{A.28})$$

$$\gamma^\mu \not{p}\not{q} \gamma_\mu = 4(p \cdot q)\mathbb{1} - (4 - D)\not{p}\not{q}, \quad (\text{A.29})$$

$$\gamma^\mu \not{p}\not{q}\not{k} \gamma_\mu = -2\not{k}\not{q}\not{p} + (4 - D)\not{p}\not{q}\not{k}. \quad (\text{A.30})$$

The so called fifth gamma matrix γ^5 defined as a multiplication of the γ matrices of the 4 dimensional case

$$\gamma^5 = i\gamma^0\gamma^1\gamma^2\gamma^3 \quad (\text{A.31})$$

obeys

$$(\gamma^5)^2 = \mathbb{1}, \quad (\text{A.32})$$

$$(\gamma^5)^\dagger = \gamma^5, \quad (\text{A.33})$$

$$\text{Tr} [\gamma^5] = 0. \quad (\text{A.34})$$

Given that

$$\{\gamma^5, \gamma^\mu\} = \gamma^5 \gamma^\mu + \gamma^\mu \gamma^5 = 0 \quad (\text{A.35})$$

still holds in D dimensions one is prepared to evaluate arising traces by the following relations:

$$\text{Tr} [\gamma^\mu \gamma^\nu] = 4g^{\mu\nu} \quad \text{and hence of course} \quad \text{Tr} [\not{p}\not{q}] = p_\mu q_\nu \text{Tr} [\gamma^\mu \gamma^\nu] = 4(p \cdot q), \quad (\text{A.36})$$

$$\text{Tr} [\gamma^\mu \gamma^\nu \gamma^5] = 0, \quad (\text{A.37})$$

$$\text{Tr} [\text{any odd \# of } \gamma^\mu] = 0, \quad (\text{A.38})$$

$$\text{Tr} [\gamma^\mu \gamma^\nu \gamma^\rho \gamma^5] = 0, \quad (\text{A.39})$$

$$\text{Tr} [\gamma^\mu \gamma^\nu \gamma^\rho \gamma^\sigma] = 4(g^{\mu\nu} g^{\sigma\rho} - g^{\mu\rho} g^{\nu\sigma} + g^{\mu\sigma} g^{\nu\rho}), \quad (\text{A.40})$$

$$\text{Tr} [\gamma^\mu \gamma^\nu \gamma^\rho \gamma^\sigma \gamma^5] = -4i\epsilon^{\mu\nu\rho\sigma}. \quad (\text{A.41})$$

A.3. Calculation of the leading order QCD contributions to weak vector boson production

In this section we will derive the partonic leading order QCD contributions to W boson production via Feynman diagrams.

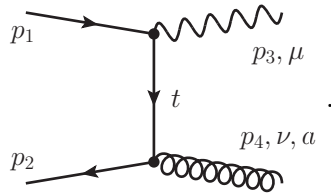
The Mandelstam variables are given by

$$s = (p_1 + p_2)^2 = (p_3 + p_4)^2, \quad t = (p_1 - p_3)^2 = (p_2 - p_4)^2, \quad u = (p_1 - p_4)^2 = (p_2 - p_3)^2 \quad (\text{A.42})$$

In addition they obey

$$s + t + u = m_W^2. \quad (\text{A.43})$$

The first contribution to the subprocess $q\bar{q}' \rightarrow Wg$ is given by the following Feynman diagram, due to exchanged momentum with respect to the Mandelstam variables called t -channel diagram:



Inserting the Feynman rules given in section A.1 the matrix element reads

$$i\mathcal{M}_t = \left[\bar{v}_{q'}(p_2, s_2) c_2^\dagger \right] (-ig_s \gamma^\nu t^a) \epsilon_\nu^*(p_4, \lambda_4) \left(i \frac{\not{p}_1 - \not{p}_3 + m_{q'} \mathbb{1}}{(p_1 - p_3)^2 - m_{q'}^2} \right) \epsilon_\mu^*(p_3, \lambda_3) \left(\frac{-ig}{\sqrt{2}} \gamma^\mu \frac{(\mathbb{1} - \gamma^5)}{2} V_{qq'} \right) [u_q(p_1, s_1) c_1] \quad (\text{A.44})$$

shorten the expression by $\bar{v}_{q'}(p_2, s_2) = \bar{v}_2$, $\epsilon_\nu^*(p_4, \lambda_4) = \epsilon_\nu^*$ etc. and using the definition of the Mandelstam variables (A.42) leads us to (color and dirac quantities commute)

$$i\mathcal{M}_t = \frac{igg_s}{\sqrt{8}} \frac{V_{qq'}}{t - m_{q'}^2} \left[c_2^\dagger t^a c_1 \right] \epsilon_\mu^* \epsilon_\nu^* \left[\bar{v}_2 \gamma^\nu (\not{p}_1 - \not{p}_3 + m_{q'}) \gamma^\mu (\mathbb{1} - \gamma^5) u_1 \right]. \quad (\text{A.45})$$

By the complex conjugate of the matrix element (using A.14, A.16, A.25, A.24, A.33,

A.35)

$$i\mathcal{M}_t^* = i\mathcal{M}_t^\dagger = \frac{-igg_s}{\sqrt{8}} \frac{V_{qq'}^*}{t - m_{q'}^2} \left[c_1^\dagger t^a c_2 \right] \epsilon_\mu \epsilon_\nu \left[\bar{u}_1 (\mathbb{1} + \gamma^5) \gamma^\mu (\not{p}_1 - \not{p}_3 + m_{q'}) \gamma^\nu v_2 \right]$$

we get for the matrix element squared (A.15)

$$\begin{aligned} |\mathcal{M}_t|^2 &= \mathcal{M}_t \mathcal{M}_t^* \\ &= \frac{g^2 g_s^2}{8} \frac{|V_{qq'}|^2}{(t - m_{q'}^2)^2} \text{Tr} \left[t^a c_1 c_1^\dagger t^a c_2 c_2^\dagger \right] \epsilon_\mu^* \epsilon_{\mu'} \epsilon_\nu^* \epsilon_{\nu'} \\ &\quad \times \text{Tr} \left[\gamma^\nu (\not{p}_1 - \not{p}_3 + m_{q'}) \gamma^\mu (\mathbb{1} - \gamma^5) u_1 \bar{u}_1 (\mathbb{1} + \gamma^5) \gamma^{\mu'} (\not{p}_1 - \not{p}_3 + m_{q'}) \gamma^{\nu'} v_2 \bar{v}_2 \right]. \end{aligned} \quad (\text{A.46})$$

Summing (averaging) over all final (initial) spins, polarizations and colors yields (A.17, A.18, A.19, A.20, A.21)

$$\begin{aligned} |\overline{\mathcal{M}}_t|^2 &= \frac{1}{2} \cdot \frac{1}{2} \sum_{\text{spins}} \sum_{\text{polarizations}} \frac{1}{3} \cdot \frac{1}{3} \sum_{\text{colors}} |\mathcal{M}_t|^2 \\ &= \frac{g^2 g_s^2}{288} \frac{|V_{qq'}|^2}{(t - m_{q'}^2)^2} \text{Tr} \left[\frac{4}{3} \cdot \mathbb{1}_{3 \times 3} \right] (-g_{\mu\mu'} + \frac{p_{3\mu} p_{3\mu'}}{m_W^2}) (-g_{\nu\nu'}) \\ &\quad \times \text{Tr} \left[\gamma^\nu (\not{p}_1 - \not{p}_3 + m_{q'}) \gamma^\mu (\mathbb{1} - \gamma^5) (\not{p}_1 + m_q) \right. \\ &\quad \left. (\mathbb{1} + \gamma^5) \gamma^{\mu'} (\not{p}_1 - \not{p}_3 + m_{q'}) \gamma^{\nu'} (\not{p}_2 - m_{q'}) \right] \\ &= \frac{g^2 g_s^2}{72} \frac{|V_{qq'}|^2}{(t - m_{q'}^2)^2} \\ &\quad \times \text{Tr} \left[\left(\gamma^\nu (\not{p}_1 - \not{p}_3 + m_{q'}) \gamma^\mu (\mathbb{1} - \gamma^5) (\not{p}_1 + m_q) \right. \right. \\ &\quad \left. \left. (\mathbb{1} + \gamma^5) \gamma_\mu (\not{p}_1 - \not{p}_3 + m_{q'}) \gamma_\nu (\not{p}_2 - m_{q'}) \right) \right. \\ &\quad \left. - \frac{1}{m_W^2} \left(\gamma^\nu (\not{p}_1 - \not{p}_3 + m_{q'}) \not{p}_3 (\mathbb{1} - \gamma^5) (\not{p}_1 + m_q) \right. \right. \\ &\quad \left. \left. (\mathbb{1} + \gamma^5) \not{p}_3 (\not{p}_1 - \not{p}_3 + m_{q'}) \gamma_\nu (\not{p}_2 - m_{q'}) \right) \right]. \end{aligned} \quad (\text{A.47})$$

 The trace consists of 288 terms. But no need to despair: many of them vanish. Using A.26, A.35, A.34, A.37 and A.39 one can see that every trace containing a single γ^5

is zero and so there are only 144 terms left.¹ Furthermore, one half of the remaining terms cancels and the other half adds up due to A.32 and A.35. Since traces consisting of an odd number of γ matrices still vanish without containing a γ^5 in addition (A.38) we can reduce the number of terms by another half ending up with only 18 non-zero traces:

$$\begin{aligned} \text{Tr} [\dots] = 2 \cdot \text{Tr} \left[\left(\gamma^\nu \not{p}_1 \gamma^\mu \not{p}_1 \gamma_\mu - \frac{1}{m_W^2} \gamma^\nu \not{p}_1 \not{p}_3 \not{p}_1 \not{p}_3 \right) (\not{p}_1 \gamma_\nu \not{p}_2 - \not{p}_3 \gamma_\nu \not{p}_2 - m_{q'}^2 \gamma_\nu) \right. \\ \left. - \left(\gamma^\nu \not{p}_3 \gamma^\mu \not{p}_1 \gamma_\mu - \frac{1}{m_W^2} \gamma^\nu \not{p}_3 \not{p}_3 \not{p}_1 \not{p}_3 \right) (\not{p}_1 \gamma_\nu \not{p}_2 - \not{p}_3 \gamma_\nu \not{p}_2 - m_{q'}^2 \gamma_\nu) \right. \\ \left. + m_{q'}^2 \left(\gamma^\nu \gamma^\mu \not{p}_1 \gamma_\mu - \frac{1}{m_W^2} \gamma^\nu \not{p}_3 \not{p}_1 \not{p}_3 \right) (-\not{p}_1 \gamma_\nu + \not{p}_3 \gamma_\nu + \gamma_\nu \not{p}_2) \right]. \end{aligned}$$

Now contracting the Lorentz-indices and commuting some of the momenta using A.27, A.28, A.29, A.30 and twice A.26 simplifies the trace to

$$\begin{aligned} \text{Tr} [\dots] = 2 \cdot \text{Tr} \left[\not{p}_1 \not{p}_2 (2 - D)^2 (p_1^2 - p_3^2 + m_{q'}^2) \right. \\ \left. - (\not{p}_3 \not{p}_2 (2 - D) + m_{q'}^2 \mathbb{1} D) 2(2 - D) (p_1^2 - p_1 \cdot p_3) \right. \\ \left. - \frac{1}{m_W^2} (\not{p}_1 \not{p}_2 (2 - D) (4(p_1 \cdot p_3)^2 - p_3^2 p_1^2 - 4p_1 \cdot p_3 p_3^2 + p_3^4 - m_{q'}^2 p_3^2) \right. \\ \left. + \not{p}_3 \not{p}_2 (2 - D) (-2p_1 \cdot p_3 p_1^2 + 2p_3^2 p_1^2 + 2m_{q'}^2 p_1 \cdot p_3) \right. \\ \left. + m_{q'}^2 \mathbb{1} D (-4(p_1 \cdot p_3)^2 + 2p_3^2 p_1^2 + 2(p_1 \cdot p_3) p_3^2) \right]. \end{aligned}$$

After all A.36 allows to evaluate the trace and plugging in the definition of the Mandelstam variables A.42 gives

$$\begin{aligned} \text{Tr} [\dots] = 2 \cdot \left[2(s - p_1^2 - p_2^2)(2 - D)^2 (p_1^2 - p_3^2 + m_{q'}^2) \right. \\ \left. - (2(p_2^2 + p_3^2 - u)(2 - D) + 4m_{q'}^2 D) (2 - D) (p_1^2 - p_3^2 + t) \right. \\ \left. - \frac{1}{m_W^2} (2(s - p_1^2 - p_2^2)(2 - D) (p_1^4 - 2p_1^2 t + t^2 - p_3^2 p_1^2 - m_{q'}^2 p_3^2) \right. \\ \left. + 2(p_2^2 + p_3^2 - u)(2 - D) ((-p_1^2 + p_3^2 + t)p_1^2 + m_{q'}^2 (p_1^2 + p_3^2 - t)) \right. \\ \left. + 4m_{q'}^2 D (-p_1^4 + 2p_1^2 t + p_3^2 t + p_1^2 p_3^2 - t^2) \right]. \quad (\text{A.48}) \end{aligned}$$

By eliminating the Mandelstam s by A.43 and putting in the on-shell masses $p_1^2 = m_q^2$, $p_2^2 = m_{q'}^2$, $p_3^2 = m_W^2$ and $p_4^2 = 0$ we have the final result for the summed matrix element

¹In addition you need to know that all γ^μ contracted with each other only contribute as sums of the unity matrix, but you do not need the explicit relations yet.

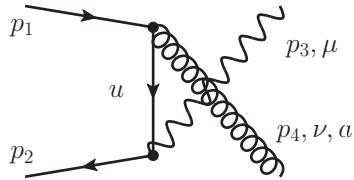
squared in the t-channel:

$$\begin{aligned}
 |\overline{\mathcal{M}}_t|^2 = & \frac{g_s^2 g_s^2}{18} \frac{|V_{qq'}|^2}{(t - m_{q'}^2)^2 m_W^2} \\
 & \left(2m_q^4 m_{q'}^2 - 2m_q^2 m_{q'}^4 - 8m_q^2 m_{q'}^2 m_W^2 + 8m_{q'}^2 m_W^4 - 2m_{q'}^4 m_W^2 \right. \\
 & + (2m_{q'}^4 + 2m_q^4 - 2m_q^2 m_{q'}^2 - 4m_q^2 m_W^2 - 8m_{q'}^2 m_W^2)t - (4m_q^2 + 2m_W^2)t^2 \\
 & + (2m_q^2 m_{q'}^2 - 4m_{q'}^2 m_W^2)u - (2m_q^2 + 2m_{q'}^2 - 4m_W^2)tu + 2(t+u)t^2 \\
 & + D \left(m_q^4 m_{q'}^2 + m_q^2 m_{q'}^4 - 4m_{q'}^2 m_W^4 + m_{q'}^4 m_W^2 - (m_q^2 m_{q'}^2 - 4m_{q'}^2 m_W^2)u \right. \\
 & \quad \left. - (m_{q'}^4 + m_q^4 + 3m_q^2 m_{q'}^2 - 4m_q^2 m_W^2 - 2m_{q'}^2 m_W^2)t \right. \\
 & \quad \left. + (2m_q^2 + 2m_{q'}^2 + m_W^2)t^2 + (m_q^2 + m_{q'}^2 - 4m_W^2)tu - (t+u)t^2 \right) \\
 & + D^2 (m_q^2 m_{q'}^2 m_W^2 - m_{q'}^2 m_W^2 t - m_{q'}^2 m_W^2 u + m_W^2 tu) \Big). \tag{A.49}
 \end{aligned}$$

Since we only deal with 5 flavors (no top quarks) as mentioned above in section 3.1 we can neglect all quark masses at LHC energy scales. This first derivation was only to show how it looks like in general. As mentioned additionally, we set $D = 4 - 2\epsilon$ in the context of regularization. Hence in the end we get:

$$|\overline{\mathcal{M}}_t|^2 = \frac{g_s^2 g_s^2}{9} |V_{qq'}|^2 \left(1 + 2\frac{u}{t} - \frac{t+u}{m_W^2} - \epsilon \left(1 + 4\frac{u}{t} - \frac{t+u}{m_W^2} \right) + \epsilon^2 \left(2\frac{u}{t} \right) \right). \tag{A.50}$$

A second diagram contributes to the process $q\bar{q}' \rightarrow Wg$, the u-channel diagram



Applying again the Feynman rules as in the t-channel case yields (neglecting the quark masses now)

$$i\mathcal{M}_u = \frac{ig g_s}{\sqrt{8}} \frac{V_{qq'}}{u} \left[c_2^\dagger t^a c_1 \right] \epsilon_\mu^* \epsilon_\nu^* \left[\bar{v}_2 \gamma^\mu (\mathbb{1} - \gamma^5) (\not{p}_1 - \not{p}_4) \gamma^\nu u_1 \right]. \tag{A.51}$$

Clearly, the only difference to the t-channel is the order of the vertices and the four-momentum of the propagator, which corresponds to $\gamma^\mu \leftrightarrow \gamma^\nu$ and $\not{p}_3 \leftrightarrow \not{p}_4$ considering A.35. So following exactly the same steps and using the same arguments to simplify

the trace as before gives for the summed matrix element squared

$$|\overline{\mathcal{M}}_u|^2 = \frac{g^2 g_s^2 |V_{qq'}|^2}{72 u^2} \times 2 \cdot \text{Tr} \left[\left(\gamma^\mu (\not{p}_1 - \not{p}_4) \gamma^\nu \not{p}_1 \gamma_\nu (\not{p}_1 - \not{p}_4) \gamma_\mu \not{p}_2 \right) - \frac{1}{m_W^2} \left(\not{p}_3 (\not{p}_1 - \not{p}_4) \gamma^\nu \not{p}_1 \gamma_\nu (\not{p}_1 - \not{p}_4) \not{p}_3 \not{p}_2 \right) \right].$$

In the first term of the trace, the new ordering of the γ matrices has been nullified by the polarization sum, indeed in the second term it has not. Analogous simplification by A.27, A.28, A.29 and twice A.26 now yields

$$|\overline{\mathcal{M}}_u|^2 = \frac{g^2 g_s^2 |V_{qq'}|^2}{36 u^2} \times \text{Tr} \left[(2-D)^2 \left(\not{p}_1 \not{p}_2 (p_1^2 - p_4^2) - 2 \not{p}_4 \not{p}_2 (p_1^2 - p_1 \cdot p_4) \right) - \frac{(2-D)}{m_W^2} \left(\not{p}_1 \not{p}_2 p_3^2 (p_4^2 - p_1^2) + 2 \not{p}_4 \not{p}_2 p_3^2 (p_1^2 - p_1 \cdot p_4) + 2 \not{p}_3 \not{p}_2 (p_1 \cdot p_3 (p_1^2 - p_4^2) + 2 p_1 \cdot p_4 (p_3 \cdot p_4 - p_1^2)) \right) \right].$$

Since now we have $p_1^2 = p_2^2 = p_4^2 = 0$ (still $p_3^2 = m_W^2$), we are only left with

$$|\overline{\mathcal{M}}_u|^2 = \frac{2}{9} g^2 g_s^2 \frac{|V_{qq'}|^2}{u^2} \left((2-D)^2 (p_4 \cdot p_2 p_1 \cdot p_4) + \frac{(2-D)}{m_W^2} (m_W^2 p_4 \cdot p_2 p_1 \cdot p_4 - 2 p_3 \cdot p_2 p_1 \cdot p_4 p_3 \cdot p_4) \right)$$

after evaluating the trace by A.36. Plugging in again the Mandelstam variables, replacing D by $4 - 2\epsilon$ and taking into account A.43 the final result is

$$|\overline{\mathcal{M}}_u|^2 = \frac{g^2 g_s^2}{9} |V_{qq'}|^2 \left(1 + 2 \frac{t}{u} - \frac{t+u}{m_W^2} - \epsilon \left(1 + 4 \frac{t}{u} - \frac{t+u}{m_W^2} \right) + \epsilon^2 \left(2 \frac{t}{u} \right) \right). \quad (\text{A.52})$$

In fact, this is just the t-channel result with $t \leftrightarrow u$. We will use such a simplification later on for the next process. For now there is one problem left: the so-called interference terms. Since \mathcal{M} is a sum of all contributing channels, there are mixing terms for the squared matrix element, in this case $\mathcal{M}_t \mathcal{M}_u^*$ and $\mathcal{M}_u \mathcal{M}_t^*$ which are the same since there are real as we will see.

At first glance one can see that the only difference compared to the former matrix elements squared lies in a mixing of the terms contributing to the Dirac trace, so we

will start at where summing/averaging was performed already:

$$\begin{aligned} \overline{\mathcal{M}_t \mathcal{M}_u^*} &= \frac{g^2 g_s^2}{72} \frac{|V_{qq'}|^2}{tu} \\ &\times \text{Tr} \left[\left(\gamma^\nu (\not{p}_1 - \not{p}_3) \gamma^\mu (\mathbb{1} - \gamma^5) \not{p}_1 \gamma_\nu (\not{p}_1 - \not{p}_4) (\mathbb{1} + \gamma^5) \gamma_\mu \not{p}_2 \right) \right. \\ &\quad \left. - \frac{1}{m_W^2} \left(\gamma^\nu (\not{p}_1 - \not{p}_3) \not{p}_3 (\mathbb{1} - \gamma^5) \not{p}_1 \gamma_\nu (\not{p}_1 - \not{p}_4) (\mathbb{1} + \gamma^5) \not{p}_3 \not{p}_2 \right) \right] . \end{aligned}$$

This time, there are four traces left containing a γ^5 after applying the same arguments as to simplify A.47, that is because we got four different momenta now. Those terms are two times (due to both γ^5 's) $\text{Tr} \left[\gamma^\nu \not{p}_3 \gamma^\mu \not{p}_1 \gamma_\nu \not{p}_4 \gamma_\mu \not{p}_2 \gamma^5 - \frac{p_3^2}{m_W^2} \left(\gamma^\nu \not{p}_1 \gamma_\nu \not{p}_4 \not{p}_3 \not{p}_2 \gamma^5 \right) \right]$. After contraction - no need to take care of the explicit expressions - we will have sums of terms like $i\epsilon^{\mu\nu\rho\sigma} p_\mu q_\nu k_\rho l_\sigma$ using A.41. But if we eliminate one of the four momenta by momentum-conservation we will have a contraction of the epsilon tensor with a sum of products of momenta which is symmetric under permutation of the two momenta that are identical in each one of the products respectively. Since the epsilon tensor is totally anti-symmetric the contraction yields therefore zero.

So in the end again every trace containing a single γ^5 vanishes. We are left with

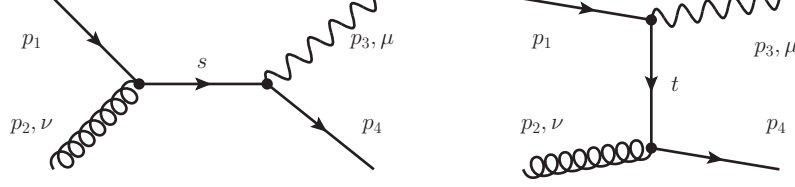
$$\begin{aligned}
\overline{\mathcal{M}_t \mathcal{M}_u^*} &= \frac{g^2 g_s^2}{36} \frac{|V_{qq'}|^2}{tu} \\
&\times \text{Tr} \left[\not{p}_1 \not{p}_2 \left((2-D)(Dp_1^2 - 4p_3 \cdot p_1 - 4p_1 \cdot p_4) - 8p_3 \cdot p_4 \right) \right. \\
&\quad + \not{p}_3 \not{p}_2 (2-D)(4-D)p_1^2 + \not{p}_4 \not{p}_2 (4-D)((2-D)p_1^2 + 4p_3 \cdot p_1) \\
&\quad + \not{p}_3 \not{p}_4 \not{p}_1 \not{p}_2 2(4-D) - (4-D)^2 \not{p}_3 \not{p}_1 \not{p}_4 \not{p}_2 \\
&\quad - \frac{(2-D)}{m_W^2} \left((\not{p}_1 \not{p}_2 - \not{p}_4 \not{p}_2) p_1^2 p_3^2 - \not{p}_3 \not{p}_2 p_1^2 (p_3^2 - 2p_3 \cdot p_4) \right. \\
&\quad \left. \left. + \not{p}_1 \not{p}_4 \not{p}_3 \not{p}_2 (p_3^2 - 2p_1 \cdot p_3) \right) \right] \\
&= \frac{g^2 g_s^2}{9} \frac{|V_{qq'}|^2}{tu} \\
&\times \left(4(2-D)p_1 \cdot p_2 (-p_3 \cdot p_1 - p_1 \cdot p_4) + (7-D)(2-D)p_1 \cdot p_2 p_3 \cdot p_4 \right. \\
&\quad - (3-D)(2-D)p_4 \cdot p_2 p_3 \cdot p_1 - (5-D)(2-D)p_3 \cdot p_2 p_4 \cdot p_1 \\
&\quad \left. + \frac{2(2-D)}{m_W^2} p_1 \cdot p_3 (p_1 \cdot p_4 p_3 \cdot p_2 - p_1 \cdot p_3 p_4 \cdot p_2 + p_1 \cdot p_2 p_4 \cdot p_3) \right) \\
D \rightarrow 4-2\epsilon &= \frac{g^2 g_s^2}{9} |V_{qq'}|^2 \left(-1 + 2m_W^2 \frac{m_W^2 - t - u}{tu} + \frac{t+u}{m_W^2} \right. \\
&\quad \left. - \epsilon \left(1 + 2m_W^2 \frac{m_W^2 - t - u}{tu} + \frac{t+u}{m_W^2} \right) + 2\epsilon^2 \right) \tag{A.53}
\end{aligned}$$

following the same steps as in the u-channel case but using A.40 here in addition.

At last, we can add up together A.50, A.52 and two times A.53 to get the final expression for the Feynman amplitude of the process $q\bar{q}' \rightarrow Wg$:

$$\begin{aligned}
|\overline{\mathcal{M}_{q\bar{q}' \rightarrow Wg}}|^2 &= |\overline{\mathcal{M}_t}|^2 + 2 \cdot \overline{\mathcal{M}_t \mathcal{M}_u^*} + |\overline{\mathcal{M}_u}|^2 \\
&= \frac{2}{9} g^2 g_s^2 |V_{qq'}|^2 (1 - \epsilon) \left((1 - \epsilon) \left(\frac{u}{t} + \frac{t}{u} \right) + 2m_W^2 \frac{m_W^2 - t - u}{tu} - 2\epsilon \right). \tag{A.54}
\end{aligned}$$

There is one more type of process contributing to the leading order, the so-called QCD "Compton" process $q\bar{q}' \rightarrow Wg$, illustrated by the involved Feynman diagrams



To get the averaged and summed matrix element squared of this second subprocess we will now make use of the so-called crossing symmetry and determine it from the yet calculated former one. As can be seen from the LSZ formula (Eq. (2.54)) since it only distinguishes final and initial states by the sign of the Fourier-transform momentum the matrix element with a particle of (three-)momentum \mathbf{p} in the initial state can be gained from the one with an anti-particle with momentum $-\mathbf{p}$ in the final state by analytical continuation. In our case this means in practice that we can just replace $p_2^{q\bar{q}' \rightarrow Wg}$ by $-p_4^{qg \rightarrow Wq'}$ and $p_4^{q\bar{q}' \rightarrow Wg}$ by $-p_2^{qg \rightarrow Wq'}$ which implies $s \leftrightarrow u$ in A.54. But for each fermion momentum flipped (only one here) there arises an additional overall minus sign after averaging and summing over spin states corresponding to the relative phase convention of the u and v spinors.

Since the gluon occurs in eight different colors instead of three we also have to adjust the color factor for the unpolarized matrix element squared, so in the end we just have

$$\begin{aligned}
 |\overline{\mathcal{M}}_{qg \rightarrow Wq'}|^2 &= -|\overline{\mathcal{M}}_{q\bar{q}' \rightarrow Wg}|^2 (s \leftrightarrow u) \\
 &= \frac{1}{12} g^2 g_s^2 |V_{qq'}|^2 (1 - \epsilon) \left((\epsilon - 1) \left(\frac{s}{t} + \frac{t}{s} \right) - 2m_W^2 \frac{m_W^2 - t - s}{ts} + 2\epsilon \right).
 \end{aligned}
 \tag{A.55}$$

Note that this result also represents the subprocess $\bar{q}g \rightarrow W\bar{q}'$ by charge conjugation.

A.4. Quark self energy one loop contribution - example of dimensional regularization

At first we remark that in the end one comes across the same kind of integral when calculating loop corrections. The integral reads

$$I_n(A) = \frac{1}{i\pi^2} \int d^D q \frac{1}{(q^2 - A + i\epsilon)^n} \quad (\text{A.56})$$

The integral is convergent if $A > 0$ and $D < 2n$. After one has performed a Wick rotation in the complex plane the integral can be solved using D dimensional spherical coordinates in the end leading to

$$I_n(A) = i(-1)^n \pi^{D/2} \frac{\Gamma(n - \frac{D}{2})}{\Gamma(n)} (A - i\epsilon)^{\frac{D}{2} - n} \quad (\text{A.57})$$

where the function $\Gamma(z)$ obeys among other things $\Gamma(z+1) = z\Gamma(z)$ and $\Gamma(n+1) = n!$ ($n=0,1,2, \dots$). It has poles at $z = 0, -1, -2, \dots$ and can be expanded as $\Gamma(z) \xrightarrow{z \rightarrow 0} \frac{1}{z} - \gamma_E + \mathcal{O}(z)$ where γ_E is the Euler constant ($\approx 0.5772 \dots$).

Furthermore, all general tensor integrals from loop diagrams growing in complexity when adding more and more propagators involving four-momenta in the numerator, can be reduced to only a few basic scalar integrals which one denotes as A_0 , B_0 , C_0 and D_0 (higher ones are usually not important). The alphabetic character indicates the power of momenta in the denominator of the integrand. We will only come across A_0 and B_0 in the considered scenario which is the one loop correction to the quark self energy $-i\Sigma^{\bar{q}q}$. The integral is given by

$$-\frac{4}{3} g_s^2 \frac{(2\pi\mu)^{4-D}}{(2\pi)^4} \int d^D q \frac{(2-D)(\not{p} - \not{q}) + Dm}{(q^2 + i\epsilon)((p-q)^2 - m^2 + i\epsilon)} \quad (\text{A.58})$$

where the arbitrary parameter μ of dimension mass accounts for the additional powers of mass from the momentum integration in D dimension. At first we have a look at the "scalar" part. Writing $C = -\frac{4}{3} g_s^2 \frac{i\pi^2}{(2\pi)^4}$ this part of the integral reads

$$C \frac{(2\pi\mu)^{4-D}}{i\pi^2} \int d^D q \frac{(2-D)\not{p} + Dm}{(q^2 + i\epsilon)((p-q)^2 - m^2 + i\epsilon)} \equiv C((2-D)\not{p} + Dm)B_0(p^2, 0, m^2) \quad (\text{A.59})$$

where we identify $B_0(p^2, m_0, m_1)$ in our case with $m_0 = 0$. To solve this integral one usually makes use of the so-called *Feynman* parametrization

$$\frac{1}{ab} = \int_0^1 dx \frac{1}{(a(1-x) + bx)^2} \quad (\text{A.60})$$

With $a = q^2 + i\epsilon$ and $b = (p - q)^2 + i\epsilon$ we have

$$\begin{aligned} B_0(p^2, 0, m^2) &= \frac{(2\pi\mu)^{4-D}}{i\pi^2} \int d^D q \int_0^1 dx \frac{1}{((q^2 + i\epsilon)(1-x) + ((p-q)^2 - m^2 + i\epsilon)x)^2} \\ &= \frac{(2\pi\mu)^{4-D}}{i\pi^2} \int d^D q \int_0^1 dx \frac{1}{((q^2 - x2pq + x(p^2 - m^2) + i\epsilon)^2} \\ &= \frac{(2\pi\mu)^{4-D}}{i\pi^2} \int d^D q \int_0^1 dx \frac{1}{(\underbrace{(q-xp)^2}_{=:q'} - \underbrace{x^2p^2 + x(p^2 - m^2)}_{=: -A} + i\epsilon)^2} \\ &= \frac{(2\pi\mu)^{4-D}}{i\pi^2} \int_0^1 dx \int d^D q' \frac{1}{(q' - A + i\epsilon)^2} \end{aligned} \quad (\text{A.61})$$

where we now can apply the generic integral $I_2(A)$ from (A.56) yielding

$$B_0(p^2, 0, m^2) = (2\pi\mu)^{\frac{4-D}{2}} \Gamma\left(\frac{4-D}{2}\right) \int_0^1 dx (x^2 p^2 - x(p^2 - m^2) - i\epsilon)^{\frac{D-4}{2}} \quad (\text{A.62})$$

Expanding the Γ -function as mentioned above and the integrand according to $x^\epsilon \approx 1 + \epsilon \ln(x) + \mathcal{O}(\epsilon^2)$ for $\epsilon \rightarrow 0$ we achieve

$$\begin{aligned} B_0(p^2, 0, m^2) &= \underbrace{\frac{2}{4-D} - \gamma_E + \ln(4\pi)}_{=: \Delta} - \int_0^1 dx \ln\left(\frac{x(xp^2 - (p^2 - m^2) - i\epsilon)}{\mu^2}\right) \\ &= \Delta + \ln(\mu^2) - \int_0^1 dx \ln(x) - \int_0^1 dx \ln\left(\frac{xp^2 - p^2 + m^2 - i\epsilon}{\mu^2}\right) \\ &= \Delta + \ln(\mu^2) + 1 - \frac{1}{p^2} \int_{m^2 - p^2 - i\epsilon}^{m^2} dx' \ln(x') \\ &= \Delta - \ln\left(\frac{m^2}{\mu^2}\right) + 2 + \frac{m^2 - p^2}{p^2} \ln\left(\frac{m^2 - p^2 - i\epsilon}{m^2}\right) + \mathcal{O}(4-D). \end{aligned} \quad (\text{A.63})$$

Now consider the other part of the self energy integral

$$C \frac{(2\pi\mu)^{4-D}}{i\pi^2} \int d^D q \frac{(2-D)\gamma_\nu q^\nu}{(q^2 + i\epsilon)((p-q)^2 - m^2 + i\epsilon)} \equiv C((2-D)\gamma_\nu B^\nu(p^2, 0, m^2)). \quad (\text{A.64})$$

The tensor integral B^ν can be reduced to scalar integrals in the following way. We use $p_\nu q^\nu = -1/2((q-p)^2 - m^2 + i\epsilon - (q^2 + i\epsilon) - (p^2 - m^2))$ and $B^\nu = p^\mu B_1$ so that

$$\begin{aligned} p^2 B_1 = p_\nu B^\nu &= \frac{(2\pi\mu)^{4-D}}{i\pi^2} \frac{1}{2} \left(\int d^D q \frac{1}{(q^2 + i\epsilon)} - \int d^D q \frac{1}{((p-q)^2 - m^2 + i\epsilon)} \right. \\ &\quad \left. + \int d^D q \frac{p^2 - m^2}{(q^2 + i\epsilon)((p-q)^2 - m^2 + i\epsilon)} \right) \\ &\Rightarrow B_1 = \frac{1}{2} (A_0(0) - A_0(m) - (p^2 - m^2)B_0(p^2, 0, m)) . \quad (\text{A.65}) \end{aligned}$$

where $A_0(m)$ can directly identified with the generic integral $\frac{(2\pi\mu)^{4-D}}{i\pi^2} \cdot I_1(m^2)$ yielding $A_0(m) = m^2 \left(\Delta - \ln \left(\frac{m^2 - i\epsilon}{\mu^2} \right) + 1 \right) + \mathcal{O}(4-D)$ (and so $A_0(0) = 0$).

Using all pieces together we obtain the final result for the self-energy correction:

$$\begin{aligned} -i\Sigma^{\bar{q}q} &= C \left((2-D)\not{p}B_1(p^2, 0, m) + ((2-D)\not{p} + Dm)B_0(p^2, 0, m) \right) \\ &= C \left((2-D)\not{p} \left(-\frac{1}{2p^2}A_0(m) + \left(\frac{1}{2} + \frac{m^2}{2p^2} \right) B_0(p^2, 0, m) \right) + DmB_0(p^2, 0, m) \right) \\ &= C \left(\left(\frac{-2+4-D}{2} \right) \not{p} \left(\Delta - \ln \left(\frac{m^2 - i\epsilon}{\mu^2} \right) + \frac{m^2}{p^2} + \frac{m^4 - (p^2)^2}{(p^2)^2} \ln \left(\frac{m^2 - p^2 - i\epsilon}{m^2} \right) \right) \right. \\ &\quad \left. + (D-4+4)m \left(\Delta - \ln \left(\frac{m^2 - i\epsilon}{\mu^2} \right) + 2 + \frac{m^2 - p^2}{p^2} \ln \left(\frac{m^2 - p^2 - i\epsilon}{m^2} \right) \right) \right) \\ &= \frac{4}{3} \frac{g_s^2}{4\pi^2} \left(\not{p} \left(\Delta - \ln \left(\frac{m^2 - i\epsilon}{\mu^2} \right) + \frac{m^2}{p^2} + \frac{m^4 - (p^2)^2}{(p^2)^2} \ln \left(\frac{m^2 - p^2 - i\epsilon}{m^2} \right) + 1 \right) \right. \\ &\quad \left. - 4m \left(\Delta - \ln \left(\frac{m^2 - i\epsilon}{\mu^2} \right) + \frac{m^2 - p^2}{p^2} \ln \left(\frac{m^2 - p^2 - i\epsilon}{m^2} \right) + \frac{3}{2} \right) \right) . \quad (\text{A.66}) \end{aligned}$$

A.4.1. Derivative of the self-energy contribution

To obtain the residue of the physical mass pole of the full quark propagator (at one loop) it is necessary to determine the derivative of the quark self energy correction evaluated at the physical mass.

We begin with

$$\begin{aligned} \frac{-i}{C} \frac{d\Sigma}{d\not{p}} = (2-D) & \left(-\frac{1}{2p^2} A_0(m) + \left(\frac{1}{2} + \frac{m^2}{2p^2} \right) B_0(p^2, 0, m) + \frac{1}{p^2} A_0(m) \right. \\ & \left. - \frac{m^2}{p^2} B_0(p^2, 0, m) + \left(\frac{p^2 + m^2}{p^2} \right) B'_0(p^2, 0, m) \right) + 2Dm\not{p}B'_0(p^2, 0, m) \end{aligned} \quad (\text{A.67})$$

As it turns out the derivative of B_0 obeys a singularity at $p^2 = m^2$ which has to be regularized. Therefor one has to take a step back. Actually its best to use the symmetry of B_0 i.e $B_0(p^2, 0, m) = B_0(p^2, m, 0)$, one arrives at

$$\begin{aligned} \frac{\partial B_0(p^2, 0, m)}{\partial p^2} &= (2\pi\mu)^{\frac{4-D}{2}} \Gamma\left(\frac{4-D}{2}\right) \int_0^1 dx \frac{\partial}{\partial p^2} (x^2 p^2 - x(p^2 + m^2) + m^2 - i\epsilon)^{\frac{D-4}{2}} \\ &= (2\pi\mu)^{\frac{4-D}{2}} \Gamma\left(\frac{4-D}{2}\right) \frac{4-D}{2} \int_0^1 dx (x-x^2) (x^2 p^2 - x(p^2 + m^2) + m^2 - i\epsilon)^{\frac{D-4}{2}-1} \\ &= (2\pi\mu)^{\frac{4-D}{2}} \Gamma\left(1 + \frac{4-D}{2}\right) \int_0^1 dx x(1-x)^{\frac{D-4}{2}} (m^2 - xp^2)^{\frac{D-4}{2}-1} \\ &\Rightarrow \left. \frac{\partial B_0(p^2, 0, m)}{\partial p^2} \right|_{p^2=m^2} = (2\pi\mu)^{\frac{4-D}{2}} \Gamma\left(1 + \frac{4-D}{2}\right) (m^2)^{\frac{D-4}{2}-1} \int_0^1 dx x(1-x)^{D-5} \end{aligned} \quad (\text{A.68})$$

where one had to consider the limit $D \rightarrow 4^+$. Expanding again all terms (up to higher orders of $(D-4)$) one obtains

$$\begin{aligned} \left. \frac{\partial B_0(p^2, 0, m)}{\partial p^2} \right|_{p^2=m^2} &= \\ &= \frac{1}{m^2} \left(1 + \frac{D-4}{2} \ln\left(\frac{m^2}{4\pi\mu^2}\right) \right) \left(1 + \gamma_E \frac{D-4}{2} \right) \left(\frac{1}{D-4} - 1 + D-4 \right) \\ &= \frac{1}{2m^2} \left(\frac{2}{D-4} + \gamma_E - \ln(4\pi) + \ln\left(\frac{m^2}{\mu^2}\right) - 2 \right) \\ &= \frac{1}{2m^2} \left(\Delta_{IR} + \ln\left(\frac{m^2}{\mu^2}\right) - 2 \right) \end{aligned} \quad (\text{A.69})$$

where we have defined $\Delta_{IR} = \frac{2}{D-4} + \gamma_E - \ln(4\pi) = -\Delta_{UV}$.

Now turning back to Eq. (A.67) and plugging in B'_0 we get the final result for the

derivative of the self-energy correction at $p^2 = m^2$:

$$\begin{aligned}
\left. \frac{d\Sigma}{d\phi} \right|_{\phi=m} &= -\frac{4}{3} \frac{g_s^2}{4\pi^2} \left((2-D) \left(\frac{1}{m^2} A_0(m) + 2m^2 B'_0(m^2, 0, m) \right) + 2Dm^2 B'_0(m^2, 0, m) \right) \\
&= -\frac{4}{3} \frac{g_s^2}{(4\pi)^2} \left(\Delta_{UV} - \ln \frac{m^2}{\mu} - 2 \left(\Delta_{IR} + \ln \frac{m^2}{\mu} - 2 \right) \right). \tag{A.70}
\end{aligned}$$

Bibliography

- [1] *The Phases of Quantum Chromodynamics: From Confinement to Extreme Environments*. Cambridge University Press. ISBN: 0521804507.
- [2] Steven Weinberg. *The Quantum Theory of Fields, Volume II: Modern Applications*. Cambridge University Press. ISBN: 0521670543.
- [3] Michael E. Peskin and Dan V. Schroeder. *An Introduction To Quantum Field Theory (Frontiers in Physics)*. Westview Press. ISBN: 0201503972.
- [4] I. J. R. Aitchison and A. J. G. Hey. *Gauge Theories in Particle Physics, Volume I: From Relativistic Quantum Mechanics to QED (Graduate Student Series in Physics)*. 3rd Rev. Taylor & Francis. ISBN: 0750308648.
- [5] “Regularization and renormalization of gauge fields”. In: *Nuclear Physics B* 44.1 (1972), pp. 189 –213. ISSN: 0550-3213.
- [6] A. A. Slavnov. In: *Theor. Math. Phys.* 10 (1972), p. 99.
- [7] “Renormalization of massless Yang-Mills fields”. In: *Nuclear Physics B* 33.1 (1971), pp. 173 –199. ISSN: 0550-3213.
- [8] “The renormalization scale-setting problem in QCD”. In: *Progress in Particle and Nuclear Physics* 72.0 (2013), pp. 44 –98. ISSN: 0146-6410.
- [9] Taizo Muta. *Foundations of Quantum Chromodynamics: An Introduction to Perturbative Methods in Gauge Theories*. Singapore: World Scientific, 1998.
- [10] “The four-loop β -function in quantum chromodynamics”. In: *Physics Letters B* 400.3–4 (1997), pp. 379 –384. ISSN: 0370-2693.
- [11] Walter Greiner, Stefan Schramm, and Eckart Stein. *Quantum Chromodynamics*. 3rd. rev. and enlarged ed. 2007. Springer. ISBN: 3540485341.
- [12] S. Bethke et al. *Workshop on Precision Measurements of α_s* . URL: <http://arxiv.org/pdf/1110.0016v3.pdf>.
- [13] F. Bloch and A. Nordsieck. “Note on the Radiation Field of the Electron”. In: *Phys. Rev.* 52 (2 1937), pp. 54–59.
- [14] Tobias Kasprzik. *Radiative Corrections to W +Jet Production at Hadron Colliders with a Leptonic Decay of the W Boson*. Dissertation. Freiburg, 2009.

- [15] “Failure of the Bloch-Nordsieck mechanism in perturbative QCD”. In: *Physics Letters B* 124.1–2 (1983), pp. 105 –108. ISSN: 0370-2693.
- [16] T. D. Lee and M. Nauenberg. “Degenerate Systems and Mass Singularities”. In: *Phys. Rev.* 133 (6B 1964), B1549–B1562.
- [17] “Lepton pair production at large transverse momentum in second order QCD”. In: *Nuclear Physics B* 211.1 (1983), pp. 106 –138. ISSN: 0550-3213.
- [18] “The complete computation of high-pT W and Z production in second-order {QCD}”. In: *Nuclear Physics B* 319.1 (1989), pp. 37 –71. ISSN: 0550-3213.
- [19] A. Denner J. Küblbeck M. Böhm. In: *Comput. Phys. Commun.* 60 (1990), p. 165.
- [20] M. Perez-Victoria T. Hahn. In: *Comput. Phys. Commun.* 118 (1999), p. 153.
- [21] A. Denner R. Mertig M. Böhm. In: *Comput. Phys. Commun.* 64 (1991), p. 345.
- [22] T. Hahn. In: *Acta Phys. Polon. B* 30 (1999), p. 3469.
- [23] “Asymptotic freedom in parton language”. In: *Nuclear Physics B* 126.2 (1977), pp. 298 –318. ISSN: 0550-3213.
- [24] John C. Collins, Davison E. Soper, and George F. Sterman. “Factorization of Hard Processes in QCD”. In: *Adv.Ser.Direct.High Energy Phys.* 5 (1988), pp. 1–91. arXiv: hep-ph/0409313 [hep-ph].
- [25] “W and Z production at next-to-leading order: From large qT to small”. In: *Nuclear Physics B* 349.2 (1991), pp. 381 –413. ISSN: 0550-3213.
- [26] Jonathan Debove. *QCD resummation for gaugino-pair hadroproduction*. PhD thesis, U. Grenoble, 2010.
- [27] “Back-to-back jets in QCD”. In: *Nuclear Physics B* 193.2 (1981), pp. 381 –443. ISSN: 0550-3213.
- [28] “Transverse momentum distribution in Drell-Yan pair and W and Z boson production”. In: *Nuclear Physics B* 250.1–4 (1985), pp. 199 –224. ISSN: 0550-3213.
- [29] F. Landry et al. “Fermilab Tevatron run-1 Z boson data and the Collins-Soper-Sterman resummation formalism”. In: *Phys. Rev. D* 67 (7 2003), p. 073016.
- [30] Wu-Ki Tung. *Perturbative QCD and the parton structure of the nucleon*. Michigan State University, USA. URL: <http://www.physics.smu.edu/~olness/cteqpp/tung2003/IntroPqcd.pdf>.
- [31] Hung-Liang Lai et al. “New parton distributions for collider physics”. In: *Phys.Rev.* D82 (2010), p. 074024. arXiv: 1007.2241 [hep-ph].

- [32] A.D. Martin et al. “Parton distributions for the LHC”. In: *Eur.Phys.J.* C63 (2009), pp. 189–285. arXiv: 0901.0002 [hep-ph].
- [33] “Impact of heavy quark masses on parton distributions and LHC phenomenology”. In: *Nuclear Physics B* 849.2 (2011), pp. 296–363. ISSN: 0550-3213.
- [34] M.R. Whalley, D. Bourilkov, and R.C. Group. “The Les Houches accord PDFs (LHAPDF) and LHAGLUE”. In: (2005). arXiv: hep-ph/0508110 [hep-ph].
- [35] M. Klasen and M. Brandt. “Parton densities from LHC vector boson production at small and large transverse momenta”. In: *Phys.Rev.* D88 (2013), p. 054002. DOI: 10.1103/PhysRevD.88.054002. arXiv: 1305.5677 [hep-ph].
- [36] CERN Program Library. PH department, CERN, CH-1211 Geneva 23, Switzerland. URL: <http://cern.ch/cernlib/>.
- [37] J. Beringer et al. Particle Data Group. *Phys. Rev. D* 86, 010001 (2012).
- [38] Serguei Chatrchyan et al. “Measurement of the Rapidity and Transverse Momentum Distributions of Z Bosons in pp Collisions at $\sqrt{s} = 7$ TeV”. In: *Phys.Rev.* D85 (2012), p. 032002. arXiv: 1110.4973 [hep-ex].
- [39] Georges Aad et al. “Measurement of the Transverse Momentum Distribution of W Bosons in pp Collisions at $\sqrt{s} = 7$ TeV with the ATLAS Detector”. In: *Phys.Rev.* D85 (2012), p. 012005. arXiv: 1108.6308 [hep-ex].

Danksagung

Ich bedanke mich bei Prof. Dr. Michael Klasen für die bereitwillige und freundliche Aufnahme in seine Arbeitsgruppe und die Bereitstellung des Themas dieser Arbeit.

Meinen Bürokollegen danke ich für das heitere Arbeitsklima.

Ein weiterer Dank geht an meine Familie, die mich auf den letzten Metern bestmöglich unterstützt hat.

Ein besonderer Dank geht an Florian König, der mit viel Geduld meinen zahlreichen Fragen begegnete.

Hiermit versichere ich, die vorliegende Arbeit selbstständig verfasst und keine anderen als die angegebenen Hilfsmittel und Quellen verwendet zu haben.

Münster, den 12. November 2013

Matthias Brandt